Dudley Knox Library, NPS
Monterey, CA 93943

NPS68-83-003

NAVAL POSTGRADUATE SCHOOL

Monterey, California

THESIS

A STATISTICAL APPROACH FOR DETERMINING
SUBSURFACE THERMAL STRUCTURE
FROM SEA SURFACE TEMPERATURE
IN THE NORTHEAST PACIFIC OCEAN

by

Terry A. Howell

June 1983

Thesis Advisor: G. H. Jung

Approved for public release; distribution unlimited

Prepared for: Naval Ocean Systems Center
Code 531
San Diego, California 92152

T209065

NAVAL POSTGRADUATE SCHOOL
Monterey, California

Rear Admiral John J. Ekelund, USN
Superintendent

David A. Schrady
Provost

This thesis was prepared in conjunction with research supported in part by Naval Ocean Systems Center under work order N6600183WR00043.

Reproduction of all or part of this report is not authorized without permission of the Naval Postgraduate School.

UNCLASSIFIED

SECURITY CLASSIFICATION OF THIS PAGE (When Data Entered)

REPORT DOCUMENTATION PAGE		READ INSTRUCTIONS BEFORE COMPLETING FORM
1. REPORT NUMBER NPS68-83-003	2. GOVT ACCESSION NO.	3. RECIPIENT'S CATALOG NUMBER
4. TITLE (and Subtitle) A Statistical Approach For Determining Subsurface Thermal Structure From Sea Surface Temperature In The Northeast Pacific Ocean		5. TYPE OF REPORT & PERIOD COVERED Master's Thesis June 1982 6. PERFORMING ORG. REPORT NUMBER
7. AUTHOR(s) Terry A. Howell in conjunction with Glen H. Jung and Calvin R. Dunlap		8. CONTRACT OR GRANT NUMBER(s)
9. PERFORMING ORGANIZATION NAME AND ADDRESS Naval Postgraduate School Monterey, California 93940		10. PROGRAM ELEMENT, PROJECT, TASK AREA & WORK UNIT NUMBERS N6600183WR00043
11. CONTROLLING OFFICE NAME AND ADDRESS Naval Ocean Systems Center Code 531 San Diego, California 92152		12. REPORT DATE June 1983 13. NUMBER OF PAGES 193
14. MONITORING AGENCY NAME & ADDRESS(if different from Controlling Office) CNO Attn: OP095 Navy Department Washington, D.C. 20350		15. SECURITY CLASS. (of this report) Unclassified 15a. DECLASSIFICATION/DOWNGRADING SCHEDULE

16. DISTRIBUTION STATEMENT (of this Report)

Approved for public release; distribution unlimited

17. DISTRIBUTION STATEMENT (of the abstract entered in Block 20, if different from Report)

18. SUPPLEMENTARY NOTES

19. KEY WORDS (Continue on reverse side if necessary and identify by block number)

Subsurface Thermal Structure
Sea Surface Temperature
Northeast Pacific Ocean
Remote Sensing
Satellite Oceanography
Fronts

20. ABSTRACT (Continue on reverse side if necessary and identify by block number)

Bathythermograph data acquired from the research vessel USNS SILAS BENT along a meridional track in the Northeast Pacific during September 1977 were statistically analyzed to determine possible associations between the subsurface thermal structure and sea surface temperature. Strongly correlated variables (thermocline gradients, mixed layer depth, and locations of the seasonal and main thermoclines) within the vertical temperature

DD FORM 1 JAN 73 1473 EDITION OF 1 NOV 65 IS OBSOLETE
S/N 0102-LF-014-6601

UNCLASSIFIED

SECURITY CLASSIFICATION OF THIS PAGE (When Data Entered)

#20. ABSTRACT (Continued)

profile were used in linear regression methods to form empirical relationships. The generated equations then are utilized to define the subsurface thermal structure from only an input of sea surface temperature. Comparison tests with temporally and spatially removed BT data were conducted with results indicating successful application within a water mass domain with uniformly changing characteristics.

Approved for public release; distribution unlimited

A Statistical Approach For Determining Subsurface Thermal Structure From Sea Surface Temperature in the Northeast Pacific Ocean

by

Terry A. Howell
Lieutenant, United States Navy
B.S., United States Naval Academy, 1974

Submitted in partial fulfillment of the
requirements for the degree of

MASTER OF SCIENCE IN METEOROLOGY AND OCEANOGRAPHY

from the

NAVAL POSTGRADUATE SCHOOL
June 1983

H 8247
c.1

Dudley Knox Library, NPS
Monterey, CA 93943

ABSTRACT

Bathythermograph data acquired from the research vessel USNS SILAS BENT along a meridional track in the Northeast Pacific during September 1977 were statistically analyzed to determine possible associations between the subsurface thermal structure and sea surface temperature. Strongly correlated variables (thermocline gradients, mixed layer depth, and locations of the seasonal and main thermoclines) within the vertical temperature profile were used in linear regression methods to form empirical relationships. The generated equations then are utilized to define the subsurface thermal structure from only an input of sea surface temperature. Comparison tests with temporally and spatially removed BT data were conducted with results indicating successful application within a water mass domain with uniformly changing characteristics.

TABLE OF CONTENTS

I. INTRODUCTION 15

A. IMPORTANCE OF DETERMINING OCEAN THERMAL STRUCTURE 15

B. SATELLITE DETERMINATION OF SUBSURFACE THERMAL STRUCTURE 16

C. PURPOSE AND GOALS OF THESIS 17

II. OCEANOGRAPHIC CHARACTERISTICS OF THE NORTHEAST PACIFIC OCEAN 19

A. WIND SYSTEMS AND CURRENTS 19

B. WATER MASSES AND FRONTS 21

1. SUBARCTIC WATER MASS CHARACTERISTICS . . . 21

2. SUBTROPIC WATER MASS CHARACTERISTICS . . . 25

3. TRANSITION ZONE 28

4. DENSITY STRUCTURE AND THE SUBARCTIC FRONT . 29

III. THERMAL STRUCTURE 32

A. THERMAL STRUCTURE IN THE NORTHEAST PACIFIC OCEAN 32

B. INTERNAL WAVE EFFECTS ON THERMAL STRUCTURE . . 36

C. HORIZONTAL SURFACE THERMAL STRUCTURE 38

IV. EXPERIMENT 40

A. OBJECTIVE 40

B. DATA ACQUISITION 42

C. ASSESSMENT OF TEMPERATURE STRUCTURE 45

D. STATISTICAL PROCEDURE 61

E. REGRESSION EQUATION ANALYSIS 81

F. THERMAL PROFILE TEST AND COMPARISON ANALYSIS . 87

1. TEST 1 87

2. TEST 2 90

3. TEST 3 101

G. REVIEW OF PREDICTED THERMAL PROFILE RESULTS . 107

V. CONCLUSIONS AND RECOMMENDATIONS 113

A. CONCLUSIONS 113

B. RECOMMENDATIONS 115

APPENDIX A. THERMAL VARIABLES VERSUS LATITUDE/DISTANCE ALONG TRACK 118

APPENDIX B. BIOMEDICAL COMPUTER PROGRAMS (DIXON AND BROWN, 1979) 132

APPENDIX C. REGIONAL SCATTER DIAGRAMS - SST VERSUS THERMAL VARIABLES 134

APPENDIX D. REGIONAL SCATTER DIAGRAMS - BOT VERSUS THERMAL VARIABLES 147

APPENDIX E. REGIONAL SCATTER DIAGRAMS - BUZ VERSUS THERMAL VARIABLES 158

APPENDIX F. CBSERVED AND PREDICTED THERMAL PROFILES ALONG TRACK 168

LIST OF REFERENCES 188

INITIAL DISTRIEUTION LIST 191

LIST OF TABLES

TABLE I. Locations and Times of XBT Measurements . . 51

TABLE II. Values of SST, MLD, Thermocline Gradients and T460 52

TABLE III. Values of Thermocline Temperatures and Depths 53

TABLE IV. Correlation Coefficients of Thermal Variables 64

TABLE V. Best-Fit Correlation Coefficients of Thermal Variables 79

LIST OF FIGURES

Figure 1. Location of OWS-P and North Pacific Ocean Surface Currents 20

Figure 2. Characteristic Temperature and Salinity Profiles 22

Figure 3. Upper Zone Domains 26

Figure 4. Lower Zone Domains 27

Figure 5. Growth and Decay of the Thermocline at Ocean Station "P" 34

Figure 6. Typical Temperature Structures at Ocean Station "P" 37

Figure 7. Surface Mean Temperature Structure For September 1977 39

Figure 8. Location of XBT DATA During 8-11 September 1977. 44

Figure 9. Meridional Cross-section of Temperature at 145W. 46

Figure 10. Model of Vertical Temperature Structure. . . 49

Figure 11. Pacific Ocean Sea Surface Temperature on 10 September 1977 55

Figure 12. Comparison of DT5, DT15, DT50 and DT100 Versus Latitude. 58

Figure 13. Comparison of MLD, BOT and BUZ Versus Latitude. 60

Figure 14. Comparison of SST, TBOT and TBUZ Versus Latitude. 66

Figure 15. Comparison of MLD and SST Versus Latitude. . 67

Figure 16. Comparison of BOT and SST Versus Latitude. . 68

Figure 17. Comparison of BUZ and SST Versus Latitude. . 69

Figure 18. Division of Regions Along Track. 71

Figure 19. Regional Scatter Diagram - DZ Versus BOT. . . 77

Figure 20. Regional Scatter Diagram - DZBUZ Versus BUZ. 78

Figure 21. Observed and Predicted Thermal Profiles - XBT Station 339. 88

Figure 22. Location of Original (•) and Test 2 (X) XBT Drops. 92

Figure 23. Observed and Predicted Thermal Profiles at 41.5N, 140.3W 94

Figure 24. Observed and Predicted Thermal Profiles at 42.3N, 150.0W 95

Figure 25. Observed and Predicted Thermal Profiles at 41.9N, 148.7W 97

Figure 26. Observed and Predicted Thermal Profiles at 42.3N, 144.0W 98

Figure 27. Observed and Predicted Thermal Profiles at 41.1N, 143.2W 99

Figure 28. Observed and Predicted Thermal Profiles at CWS-P 100

Figure 29. Location of Original (•) and Test 3 (X) XBT Data. 102

Figure 30. Observed and Predicted Thermal Profiles for 182030Z SEP 77 104

Figure 31. Observed and Predicted Thermal Profiles for 240000Z SEP 77 106

Figure 32. Observed and Predicted Thermal Profiles for 300000Z SEP 77 109

Figure 33. Example Predicted Profile Error Due to "Afternoon Effect". 111

Figure A.1. SST Versus Latitude/Distance. 118

Figure A.2. MLD Versus Latitude/Distance. 119

Figure A.3. DT5 Versus Latitude/Distance. 120

Figure A.4. DT15 Versus Latitude/Distance. 121

Figure A.5. DT50 Versus Latitude/Distance. 122

Figure A.6. DT100 Versus Latitude/Distance. 123

Figure A.7. BCT Versus Latitude/Distance. 124

Figure A.8. TBOT Versus Latitude/Distance. 125

Figure A.9. DT Versus Latitude/Distance. 126

Figure A.10. DZ Versus Latitude/Distance. 127

Figure A.11. BUZ Versus Latitude/Distance. 128

Figure A.12. TBUZ Versus Latitude/Distance. 129

Figure A.13. DTBUZ Versus Latitude/Distance. 130

Figure A.14. DZBUZ Versus Latitude/Distance. 131

Figure C.1. Regional Scatter Diagram - SST Versus MLD. 134

Figure C.2. Regional Scatter Diagram - SST Versus DT5. 135

Figure C.3. Regional Scatter Diagram - SST Versus DT15. 136

Figure C.4. Regional Scatter Diagram - SST Versus DT50. 137

Figure C.5. Regional Scatter Diagram - SST Versus DT100. 138

Figure C.6. Regional Scatter Diagram - SST Versus BCT. 139

Figure C.7. Regional Scatter Diagram - SST Versus TBOT. 140

Figure C.8. Regional Scatter Diagram - SST Versus DT. 141

Figure C.9. Regional Scatter Diagram - SST Versus DZ. 142

Figure C.10. Regional Scatter Diagram - SST Versus BUZ. 143

Figure C.11. Regional Scatter Diagram - SST Versus TBUZ. 144

Figure C.12. Regional Scatter Diagram - SST Versus DTBUZ. 145

Figure C.13. Regional Scatter Diagram - SST Versus DZBUZ. 146

Figure D.1. Regional Scatter Diagram - BOT Versus DT5. 147

Figure D.2. Regional Scatter Diagram - BOT Versus DT15. 148

Figure D.3. Regional Scatter Diagram - BOT Versus DT5C. 149

Figure D.4. Regional Scatter Diagram - BOT Versus DT100. 150

Figure D.5. Regional Scatter Diagram - BOT Versus TBOT. 151

Figure D.6. Regional Scatter Diagram - BOT Versus DT. 152

Figure D.7. Regional Scatter Diagram - BOT Versus DZ. 153

Figure D.8. Regional Scatter Diagram - BOT Versus BUZ. 154

Figure D.9. Regional Scatter Diagram - BOT Versus TBUZ. 155

Figure D.10. Regional Scatter Diagram - BOT Versus DTBUZ. 156

Figure D.11. Regional Scatter Diagram - BOT Versus DZBUZ. 157

Figure E.1. Regional Scatter Diagram - BUZ Versus DT5. 158

Figure E.2. Regional Scatter Diagram - BUZ Versus DT15. 159

Figure E.3. Regional Scatter Diagram - BUZ Versus DT50. 160

Figure E.4. Regional Scatter Diagram - BUZ Versus DT100. 161

Figure E.5. Regional Scatter Diagram - BUZ Versus TBOT. 162

Figure E.6. Regional Scatter Diagram - BUZ Versus DT. 163

Figure E.7. Regional Scatter Diagram - BUZ Versus DZ. 164

Figure E.8. Regional Scatter Diagram - BUZ Versus TBUZ. 165

Figure E.9. Regional Scatter Diagram - BUZ Versus DTBUZ. 166

Figure E.10. Regional Scatter Diagram - BUZ Versus DZBUZ. 167

Figure F.1. Observed and Predicted Thermal Profiles at XBT Sta. 340. 168

Figure F.2. Observed and Predicted Thermal Profiles at XBT Sta. 341. 169

Figure F.3. Observed and Predicted Thermal Profiles at XBT Sta. 342. 170

Figure F.4. Observed and Predicted Thermal Profiles at XBT Sta. 343. 171

Figure F.5. Observed and Predicted Thermal Profiles at XBT Sta. 344. 172

Figure F.6. Observed and Predicted Thermal Profiles at XBT Sta. 345. 173

Figure F.7. Observed and Predicted Thermal Profiles at XBT Sta. 346. 174

Figure F.8. Observed and Predicted Thermal Profiles at XBT Sta. 347. 175

Figure F.9. Observed and Predicted Thermal Profiles at XBT Sta. 348. 176

Figure F.10. Observed and Predicted Thermal Profiles at XBT Sta. 349. 177

Figure F.11. Observed and Predicted Thermal Profiles at XBT Sta. 350. 178

Figure F.12. Observed and Predicted Thermal Profiles at XBT Sta. 351. 179

Figure F.13. Observed and Predicted Thermal Profiles at XBT Sta. 352. 180

Figure F.14. Observed and Predicted Thermal Profiles at XBT Sta. 353. 181

Figure F.15. Observed and Predicted Thermal Profiles at XBT Sta. 354. 182

Figure F.16. Observed and Predicted Thermal Profiles at XBT Sta. 355. 183

Figure F.17. Observed and Predicted Thermal Profiles at XBT Sta. 356. 184

Figure F.18. Observed and Predicted Thermal Profiles at XBT Sta. 357. 185

Figure F.19. Observed and Predicted Thermal Profiles at XBT Sta. 358. 186

Figure F.20. Observed and Predicted Thermal Profiles at XBT Sta. 359. 187

I. INTRODUCTION

A. IMPORTANCE OF DETERMINING OCEAN THERMAL STRUCTURE

An important physical property and product of various dynamical processes occurring in the oceans is the thermal structure. Although it is derived from only a few mechanisms such as air-sea thermal energy exchange, forced and free convective mixing and horizontal ocean thermal advection, the interaction of these processes along with other hydrodynamic motions can become immensely complicated. Since the temperature profile has important implications for climatic weather prediction, commercial fisheries and military acoustic surveillance, to mention a few, the ability to predict this structure is of major importance.

Climatological atlases present an averaged profile for a certain period and location. However, this results in a generalized thermal structure which is not accurate enough to accomplish the precise needs of underwater sound propagation forecasting. Recent developments in numerical modeling of the upper-ocean temperatures have produced vast improvements in the analysis and prediction of mixed layers and other synoptic oceanic features (Clancy et al., 1981). It is inevitable that this method will reach the sophistication

of today's meteorological forecasting, but with the complexity of the physical processes involved and with present data sparsity in many ocean areas, many inaccuracies still exist.

The bathythermograph (BT) provides an accurate temperature profile at a point location in the upper ocean. Since the vertical thermal structure over a large area provides the main factor which affects the propagation characteristics of underwater acoustics, the need for many temperature profiles in Navy ASW operations is obvious. The expense involved in ship and aircraft deployment of BT's for an ocean area of interest often prohibits the use of this most accurate means of obtaining a detailed thermal description.

B. SATELLITE DETERMINATION OF SUBSURFACE THERMAL STRUCTURE

The study of the oceans by satellites has become a major arena for scientific scrutiny and investigation. Already it has given added insight into the numerous processes that govern oceanic behavior. The Gulf Stream eddies and fronts, the coastal upwelling off the Somali and Arabian coasts, and other applications in biological, geophysical and dynamical fields are becoming well known. However, in spite of great progress, satellite remote sensing techniques for observing oceanic processes are far from being fully realized.

The fundamental problem which continuously arises, besides atmospheric effects which will not be discussed, is that satellite observations are made at the surface alone and that all conclusions about subsurface processes are obtained from inference rather than by direct measurement. Consequently, the applications of satellites for oceanography are limited to those phenomena that generate surface signatures detectable by electromagnetic waves. Once these surface manifestations are observed, it is necessary to have knowledge of the physical processes involved to interpret their meaning. Currently there are few methods available where a qualitative "feel" for subsurface features can be directly expressed as empirical relationships from remotely sensed measurements at the sea surface. If a linkage is found to exist between the air-sea interface and the thermal structure below, a satellite would then be the perfect platform to collect sea surface data rapidly over all the world's oceans. This surface information could then be used to infer the subsurface vertical temperature structure.

C. PURPOSE AND GOALS OF THESIS

The primary purpose for the ongoing research into the prediction of subsurface thermal structure is to understand

the processes and relationships that govern the ocean's behavior. Roles that are performed by ships and aircraft (via expendable bathythermographs) in determining the temperature profiles could be played better by satellites, provided a "link" is found to read the below-surface events from the sea surface signatures. Therefore, if strong correlations and relationships could be ascertained between satellite-derived sea surface temperatures and vertical temperature profiles, then the areas of acoustical oceanography and naval tactical applications would benefit greatly.

The goal of this thesis is to determine the possible correlations that exist between the subsurface thermal structure and the temperature at the surface. Then, from these relationships and use of regression formulas, predicted vertical temperature profiles could be computed from an input of sea surface temperature alone.

II. OCEANOGRAPHIC CHARACTERISTICS OF THE NORTHEAST PACIFIC OCEAN

A. WIND SYSTEMS AND CURRENTS

The Northeast Pacific has been studied extensively for many years and it has revealed a complex arrangement of environmental conditions. Severe storms, high winds, varied water masses, numerous currents and unique temperature and salinity structures are a normal occurrence for the region.

In the winter the North Pacific is usually under the influence of the Aleutian Low in the atmosphere while for the summer months a high pressure system dominates (Uda, 1963). The distribution of the mean surface winds are controlled by these two systems. At the location of the now retired Ocean Weather Station "P" (OWS-P, positioned at 50N, 145W in the Gulf of Alaska) the prevailing winds are from the southwest (Tabata, 1965). From the influence of these wind patterns, the surface waters flow eastward across the Pacific Ocean in the vicinity of Station "P". This flow consists of the West Wind Drift and Subarctic Current which then diverge to form the southward flowing California Current and the northward flowing Alaskan Current (Tabata,

1978). Fig. 1 shows the location of Ocean Weather Station "P" and the major surface currents of the North Pacific.

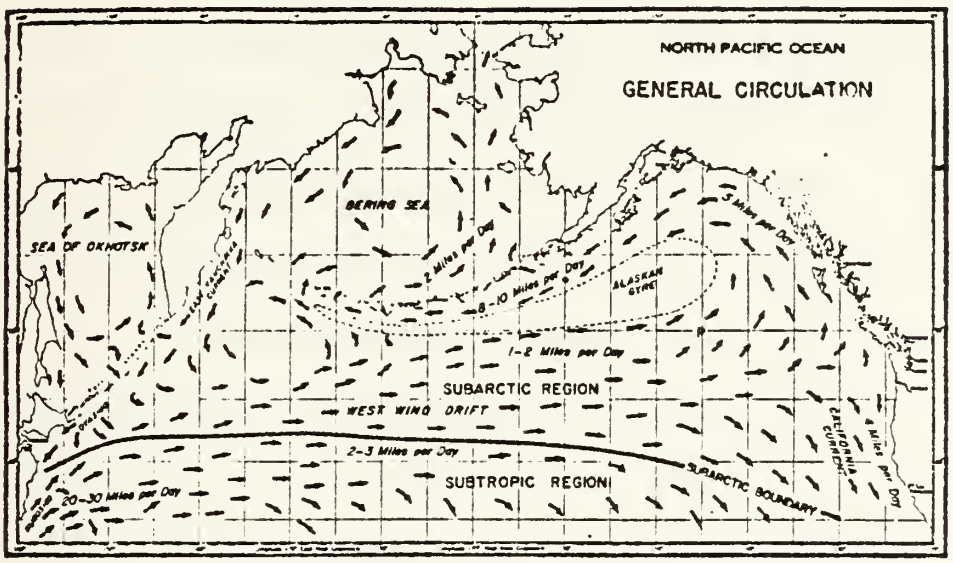

Figure 1. Location of OWS-P and North Pacific Ocean Surface Currents (From Tully, 1960).

B. WATER MASSES AND FRONTS

The Northeast Pacific can be divided into three major regions based upon their water characteristics. Near the vicinity of OWS-P and northward is the Subarctic Pacific Water Mass in which the upper 100-150 m layer is composed of cold and low-salinity water. To the south warm and highly saline water exists in the upper layers of the Subtropic Water Mass. In between and along the coast lies a region in which characteristics from both water masses are combined. This is known as the Transition Zone where there is a marked gradation of oceanographic properties from one region to another, with the boundaries separating these water masses having complicated thermohaline structures (Roden, 1970). The location of the Subarctic Front between the two water masses remains fairly constant, from 40N to 45N, and is largely dependent on the prevailing winds (Roden, 1975).

1. SUBARCTIC WATER MASS CHARACTERISTICS

The main feature of the vertical structure of oceanic properties is the existence of an upper zone, a halocline and a lower zone (Uda, 1963). The temperature, salinity and density profiles of these three zones for summer and winter are depicted in Fig. 2.

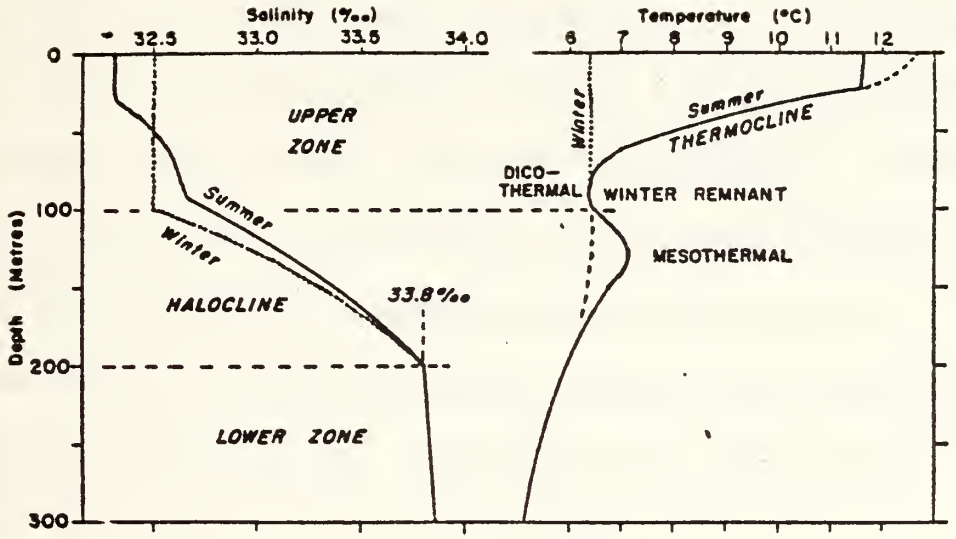

Figure 2. Characteristic Temperature and Salinity Profiles (From Tully, 1964).

The upper zone, which extends from the surface to a depth of about 100 m, generally has a low salinity level of less than 33 g/kg with the lowest values being closest to the coastal regions in the late spring (Uda, 1963). In the winter, the water in this zone is thoroughly mixed with all physical properties becoming homogeneous. During the summer, due to lighter surface winds, a shallow isohaline and isothermal layer exists from 10 to 30 m below the sea surface. Below this mixed layer is a strong negative thermocline with temperature decreasing as much as 8C in 20 m; in the same zone a small halocline extends above another near-isohaline layer to the bottom of the upper zone (Tabata, 1965).

Below the upper zone lies the main halocline which is permanent, as the salinity increases by as much as 1 g/kg from 100 to 200 m (Tabata, 1960). The temperature generally decreases with depth in this region, but at times a temperature inversion occurs to a depth of about 150 m. This positive temperature gradient is in a stable layer (density increases with depth) since it is located within the main halocline (Uda, 1963).

In the lower zone, below the halocline, the properties of the water change gradually with depth. Salinity increases slightly by about 0.6 g/kg in 1000 m while the temperature decreases to a value of approximately 2.8C at a depth of 1000 m (Tabata, 1965).

The variations of salinity are most pronounced in the upper zone and halocline and are less in the lower zone. The annual salinity variations in the upper zone are characterized by a decrease in the upper 30 m in the late summer or early fall with a maximum in late winter or early spring. These seasonal fluctuations result primarily from the evaporation and precipitation imbalances common to the region. Annual variation is similar at great depths, but lags the surface layers in time (Tabata, 1965).

At the surface, several features are observed in the salinity pattern. Basically, the trend of the surface isohalines appears to be east-west throughout the year with major changes occurring along the coast. Also, a permanent salinity maximum of about 33 g/kg exists near the center of the Gulf of Alaska, south of Kodiak Island. The salinity decreases southward to a minimum of about 32.6 g/kg in the vicinity of 50N and then increases further south into the Subtropical Water Mass (Uda, 1963).

The "three-zone" structure of the water column is characteristic of the deep ocean region of the Subarctic Domain. However, it does not always exist in near-coastal waters as current systems, coastal winds and fresh water runoff from land can modify the profiles. As shown in Figs. 3 and 4, this coastal regime primarily alters the upper zone. Along the western United States this domain exists out to about 130W. The lower zone also becomes affected by the proximity to land of the California Undercurrent (Dodimead et al., 1962).

2. SUBTROPIC WATER MASS CHARACTERISTICS

To the south of the Subarctic region is the Subtropic Water Mass which is basically warmer and more saline than the Subarctic Water. In the upper layer the high values of salinity (greater than 34 g/kg) due to higher evaporation decrease to a minimum at 200 to 600 m and are typical of the values throughout the year. Sea surface temperatures remain fairly constant with an isothermal upper zone averaging about 20 m in thickness below the sea surface, due to the prevailing winds. Below this zone exists a negative permanent thermocline reaching down to a depth of 500-600 m. Also, there is no characteristic halocline or major

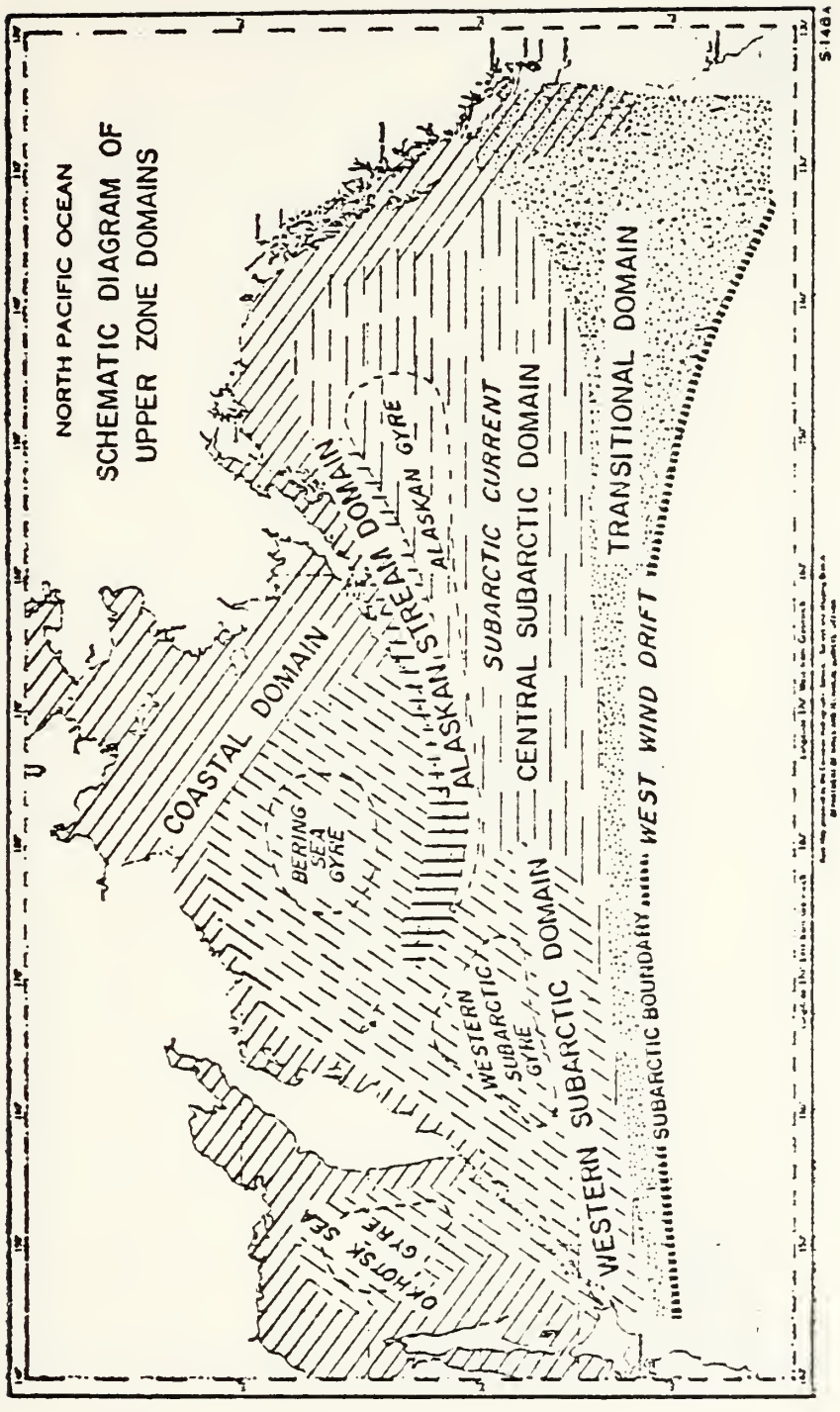

Figure 3. Upper Zone Domains (From Dodimead et al., 1962).

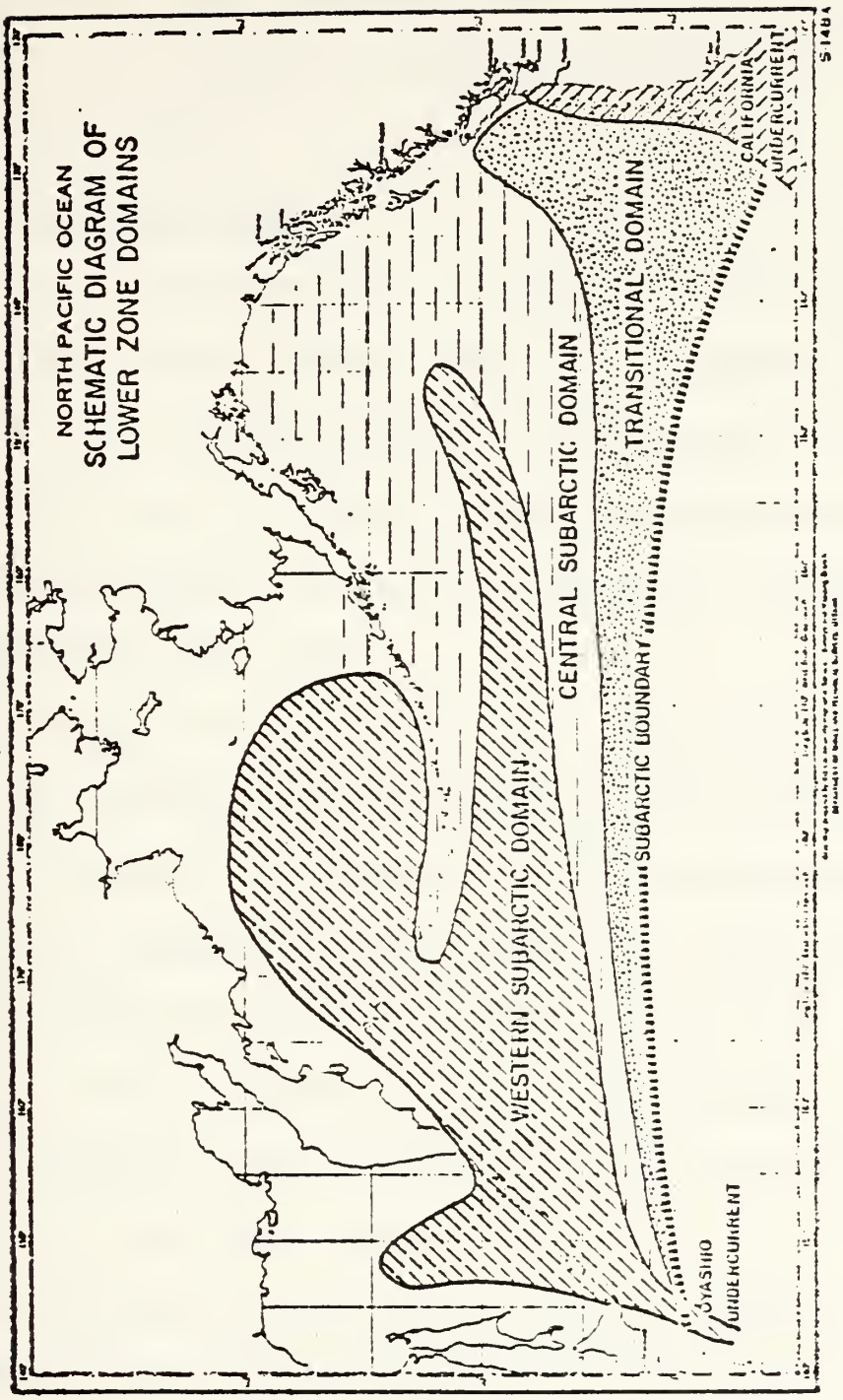

Figure 4. Lower Zone Domains (From Dodimead et al., 1962).

temperature inversion as there was in the water mass to the north (Tabata, 1965). The deep water structure is basically continuous and similar from the Subarctic to Subtropic regions (Uda, 1963).

3. TRANSITION ZONE

The Transition Zone, located in the central and eastern North Pacific between 45N and 35N, separates Subarctic Water from Subtropic Water. It consists of the mixed water originating in the warm, saline Kuroshio and the cold, low salinity Oyashio currents as they move eastward in the West Wind Drift (Uda, 1963).

The width of this zonal belt, which is about 2 to 4 degrees of latitude, and the strength of its boundaries, are primarily determined by the wind stress at the sea surface. The northern boundary is characterized by many temperature inversions and by the gradual disappearance of the Subarctic halocline. At the southern boundary the vertical structure becomes basically isohaline with a strong negative thermocline in the upper layer (Roden, 1970).

The Transition Zone is primarily a property of the upper ocean, as its characteristics fade below a few hundred meters. At the surface this region has a distinctive

meridional (N-S) temperature gradient of approximately 1.0C per 100km as it stretches eastward across the Pacific Ocean. The horizontal surface salinity pattern exhibits similar structure along a latitude band throughout the year with values increasing as much as 0.8 g/kg meridionally (Uda, 1963).

The upper layers are often characterized by temperature inversions which can occur because of the existence of the associated halocline. These inversions decrease in magnitude and slowly increase in depth toward lower latitudes.

The vertical distribution of properties at intermediate depths shows that the salinity becomes effectively isohaline, with a slight minimum developing below 300 m at the southern boundary (Uda, 1963).

4. DENSITY STRUCTURE AND THE SUBARCTIC FRONT

The density of sea water is calculated primarily from its temperature and salinity at depth. In the Subarctic waters, salinity governs the density structure. The seasonal variability illustrates some of the features that occur in the vertical profiles. In winter, basically isopycnal conditions are found throughout the upper zone as

temperature and salinity are well mixed. In summer, a minor pycnocline corresponding to the shallow thermocline is observed. However, a large and permanent pycnocline occurs along with the main halocline. In the lower zone, the density increases gradually with depth (Uda, 1963).

In Subtropic Water, the density is controlled by the temperature. Here the warm surface layer of about 10 to 30 m is isopycnal from the mixing of the prevailing winds. A permanent pycnocline exists at lower depths due to the thermocline in the region (Uda, 1963).

The Transition Region has a complex density structure as numerous minor density fronts occur at depth due to the temperature and salinity inversions.

The Subarctic Front in the eastern North Pacific is a narrow, meandering band located in the latitude range of 40N to 45N. This front has a unique structure in its lack of a density front in the upper 100 m. The strong horizontal temperature and salinity gradients are in almost complete balance. Below this upper layer a density front of moderate intensity slopes slightly to the south (Roden, 1975).

The mixed layer depth can strongly change across the Subarctic Front. To the north, the mixed layer extends to the top of the halocline at about 100 m. To the south, there is no halocline and, during the stormy, winter season, the mixed layer depth can extend to almost 300 m. In the summer months the seasonal thermocline controls the depth of the mixed layer and there is little difference across the Subarctic Front (Roden, 1975).

III. THERMAL STRUCTURE

A. THERMAL STRUCTURE IN THE NORTHEAST PACIFIC OCEAN

The interaction between the sea and atmosphere is the dominant process determining temperature structure in the upper layers. Below, temperature is a fairly constant property with the structure being determined by internal processes, such as advection and mixing.

Two heating cycles occur in the ocean: diurnal and seasonal. In the daily cycle the surface layer is heated during the daylight hours and cooled during the night. In the higher latitudes during the heating season, i.e., the middle six months of the year, a daily net heat gain occurs (Uda, 1963). Fig. 5 illustrates the annual cycle of heating and cooling and its relation to the thermal structure. In March, at the end of the cooling season, the waters are nearly isothermal to the top of the halocline located at about 100 m in depth. With the beginning of the heating season in April, the heat is accumulated as small temperature inversions are gradually mixed downward by light winds. During subsequent short periods of high winds these

transients are quickly eroded and a shallow isothermal surface layer results.

Below the surface layer, a sharp negative thermocline is formed between 30 and 60 m in a temperature transition layer adjacent to the deeper cold waters. From the end of the heating season until the waters are again nearly isothermal in March, the thermocline deepens to about 100 m.

In this ocean region, below the thermocline there is usually a cooler layer nearly 120 m in depth which is stable, since it occurs within the main halocline. Below the cooler layer there may be an increase in temperature with depth, an inversion. Temperature inversions can be classified into three types according to their method of formation and behavior. The first type, which is the most common in the eastern North Pacific, is a result of the seasonal cycle of heating and cooling. The upper layers in an extremely cold winter can become colder than the waters in the halocline below and a positive temperature gradient is formed. With the advent of the following heating season the temperature of the surface waters increase causing a (negative) thermocline to form above the positive thermal gradient. The temperature minimum thus generally is located

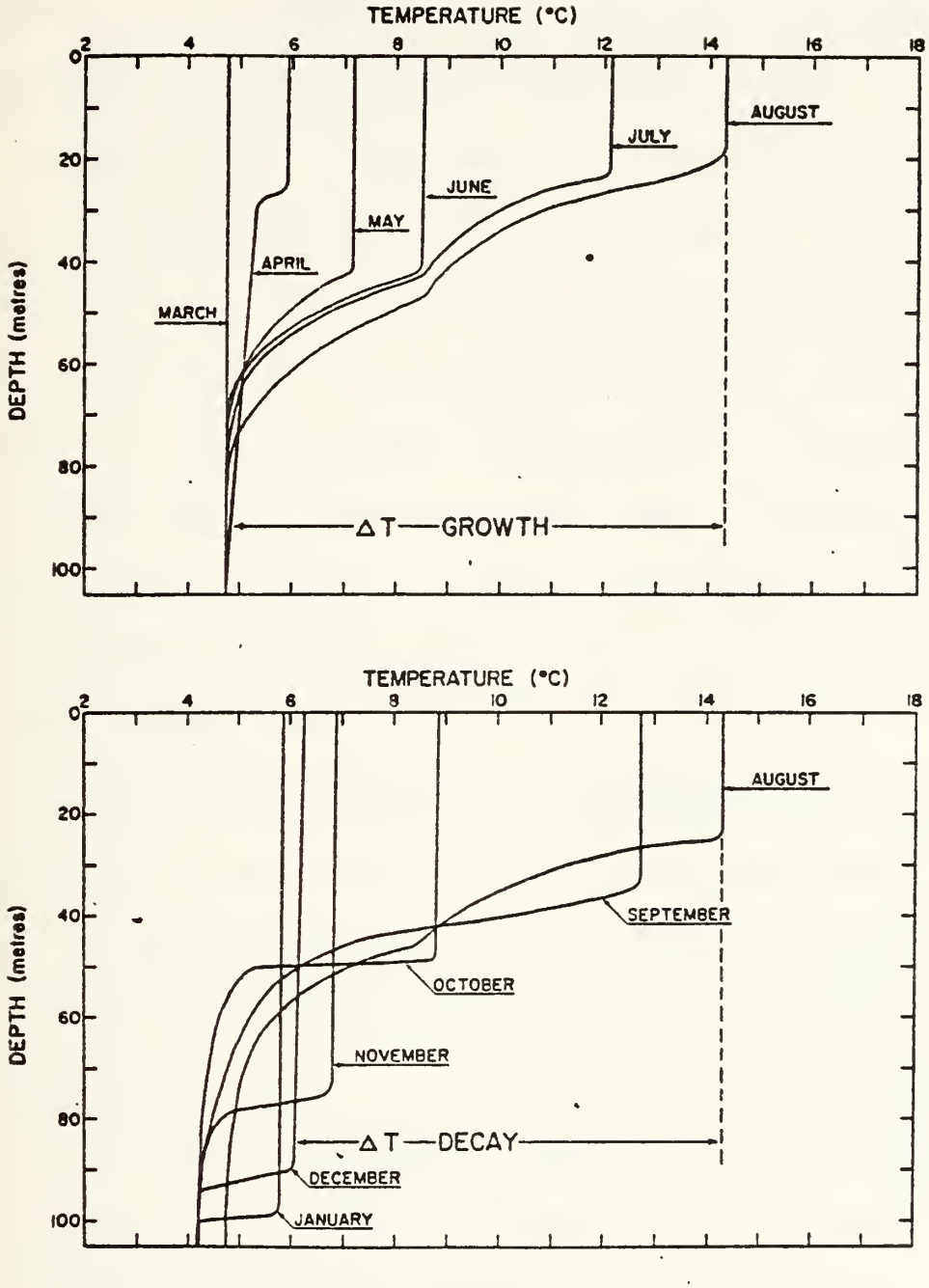

Figure 5. Growth and Decay of the Thermocline at Ocean Station "P" (From Tully and Giovando, 1963).

just above the halocline at 120 m and changes very little during the course of the summer heating period. During the follcwing winter season the upper thermocline decays and the temperature inversion may be erased (Uda, 1963).

Another prccess which can cause temperature inversions is the formation of sea-ice in the western Pacific. The remaining cold (-1C), high salinity surface layer sinks tc a level of stability in the existing halocline and is carried eastward in the West Wind Drift where it completely mixes with other waters before reaching 140W. Depending on the amount of heating of the surface layers during the transit, the temperature inversion may or may not persist throughcut the year (Eoden, 1964).

A third prccess results in a subsurface temperature maximum when the warm, more saline Subtropical Water intrudes under the colder Subarctic Waters. The advecting water then is slightly cccled and sinks; it remains warmer than the surrcundings, however, and forms the temperature maximum at depth. Its upper boundary is generally limited by the stability criterion of the main halocline (Uda, 1963).

As the cccling period begins in late September, the surface waters are cooled and mixed downward by convection as

well as by the strong winds of the fall and winter months. The seasonal thermocline sinks and narrows until it reaches the halocline. By late winter the upper zone has reached its minimum temperature of the year.

At depths below 500 m temperature variations are small, seldom exceeding standard deviations of 0.04C (Tabata, 1960). Fig. 6 shows the typical temperature structure at Ocean Station "P" for both summer and winter months.

B. INTERNAL WAVE EFFECTS ON THERMAL STRUCTURE

In many vertical temperature structure analyses, the depths of the isotherms fluctuate considerably. Periodicity and amplitude of the fluctuations appear non-systematic, but result from the superposition of a large number of internal wave trains. The limiting frequencies range from the Brunt-Väisälä to inertial; in the Subarctic Region, periods from 5 minutes to at least half a day have been observed. The vertical displacement of isotherms is of the order of 5 m at the top of the thermocline and perhaps as large as 25 m at the level of the principal halocline (Tully and Giovando, 1963).

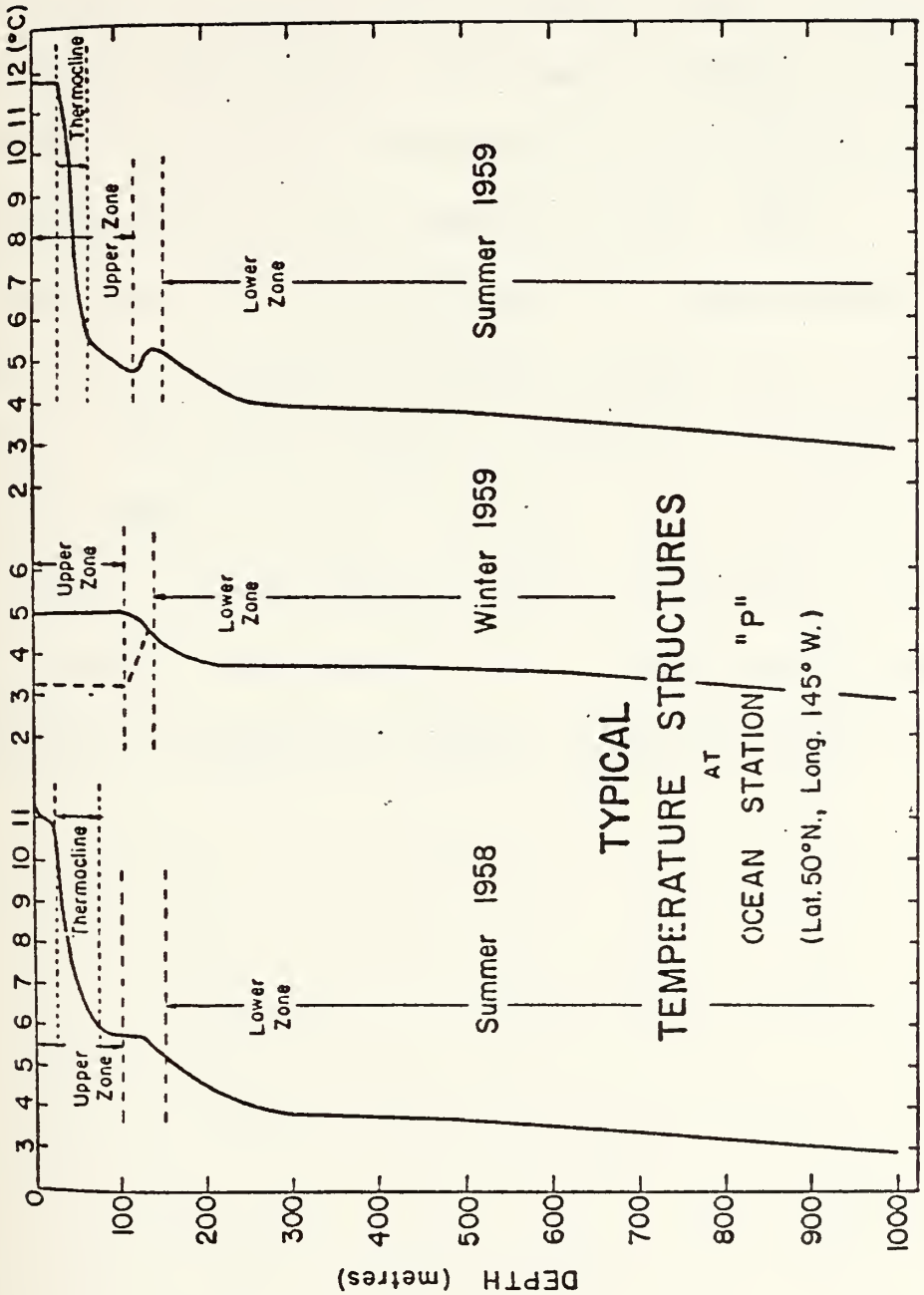

Figure 6. Typical Temperature Structures at Ocean Station "P" (From Tully and Giovando, 1963).

C. HORIZONTAL SURFACE THERMAL STRUCTURE

Near the center of the Gulf of Alaska is located an area of temperature minimum that coincides with the dynamic center of the Alaskan Gyre. In summer it roughly overlies the center of the gyre as determined by the salinity maximum, but in winter the two are separated (Uda, 1963).

South from the cold core dome to approximately 35N the thermal field is oriented zonally except near the coastal regions. This configuration continues year round with a seasonal range of 7.0C throughout the Transition Region (Uda, 1963). The horizontal thermal gradient in the north-south direction is strongest in the Transition Zone where gradients of 1C/100km are common, as shown in Fig. 7.

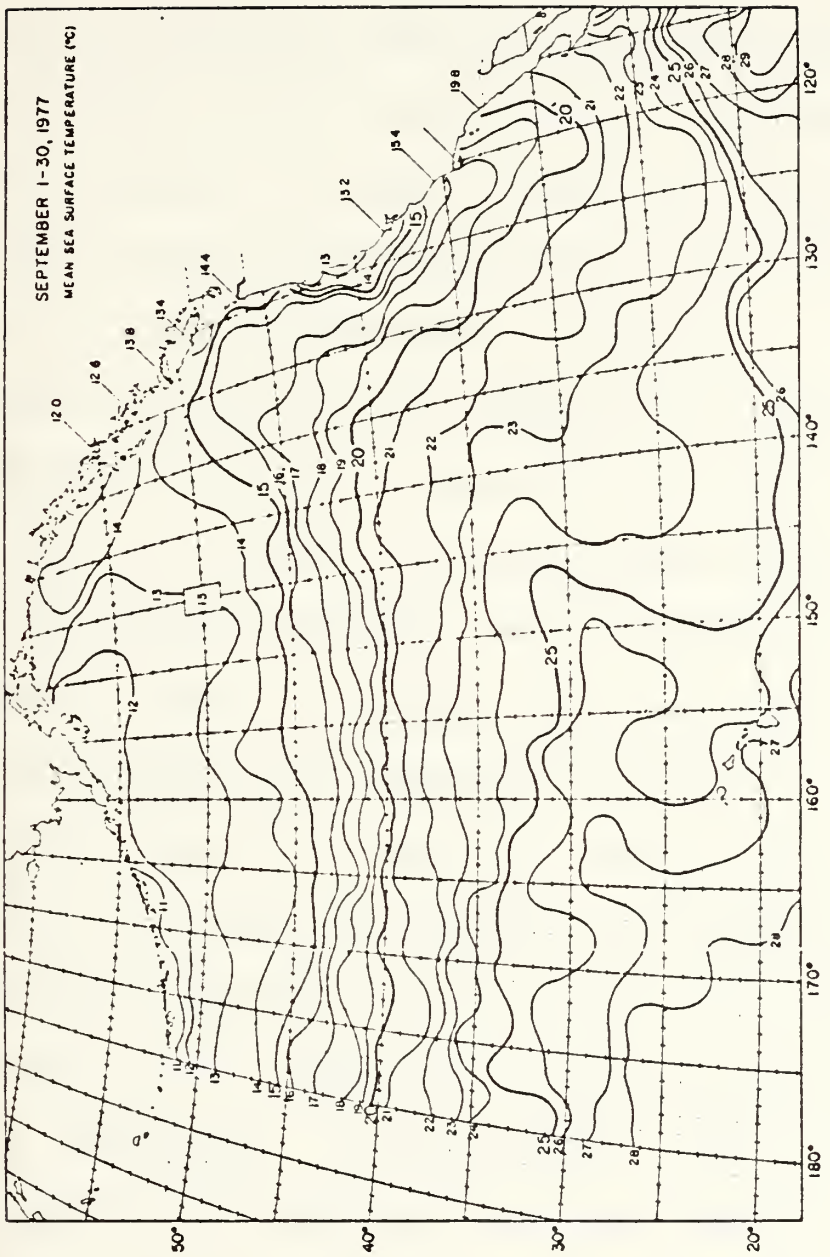

Figure 7. Surface Mean Temperature Structure For September 1977 (From Renner, 1977).

IV. EXPERIMENT

A. OBJECTIVE

For ocean monitoring from space to become effective, the interior motions of the oceans must be inferred from the resulting signature of surface properties. The ability to define the subsurface structure accurately by this method is becoming increasingly utilized and understood.

Legeckis and Gordon (1982) described the ability of satellite infrared imagery to locate sea surface temperature fronts, and the relation of these surface features to subsurface temperature structure. For the Brazil Current and two warm core eddies, they noted the mixed layer depth correlated with the surface temperature patterns.

Bernstein, Breaker and Whritner (1977) examined the eddy formations in the California Current from combined ship, air and satellite platforms and found that the sea surface temperature patterns conformed to subsurface warm and cold mesoscale variations. They concluded that in unstable regions such as the California Current, surface and main thermocline temperature distributions have relationships to each other. Thus, in such a region, remotely sensed sea

surface temperature patterns would be able to interpret subsurface circulation.

From these recent examples of satellite-determined subsurface structure and from other oceanographic literature, it appears that the regions of the world's oceans where large instabilities occur (i.e., boundary currents, coastal upwelling zones, etc.), the subsurface dynamic features are readily deduced from the surface observations. Areas of the seas which are quiescent and usually located in the central oceans have not been as easy to describe accurately. In these regions, the use of either dynamical or empirical methods could be the only means of forecasting the thermal structure of the oceans.

Numerical models are based on dynamical principles and will ultimately provide the basis for predicting oceanic processes. Empirical methods have been determined in the past for certain regions and for limited time periods, but do not appear to be valid universally. If relationships could be devised for certain water masses or oceanic regimes, then the possibility exists of piecing together the subsurface thermal features in the different regions by utilizing remote sensing to define certain surface measurements.

Toward this goal, the first objective of this thesis is to determine what particular relationships exist between sea surface temperature and subsurface thermal structure for a relatively "quiet" region in the northeast Pacific Ocean. By examining the climatology, an empirical set of equations could then be derived between sea surface temperature, mixed layer depth, thermocline gradient and the depths of prominent points within the structure.

The second objective is to produce a predicted vertical temperature profile from the best fit regression equations for a particular water region and SST at a future time and different location. When these profiles are compared to actual temperature-depth profiles, accuracy of this statistical method will be determined.

B. DATA ACQUISITION

During the period 5 to 14 September 1977, the U.S. Naval oceanographic survey vessel USNS SILAS BENT conducted oceanographic surveys to determine the thermohaline and sound velocity structures across the California Current, the Transition Zone and Subtropical Water. For this thesis, the only data utilized were along a 1155 km meridional track south of Ocean Weather Station "P", as displayed in Fig. 8.

The data consisted of 28 vertical temperature profiles spaced approximately 42 km apart; they spanned the period 9 to 11 September 1977.

Weather conditions during this period were governed by a weak staticnary low pressure system with mostly low cloud cover and pericds of light drizzle and showers. The wind speed varied from 5 to 20 knots from several directicns causing wave heights of approximately 3 to 6 m along the entire track (FNOC, 1977).

Expendable bathythermographs (XBT's) were used to define the thermal structure. The resulting temperature traces plotted cnboard ship were coded on bathythermograph log sheets, which were utilized as the data points for reconstruction cf the thermal profiles. Characteristic of this procedure is the loss of the fine thermal structure, as only prominent points cn the temperature profile are recorded to give the general shape and location of important features.

Another prcblem associated with this method of data acquisition is the varying probability that the observer on the vessel at the time of the XBT drop correctly chose the proper points to reflect adequately the mixed layer depth, thermocline gradient and temperature inversions. Incorrect

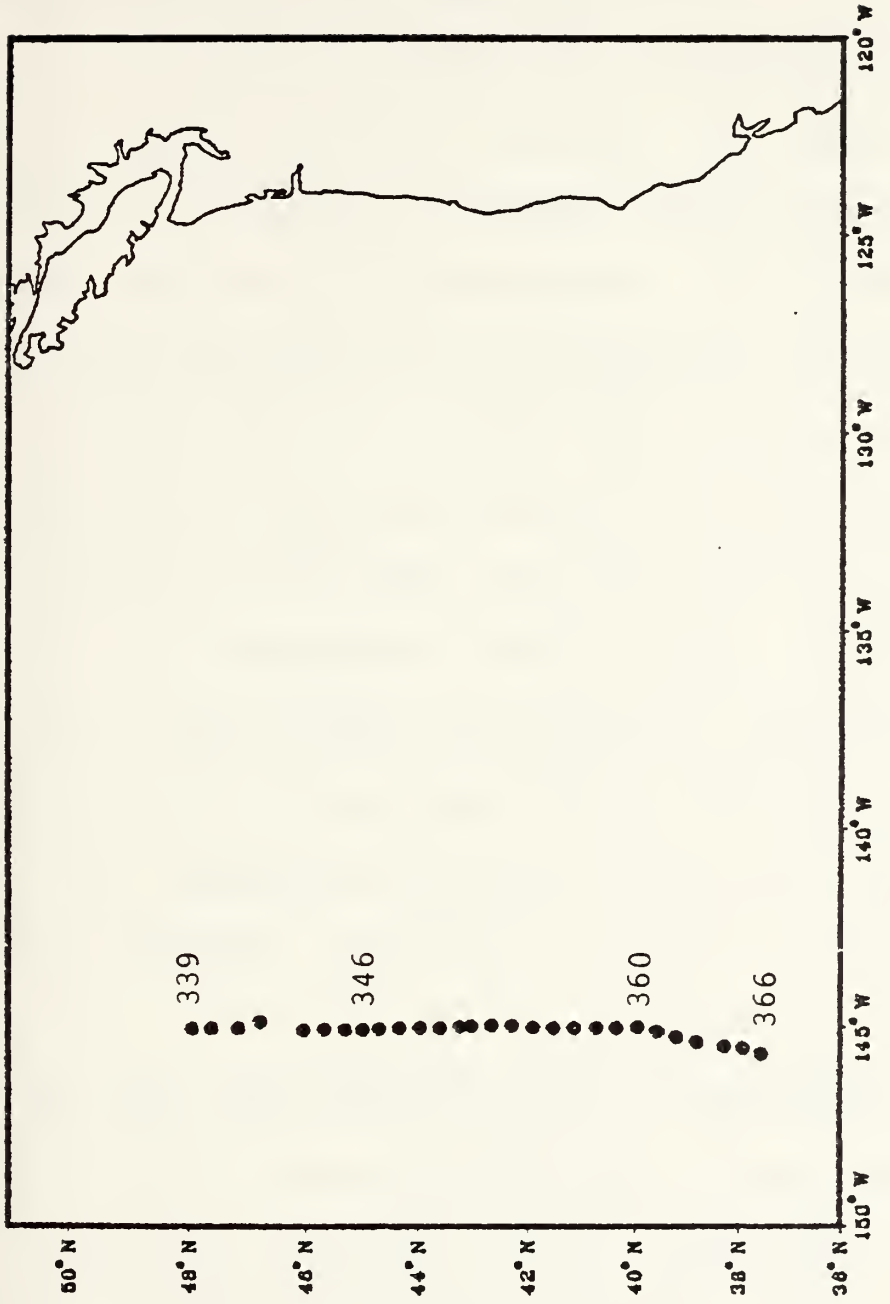

Figure 8. Location of XBT DATA During 8-11 September 1977.

recording of the values along with malfunctioning in 5 to 10% of the XBTs can also be a source of potential error.

C. ASSESSMENT OF TEMPERATURE STRUCTURE

To begin the analysis of subsurface thermal structure, realizing the "crude" nature of the data, the temperature-depth points were plotted on a computer graphics system and the 28 thermal profiles were reconstructed. From these profiles a vertical cross-section of the meridional temperature structure was drawn, Fig. 9. It was noted immediately that numerous temperature inversions existed along the northern and central regions of the track, but they ceased at approximately 41N. This subsurface border clearly defines the Subarctic Front which divides the Subarctic from Subtropic Waters; while at the surface there is no indication of the division. The temperature inversions varied in strength, but generally showed an increase in depth in a southward direction.

The upper mixed layer displayed little variability with few transients found within the structure. There were no large eddies noted in the surface layer and the mixed layer depth appeared relatively constant along the entire track. Weak mesoscale features are probably present, but the

Figure 9. Meridional Cross-section of Temperature at 145W.

spatial resolution prohibits their detection. The thermocline was also fairly constant in depth with the strongest gradients between 30 to 60 m. The isotherms in the lower layers characteristically deepened to the south, with several areas of large variability located near the temperature inversions. The large warm intrusion located at 47N may be caused by errors in the data, as a structure this size in the Subarctic Region does not appear to be congruent with the other features, and is not mentioned in the research literature.

To assess further the vertical thermal structure, prominent points, gradients and zones were defined on a typical temperature profile from the test region. Fig. 10 illustrates the variables that were used to analyze statistically the thermal profile. Descriptions of these variables are:

- SST - Sea surface temperature was defined as the surface temperature reported on the bathythermograph logs. Since this is the temperature recorded on the XBT trace when the XBT probe entered the water, a slight disparity from remotely-sensed SST may occur due to the response time of the XBT system.

- MLD - Mixed layer depth was visually determined as the greatest depth where the isothermal or slightly negative temperature gradient in the surface layer changed to the stronger gradient of the underlying thermocline.

- BOT - Bottom of seasonal thermocline was visually determined as the depth where the seasonal thermocline markedly changes into a weaker negative temperature gradient below.

- TBOT - Temperature at the bottom of the seasonal thermocline.

- DT - Difference in temperature between the temperature at the mixed layer depth and at the bottom of seasonal thermocline.

- DZ - Difference in depth between the mixed layer depth and bottom of seasonal thermocline.

- BUZ - Depth of the bottom of the main thermocline was visually determined as the depth where the thermocline changes to an isothermal or positive temperature gradient just above the temperature inversion region.

- TBUZ - Temperature at the bottom of the main thermocline.

- DTBUZ - Difference in temperature between the temperature at the mixed layer depth and at the bottom of main thermocline.

- DZBUZ - Difference in depth between the mixed layer depth and the bottom of main thermocline.

- T460 - Temperature at reference depth of 460 m which was selected arbitrarily at maximum depth of XBT reports.

- DT5 - Temperature change in upper 5 m of thermocline below the mixed layer depth.

- DT15 - Temperature change in upper 15 m of thermocline below the mixed layer depth.

- DT50 - Temperature change in upper 50 m of thermocline below the mixed layer depth.

- DT100 - Temperature change in upper 100 m of thermocline below the mixed layer depth.

- DIS - Distance from northern most XBT drop.

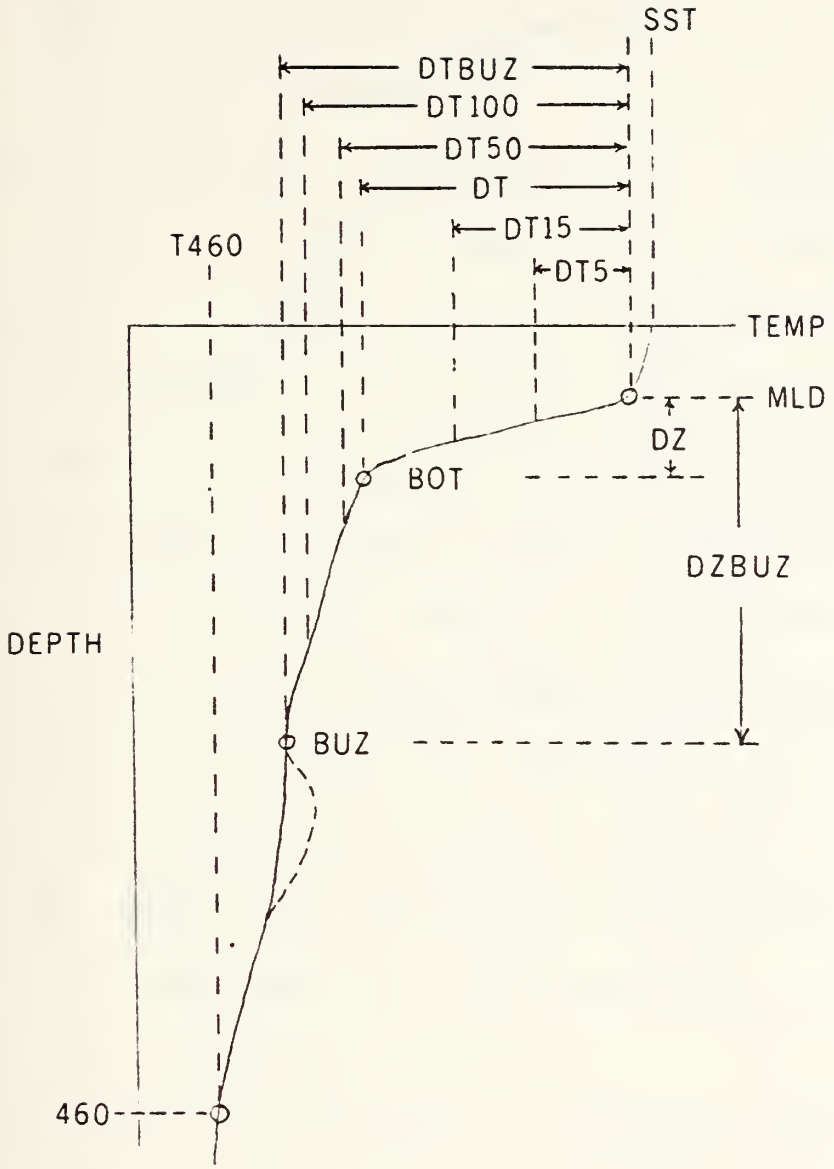

Figure 10. Model of Vertical Temperature Structure.

This assessment defines the general structure primarily in the upper layers above the permanent halocline. The detail of the smaller structure such as transients in the mixed layer and multiple thermoclines are not included because they are variable and minor with respect to the principal structure. The temperature inversion feature below the main thermocline was not characterized as its occurrence in the region varies in location and intensity during the test period. In those zones within the Subarctic Region where a sub-thermocline temperature maximum exists permanently during the heating season, additional variables should be used to define this part of the thermal profile.

Initially, the sea surface temperature gradient was used as a variable in the analysis. However, problems occurred in computing consistent gradients along the track as the calculated values were unrealistic and inaccurate compared with actual conditions at the time; this variable was dropped from this study.

These varibles provided the statistical base from which all correlations and regression equations were derived. The values could then distinguish the fluctuating and transient features from the median thermal structure. Tables I, II

and III list the values from the analyzed thermal profiles by XBT drop number.

TABLE I

Locations and Times of XBT Measurements

XBT	DATE/TIME(Z)	LAT(N)	LONG(W)	DISTANCE(km)
339	090613 SEP 77	47.98	144.98	0
340	090804 SEP 77	47.65	144.98	36
341	091003 SEP 77	47.20	144.98	86
342	091200 SEP 77	46.82	144.82	128
343	091800 SEP 77	46.07	145.05	212
344	092000 SEP 77	45.70	145.04	253
345	092205 SEP 77	45.33	145.04	294
346	100000 SEP 77	45.02	145.04	329
347	100308 SEP 77	44.73	145.00	361
348	100508 SEP 77	44.37	144.98	401
349	100708 SEP 77	44.00	144.98	442
350	100904 SEP 77	43.63	144.98	483
351	101100 SEP 77	43.28	144.97	522
352	101400 SEP 77	43.07	144.95	546
353	101600 SEP 77	42.70	144.93	587
354	101800 SEP 77	42.32	144.95	629
355	102000 SEP 77	41.93	144.98	672
356	110002 SEP 77	41.55	145.00	714
357	110203 SEP 77	41.17	145.00	757
358	110406 SEP 77	40.75	145.00	803
359	110604 SEP 77	40.37	145.00	846
360	111000 SEP 77	39.97	144.98	890
361	111200 SEP 77	39.60	145.10	931
362	111400 SEP 77	39.22	145.25	973
363	111600 SEP 77	38.83	145.37	1017
364	112304 SEP 77	38.30	145.47	1076
365	120107 SEP 77	37.93	145.53	1117
366	120307 SEP 77	37.58	145.67	1156

TABLE II

Values of SST, MLD, Thermocline Gradients and T460

XBT	SST (c)	MLD (m)	DT5 (c)	DT15 (c)	DT50 (c)	DT100 (c)	T460 (c)
339	13.4	-33	1.5	4.6	7.1	6.6	4.0
340	13.6	-24	0.3	1.5	6.6	7.4	4.1
341	14.1	-25	2.5	4.3	6.0	6.2	5.0
342	14.4	-25	2.3	5.6	7.1	7.6	4.2
343	15.1	-19	2.4	4.8	7.3	8.1	4.6
344	15.3	-32	0.3	4.6	7.7	7.4	4.9
345	15.6	-29	3.1	4.9	7.3	7.9	6.2
346	15.7	-19	0.4	4.7	6.7	7.9	4.7
347	16.6	-27	0.2	4.8	7.9	9.1	4.7
348	16.2	-20	0.5	4.7	7.4	8.4	4.8
349	17.0	-21	0.4	5.3	8.0	8.5	4.9
350	18.1	-20	0.2	6.2	9.1	10.3	4.9
351	18.3	-30	3.6	4.2	7.8	10.2	5.0
352	18.1	-20	0.3	5.8	8.4	8.7	5.1
353	18.4	-20	0.7	4.0	9.0	9.9	5.0
354	18.1	-20	0.6	5.4	8.6	9.3	5.2
355	19.3	-21	0.6	5.4	9.3	10.3	5.3
356	19.7	-15	0.2	6.9	9.6	10.8	5.3
357	19.5	-23	0.6	6.4	9.7	10.7	5.3
358	20.1	-16	0.3	2.1	9.4	10.3	5.6
359	20.3	-22	0.8	7.0	10.0	10.8	5.6
360	20.1	-16	0.5	2.6	8.3	10.3	5.9
361	20.5	-30	2.4	6.1	9.3	10.4	5.5
362	21.5	-22	0.3	5.7	10.5	11.6	5.8
363	21.4	-32	3.8	6.4	9.8	11.4	5.8
364	22.5	-27	0.4	6.2	9.8	11.1	6.5
365	22.3	-22	0.4	5.6	7.6	9.6	6.9
366	22.7	-20	3.3	5.2	8.1	10.4	6.8

TABLE III

Values of Thermocline Temperatures and Depths

XBT	EOT (m)	TECT (C)	DT (c)	IZ (m)	BUZ (m)	TBUZ (c)	DTBUZ (c)	DZBUZ (m)
339	-88	5.4	7.4	55	-95	5.3	7.2	62
340	-80	6.5	6.8	56	-109	5.9	7.4	85
341	-70	7.8	5.9	45	-110	7.4	6.3	85
342	-79	6.6	7.2	54	-128	6.2	7.6	103
343	-81	6.6	8.0	62	-138	6.5	8.1	119
344	-81	7.1	7.7	49	-112	6.7	8.1	80
345	-68	7.8	7.1	39	-112	7.0	7.9	83
346	-57	8.4	6.8	38	-100	7.3	7.9	81
347	-68	8.6	7.8	41	-114	7.3	9.1	87
348	-65	8.4	7.3	45	-143	7.6	8.1	128
349	-50	9.1	7.5	29	-109	8.1	8.5	88
350	-56	8.8	9.0	36	-123	7.5	10.3	103
351	-57	10.7	7.0	27	-148	7.2	10.5	118
352	-73	9.0	8.5	53	-158	7.8	9.7	138
353	-67	9.4	8.8	47	-132	7.7	10.5	112
354	-63	9.3	8.6	43	-120	8.6	9.3	100
355	-59	9.9	9.1	38	-130	8.6	10.4	109
356	-54	9.9	9.5	39	-134	8.5	10.9	119
357	-62	10.1	9.1	39	-127	8.4	10.8	104
358	-50	11.3	8.6	34	-120	9.3	10.6	104
359	-53	10.8	9.4	31	-95	9.4	10.8	73
360	-78	10.5	9.5	62	-180	9.3	10.7	164
361	-99	9.5	10.2	69	-127	9.3	10.4	97
362	-68	11.0	10.4	46	-157	9.4	12.0	135
363	-100	10.2	11.0	68	-155	9.7	11.5	123
364	-91	12.2	10.0	64	-173	10.5	11.7	144
365	-100	12.5	9.3	78	-196	10.7	11.3	174
366	-100	12.2	10.2	80	-188	10.7	11.7	168

To examine the variations and trends of the individual thermal profile features along the track, graphs of the variables as related to distance and latitude are plotted in Appendix A. These diagrams illustrate some of the concepts that were discussed in previous chapters pertaining to the variability in thermal structure within a particular region.

The sea surface temperature over the entire track as shown in Fig. A.1 increases linearly to the south where the mean gradient was 0.8C/100km. The strongest gradient occurred in the vicinity of 44N and reached a value of 2.3C/100km. Fig. 11 shows the sea surface temperature in the North Pacific as compiled from ship reports and climatology by Fleet Numerical Oceanography Center for 10 September 1977. In the region of data acquisition, the meridional temperature gradient and surface isotherm structure closely compare to the surface temperature versus distance plot (Fig. A.1). Satellite infrared imagery during this time period was obstructed due to the thick cloud cover over the area; therefore, this method of sea surface temperature determination was not used as was desired (Tabata and Kimber, 1979).

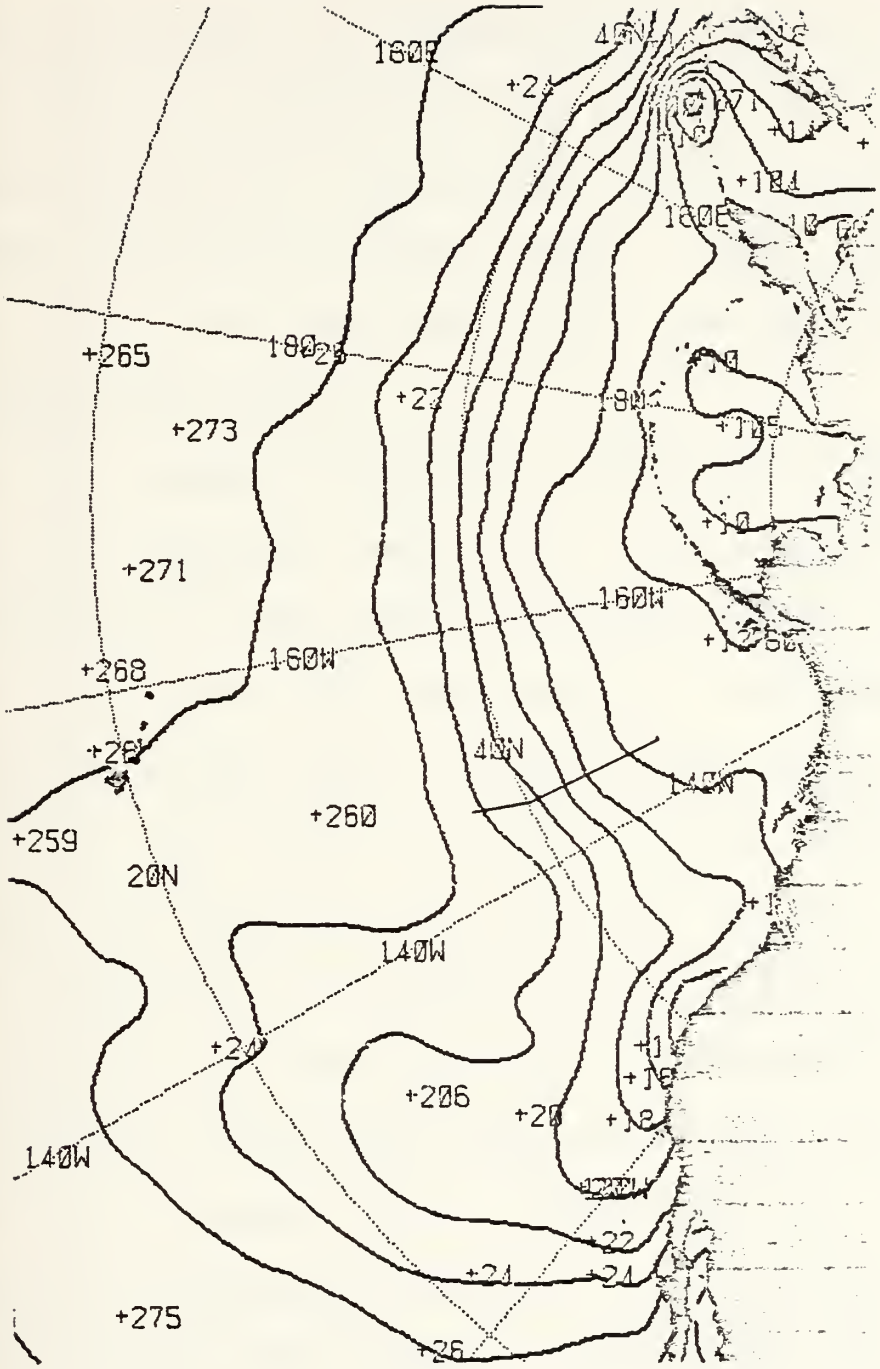

Figure 11. Pacific Ocean Sea Surface Temperature on 10 September 1977 (Fleet Numerical Oceanography Center, 1977).

Fig. A.2 shows the depth of the mixed layer along the track. The mean depth was -22.9 m with a maximum and minimum depth of -32 and -15 m, respectively. The layer's general trend of a slight shallowing by about 5 m in the southward direction is observed until 40N is reached where the trend reverses and becomes deeper. This location of change in the mixed layer depth trend accurately coincides with the Subarctic Front.

The four thermocline gradient variables in Figs. A.3 through A.6 displayed a measurable trend along the track. The variability of the temperature change in the upper 5 m of the thermocline (DT5) was large in the northern and southern ends of the track. In the center, with the exception of one data point, a mean value of 0.3C/5m was observed. The boundaries of these three zones of the DT5 variable agreed with the division of the track into the three regions, i.e., Subarctic Water, Transitional Zone and Subtropic Water. This effect was noted in many of the thermal structure variable plots. DT15, DT50 and DT100 all increased with decreasing latitude, but the general trends differed between each variable. DT15 showed the largest range of variability with only a slight increase in

temperature gradient, while DT50 and DT100 both increased at a greater rate. When plotted collectively, as shown in Fig. 12, the relationships become apparent. Generally, with increasing sea surface temperature, the negative temperature gradient of the thermocline increases slowly at a relatively constant rate.

Two other depth-dependent variables on the vertical temperature profile, besides the mixed layer depth, are the bottom of the seasonal and main thermoclines, BOT and BUZ, respectively. Figs. A.7 and A.11 display these variables as they vary with latitude. The variability of the plots may be due in part to internal waves with typical amplitudes of 15 m for the BOT and 30 m for the BUZ.

The BOT's general trend southward along the track to about 40N showed a slight decrease in depth from -80 to -60 m. Again, this location coincides with the Subarctic Front as did the MLD. The BOT then increases sharply as the trend reverses to a depth of -90 m.

For the BUZ, the trend is just the opposite of the BOT in the Subarctic Water and Transitional Zone. The depth of the bottom of the main thermocline increases slowly until reaching the Subarctic Front, where the maximum variation in

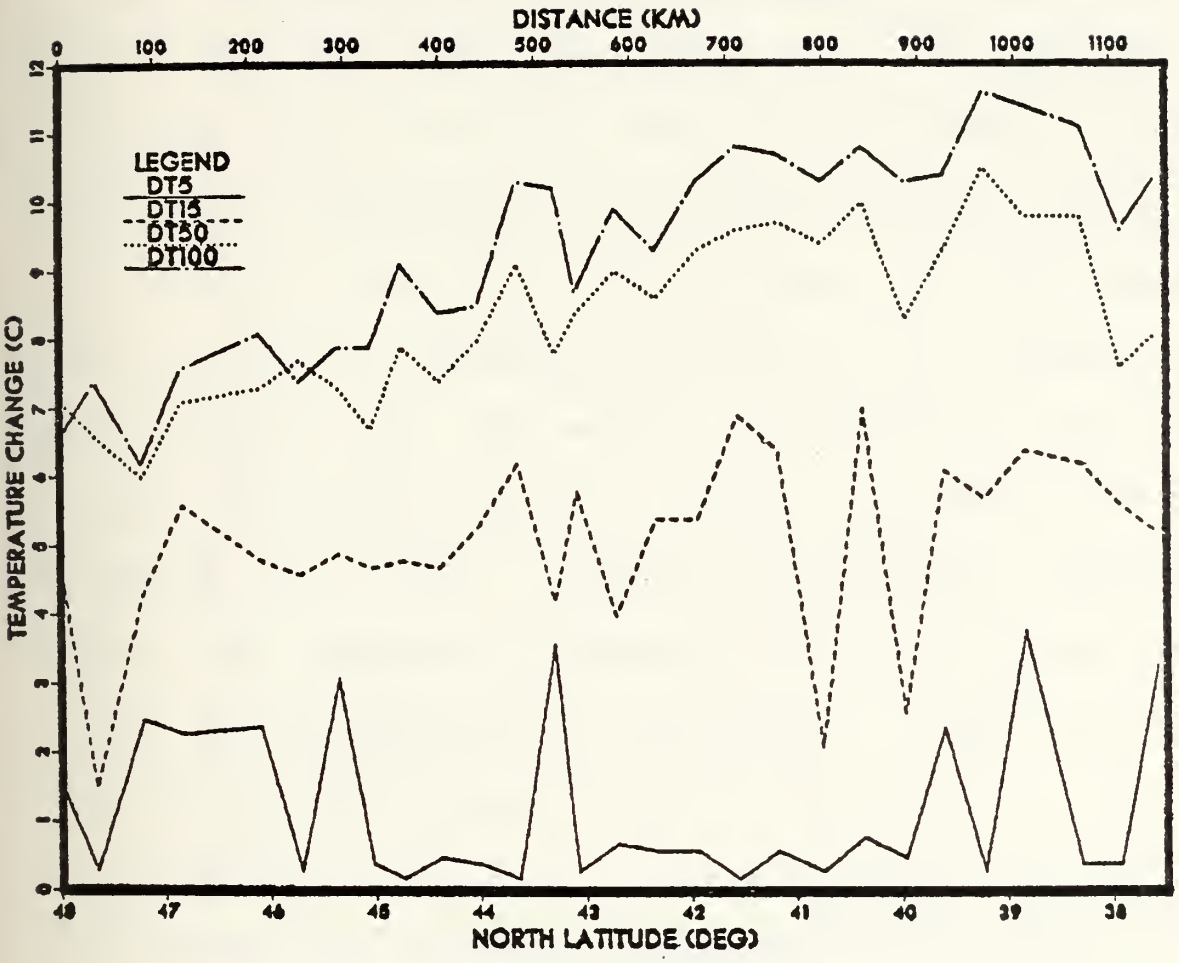

Figure 12. Comparison of DT5, DT15, DT50 and DT100 Versus Latitude.

depth is approximately 85 m. In Subtropic Water, the trend of the BUZ increases in depth at a greater rate along the southern end of the track.

When the MLD, BOT and BUZ are plotted together, as shown in Fig. 13, additional relationships appear. In the Subarctic and Transition Regions, north of 40N, the thickness of the upper layers above the bottom of the seasonal thermocline (BOT) decreased in a southward direction. With the MLD trend at a relatively constant depth, the only thermal layer to change in magnitude appreciably is the thermocline. This suggests that the seasonal thermocline, with its negative temperature gradient, becomes stronger as the SST increases and as the thermocline thickness decreases. Indeed, the temperature difference (DT) and thickness (DZ) of the seasonal thermocline displayed in Figs. A.9 and A.10, respectively, agree with this suggestion.

As previously mentioned, the depth of the bottom of the main thermocline gradually deepens toward the south along the track. Figs. A.13 and A.14 show the increasing difference in temperature and depth from the mixed layer depth, DTBUZ and DZBUZ, respectively. These tendencies, in conjunction with the trend of the BOT, indicate that the

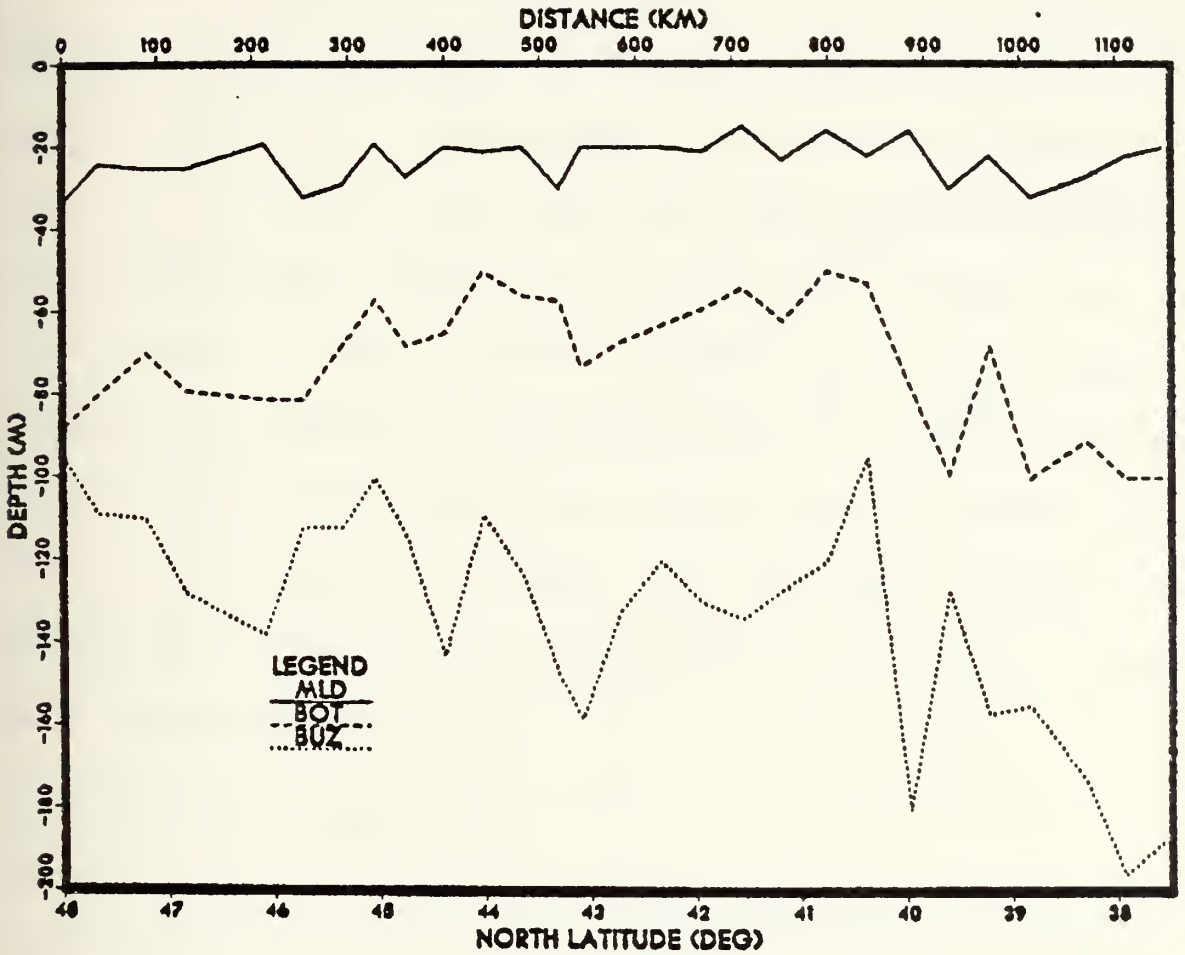

Figure 13. Comparison of MLD, BCT and BUZ Versus Latitude.

negative temperature gradient at the lower part of the main thermocline becomes weaker and thicker toward the south in the Subarctic and Transitional Regions.

For Subtropical Water, south of 40N, the BOT has reversed its trend at the Subarctic Front and increases in depth. The BUZ continues to deepen, but at a greater rate than to the north. Temperatures at these two locations on the thermal profile, TBOT and TBUZ, slowly increase linearly with decreasing latitude at nearly the same rate of 0.5C/100km. These values suggest that the negative temperature gradient at the lower part of the main thermocline continues to weaken and thicken, but at a deeper depth than in the northern waters. At the upper layers, the parameters of the seasonal thermocline, DT and DZ, increase with increasing SST.

D. STATISTICAL PROCEDURE

To predict the subsurface thermal structure from a given sea surface temperature, a statistical approach was utilized to determine the relationships between the thermal structure variables. The data analysis was done using the BIOMED statistical computer programs on the Naval Postgraduate School's IBM 3033 computer system. Details of the BIOMED

computer programs used in the analysis are provided in Appendix E. Basic statistics (mean and standard deviations), scatter diagrams, correlation and linear regression analysis were performed on all variables.

As part of the regression analysis, the correlation coefficients for all combinations of pairs of the sixteen variables were computed. These simple correlations are an estimate of the strength of the linear association between two variables and do not imply the cause for the relationship or which variables affect the variation of the other.

Scatter diagrams were used in conjunction with the regression analysis to assist in refining the correlations between variables. By visually removing poor data points that detracted from trends within specific regions, the analysis could be improved. After determining the best fit correlations, least square linear regression equations are computed between variables and also with sea surface temperature as the independent variable. This enabled a vertical temperature profile to be determined by calculating the values for the variables with the only input being the sea surface temperature.

The values of the 16 thermal structure variables from the 28 temperature profiles along the track were correlated for all combinations with the results shown in Table IV. Several strong relationships appear with the correlation coefficients of a few variables being greater than 0.750.

The sea surface temperature had the greatest number of strong correlations which greatly enhances the idea of prediction of the thermal profile from the SST. The highest correlation coefficient (0.993) occurred when the SST was compared with the distance along the track. This was expected due to the relatively constant north-south surface temperature gradient in this region of the Northeast Pacific.

Other strong correlations with the sea surface temperature were the temperatures at the bottom of the seasonal and main thermocline, TBOT (0.944) and TBUZ (0.949), respectively. When plotted together, as shown in Fig. 14, the trends clearly appear. The variables' similar relationships imply that the entire vertical temperature profile "leans" toward warmer temperatures as the small negative thermal gradient in the deeper layers increase with increasing sea surface temperature. The change in temperature in

TABLE IV

Correlation Coefficients of Thermal Variables

MLD	MLD														
SST	.224	SST													
DT5	-.484	-.028	DT5												
DT15	-.121	.385	.080	DT15											
DT50	.157	.770	-.211	.485	DT50										
DT100	.235	.905	-.065	.393	.902	DT100									
DT	.128	.835	-.026	.466	.843	.867	DT								
DZ	-.156	.305	.280	.018	-.082	.050	.425	DZ							
BOT	.459	-.203	-.406	-.055	.124	.030	-.341	-.949	BOT						
TBOT	.296	.944	-.065	.251	.632	.822	.688	.150	-.041	TBOT					
BUZ	-.202	-.682	-.124	-.098	-.239	-.496	-.566	-.643	.514	-.653	BUZ				
TBUZ	.267	.949	-.035	.334	.630	.770	.792	.355	-.234	.932	-.654	TBUZ			
DTBUZ	.217	.960	-.068	.368	.842	.961	.891	.204	-.114	.885	-.638	.830	DTBUZ		
DZBUZ	.374	.678	-.031	.068	.246	.505	.551	.578	.401	.665	-.983	.661	.634	DZBUZ	
DIS	.217	.993	-.012	.365	.738	.878	.885	.356	-.251	.931	-.688	.963	.934	.684	DIS
T460	.114	.831	.139	.265	.435	.569	.644	.405	-.318	.835	-.686	.832	.706	.663	.846
MEAN	-23.2	18.1	1.2	5.0	8.3	9.3	8.5	48.8	-72.0	9.3	-133.3	8.1	9.6	110.2	580.9
STD DEV	5.1	2.8	1.2	1.3	1.2	1.5	1.3	14.3	15.9	1.8	27.4	1.4	1.6	28.9	343.6

the upper 50 and 100 m of the thermocline also displayed strong direct relationships with the SST.

Two pairs of variables which exhibited strong negative correlations, and for similar reasons, were BOT-DZ (-0.949) and BUZ-DZBUZ (-0.983). These combinations indicate that a relationship exists between both the BOT and BUZ and the MLD. This is due to the relatively small variations in the mixed layer depth when compared to the large fluctuations of the BOT and BUZ. Therefore, as the bottom of the seasonal and main thermoclines varied, the depth difference between these variables and the MLD similarly changed. This could provide an important link in determining the mixed layer depth if a viable connection could be established between the BOT or BUZ and SST. However, according to the correlation coefficients comparing the SST to MLD (0.224), to BOT (-0.203) and to BUZ (-0.682), the strength of these relationships was weak as shown in Figs. 15, 16, and 17. Correlations of the other variables with the mixed layer depth revealed little as to possible methods to determine this important thermal structure variable.

Due to the noticeable differences in thermal structure characteristics among the various regions encountered along

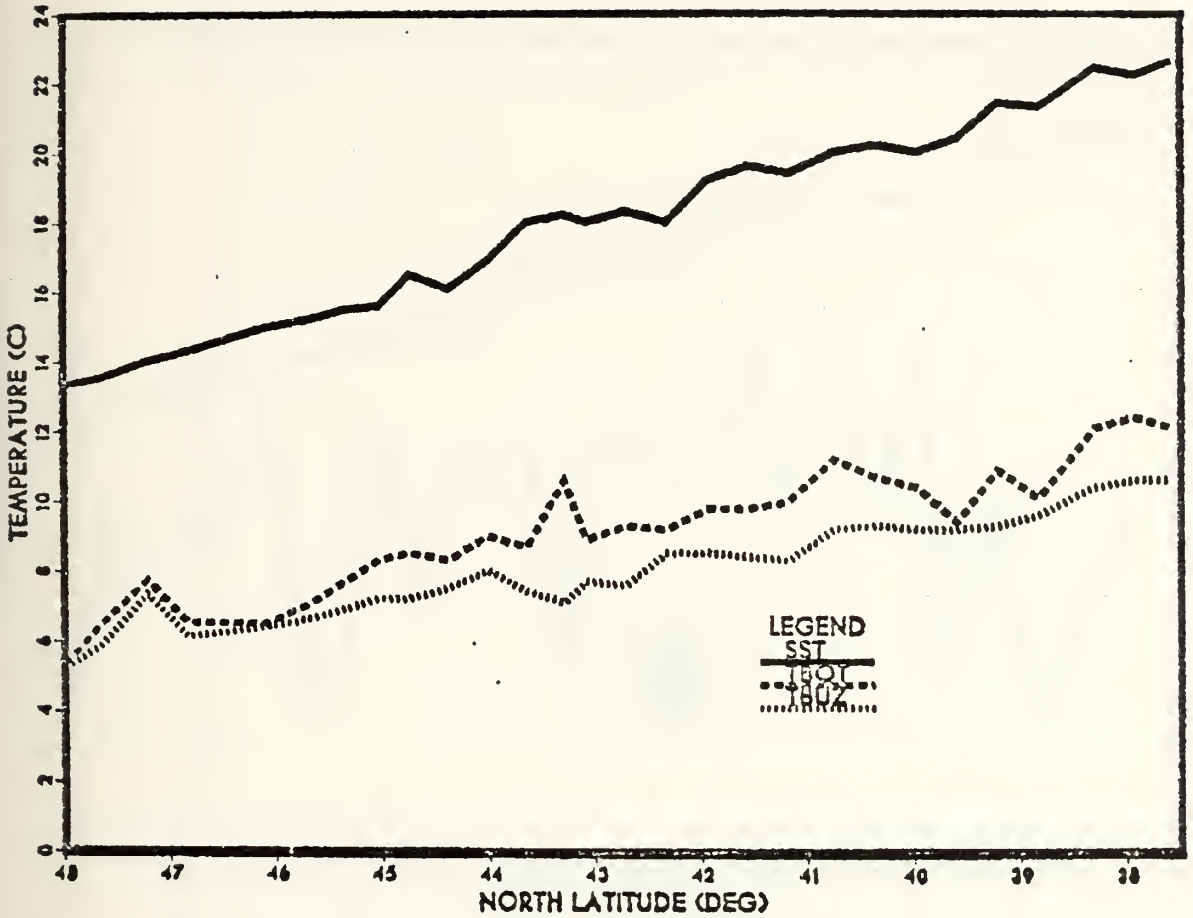

Figure 14. Comparison of SST, TBOT and TBUZ Versus Latitude.

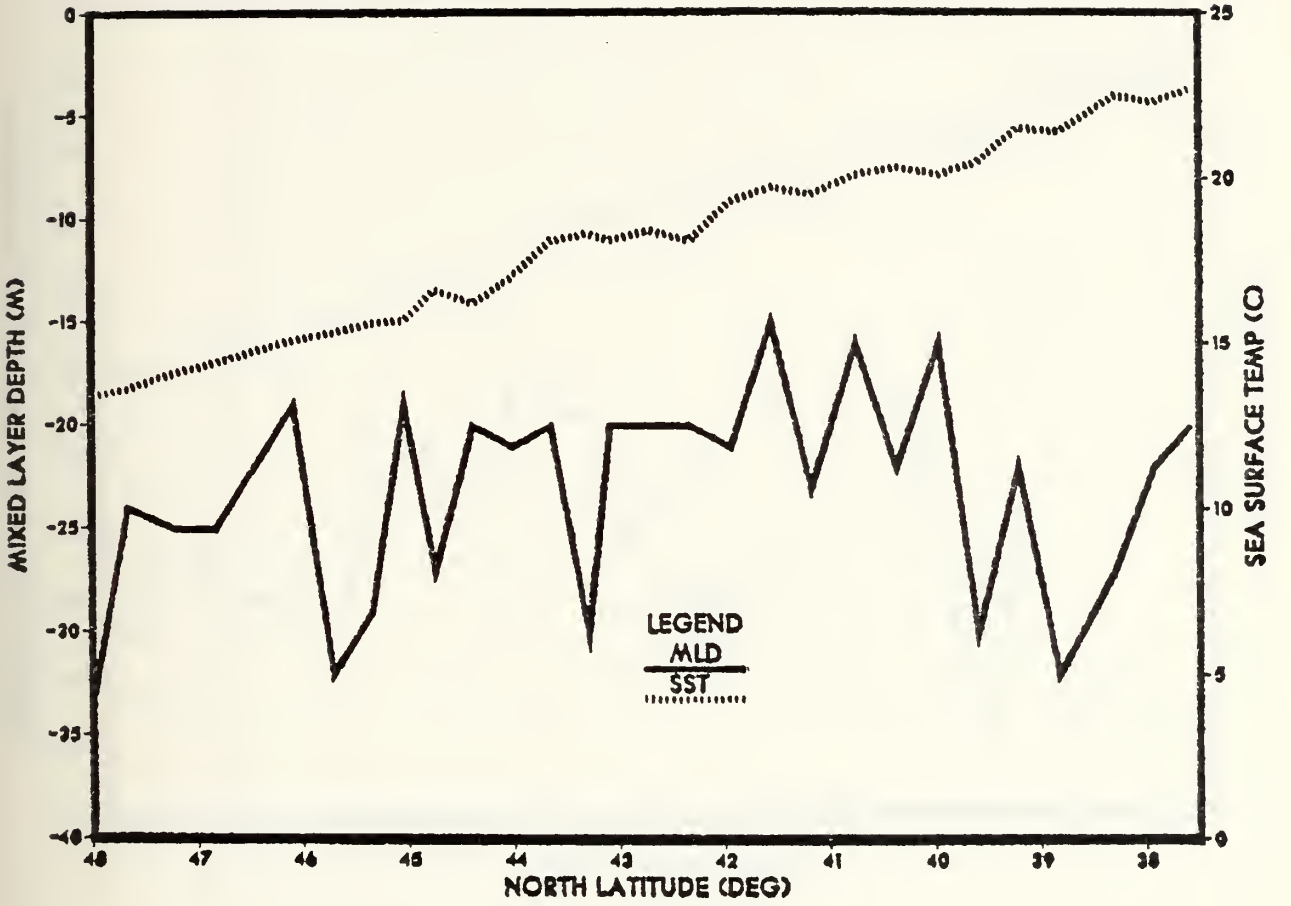

Figure 15. Comparison of MLD and SST Versus Latitude.

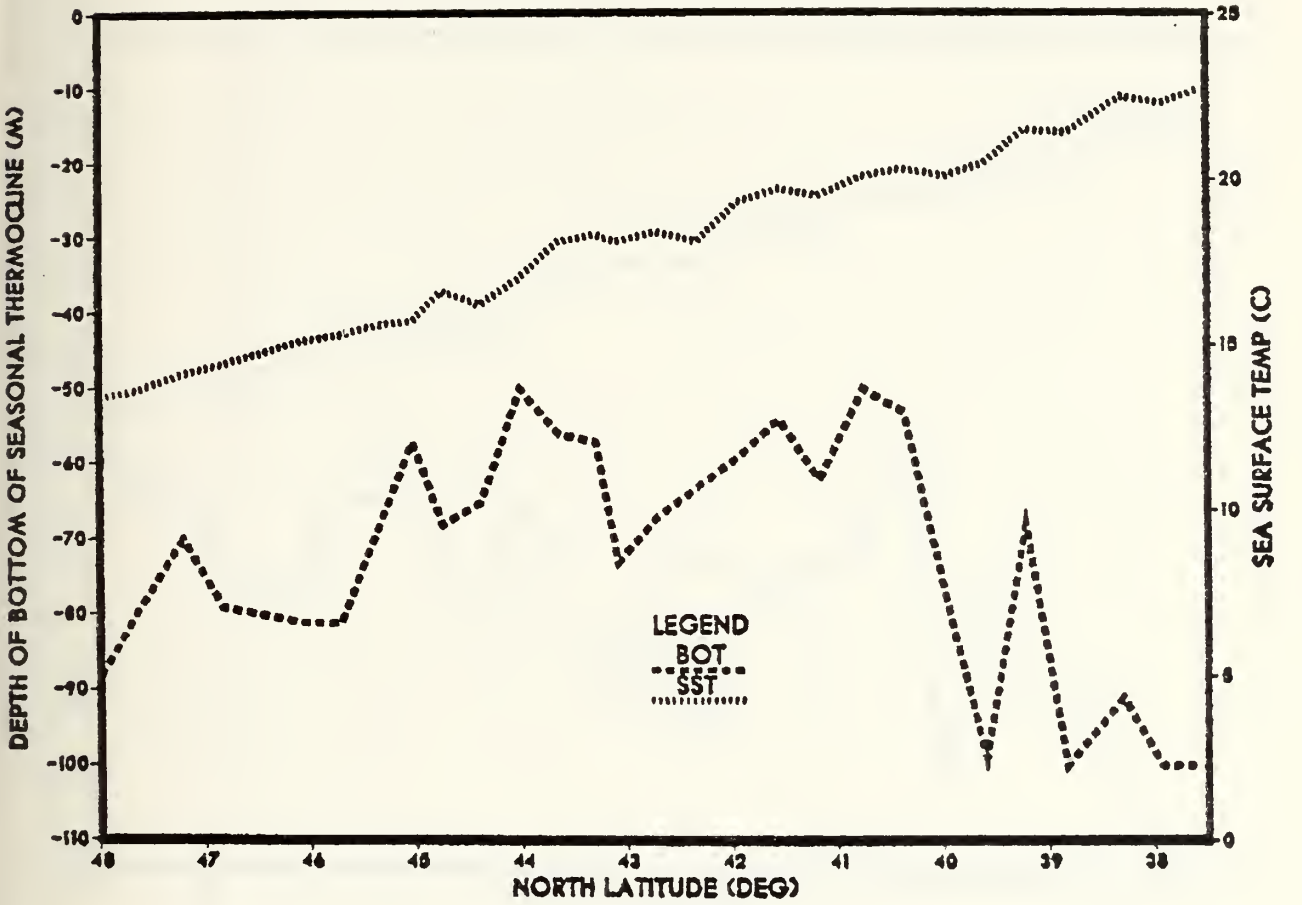

Figure 16. Comparison of BOT and SST Versus Latitude.

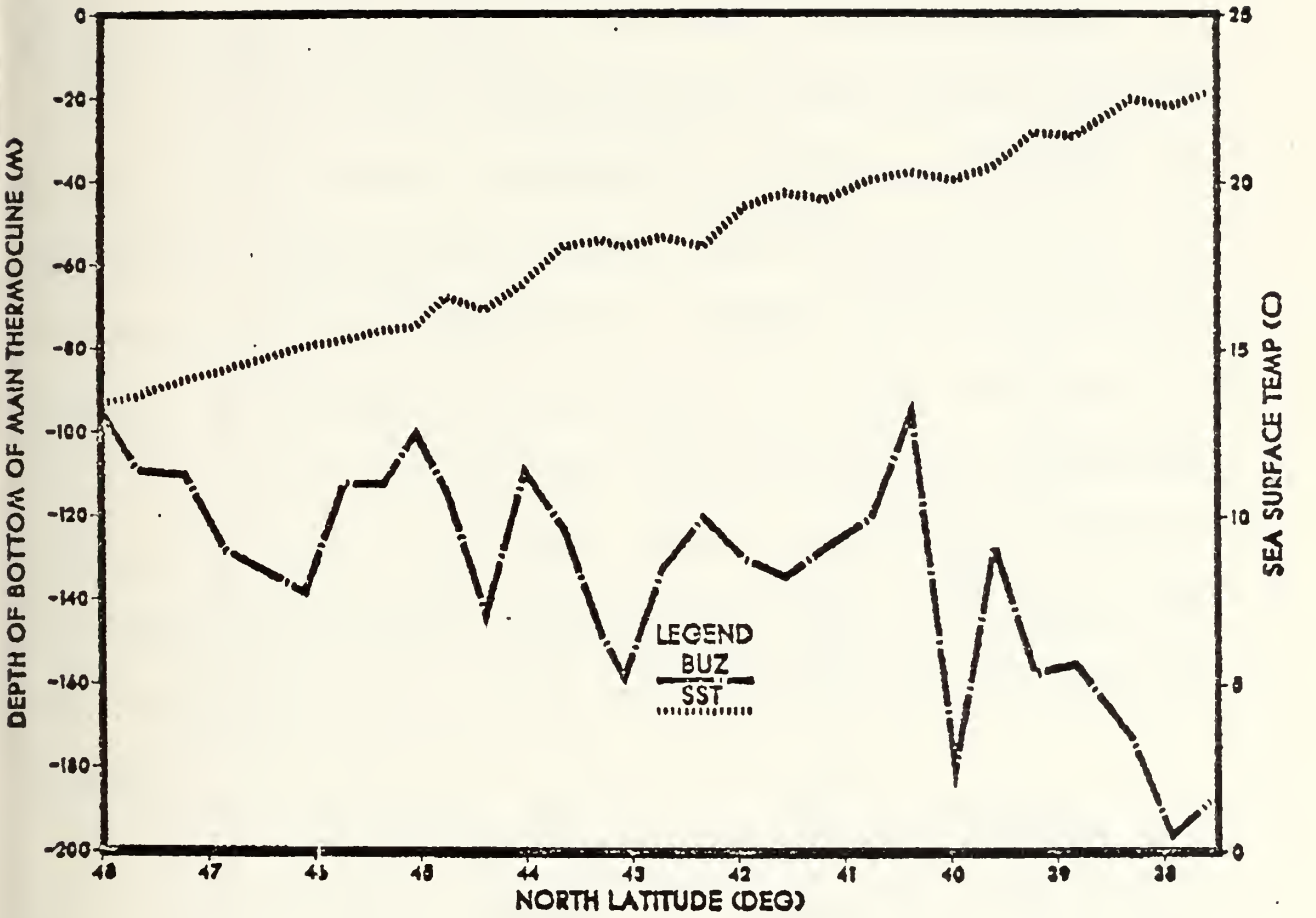

Figure 17. Comparison of BUZ and SST Versus Latitude.

the track, the data were next divided into Subarctic, Transitional, Frontal and Subtropical groupings. These divisions were determined from the previously discussed regional characteristics and thermal analysis of Chapters II and III, and in retrospect, they proved to be an accurate reflection of the boundary locations at the time of data acquisition.

The Subarctic Water characteristics were traced from the northern-most vertical temperature profile on the track to XBT station number 345 at 45.33N. The Transitional Zone was observed from XBT station 346 to station 357 at 41.17N followed by the Subarctic Front between stations 358 and 359. Beginning at XBT station 360 at (39.97N), and continuing south to the end of the track, was an ocean region containing properties of the Subtropic Water. Fig. 18 illustrates the divisions of the track data points into the various regions.

To observe the separation of the data by groupings better, and to refine further the correlation coefficients, scatter diagrams of several of the thermal variables were plotted using the BIOMED computer programs. Since the only variables that correlated strongly with SST were other temperature-dependent variables such as TBOT, DT, TBUZ and

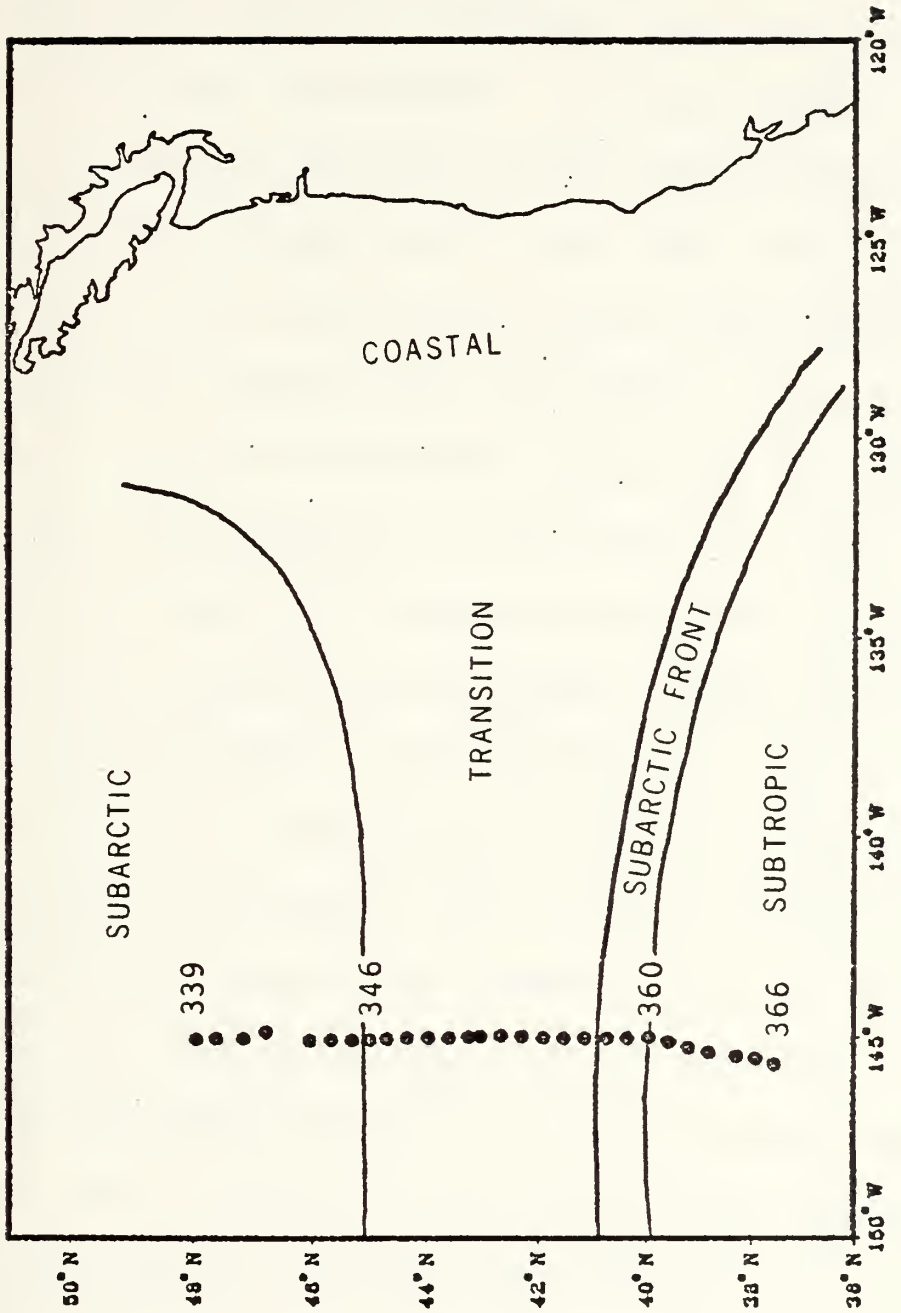

Figure 18. Division of Regions Along Track.

DTBUZ, a closer inspection of the depth-dependent variables was desired. To ascertain whether the sea surface temperature can define the depth of certain variables is necessary in the development of the thermal profile. Therefore, regional scatter diagrams for the three primary depth dependent variables (MLD, BOT, BUZ) and SST as compared to the other variables were plotted and analyzed.

The scatter diagrams for sea surface temperature when compared to the other variables are listed in Appendix C. Due to the high correlation coefficients of these thermal variables the trends of the data points were clearly visible. Obvious linear relations occur between SST and DT50, DT100, DT, TBCT, TBUZ and DTBUZ through the various regions. DT5 and DT15 also displayed an element of linearity when several of the more distant data points were removed. The computer-derived correlation coefficients for these two variables were excessively low due to the remote points. For the variable DT5 shown in Fig. C.2, the data behaved in a strong linear fashion in the Transitional Region as a temperature change of 0.3C in the upper 5 m of the thermocline was the mean. All of the thermocline gradient variables, DT5, DT15, DT50 and DT100, could then be modeled by a

linear equation related to the SST, at least in the Transition Region.

Two scatter diagrams which compare SST to BUZ and DZBUZ, Figs. C.10 and C.13, illustrate a perceivable linear trend between the variables while the correlation coefficients reflect a moderate level of association, (-0.687) and (0.678), respectively. Again, with several of the remote data points removed, an improved correlation coefficient could be computed which better portrays the relationship with SST.

Other depth-dependent variables, for which a visual relationship was observed with SST in the scatter diagrams, were for BCT and DZ, Figs. C.6 and C.9. Both exhibited a "V" or wedge shape with data for the Subarctic and Subtropical Waters on either wing and data for the Transitional Zone in the center. If the northern or southern regional data were removed, then a higher correlation could be obtained utilizing that from the Transitional Region alone. However, with the visual trend in this region closely following the trend of data from the Subarctic Water, data from the northern end of the track could be used to assist in the accurate determination of relationships with the SST. The

combination of data from these two regions is reasonable since the location of the Subarctic Front is on the southern boundary of the Transition Zone, and the water characteristics are similar. Therefore, the Subtropic Water data points should be removed to derive the correlations with data from only the two northern regions.

The two data points in the regional scatter diagrams for the Subarctic Front consistently followed the Transitional Zone data trends. As shown in Appendix C, for the thermal variables BOT, DZ, BUZ and DZBUZ, the Front provided the sharp break between the Transitional and Subtropical Regions, but in the scatter plots for the remaining thermal variables the Subarctic Front fell within the trend of the two northern regions.

The scatter plot comparing mixed layer depth to SST, shown in Fig. C.1, initially appears not to reveal any pattern which could be used to infer a relationship with the SST. However, if the Subtropical Water data points are not included, a trend of decreasing depth is noticed and the correlation coefficient value of 0.224 between these two variables should increase appreciably.

The regional scatter diagrams comparing mixed layer depth to the other variables did not exhibit any strong correlations and were not included. However, several weak patterns were observed which indicated a trend of the MLD slowly decreasing in depth in a southward direction for the northern two regions. All scatter plots displayed large variability among the data points which agrees with the low correlation coefficients for the variable.

Appendices D and E contain the regional scatter diagrams for BOT and BUZ, respectively. These plots show a greater linear dependence among the variables, and therefore higher correlation coefficients, than was shown by the mixed layer depth. In most cases when the Subtropical Water data are removed, leaving only data from the Subarctic, Transition and Frontal regions, a stronger relationship was observed.

Two noteworthy scatter diagrams which had strong negative correlations were BOT-DZ and BUZ-DZBUZ as shown in Figs. 19 and 20. As previously noted, these two variables with high correlation coefficients could provide the necessary link to determine the mixed layer depth. Since DZ and DZBUZ are the differences in depth from the MLD to the BOT and BUZ, respectively, a pair of simple equations define the relationship.

$$MLD = BOT + DZ$$

$$MLD = BUZ + DZBUZ$$

note: MLD, BOT and BUZ are negative values (depth)

The only weak "link" in the two equations is the determination of the BOT and BUZ directly from SST. To improve the correlation coefficients for these two variables as suggested by the regional scatter diagrams, data from the Subtropical Water and several distant data points which detracted from the established trends were removed. In several of the plots, primarily for the temperature-dependent variables, where the trend was actually stronger and more accurate with data from the Subtropical Region included, the correlation coefficients were improved. The correlation coefficients for the best-fit trends are listed in Table V. Indications are made to show which coefficients increased or decreased from the values presented in Table IV.

An example of a correlation coefficient that decreased due to the removal of data points and yet provided a stronger trend was the MLD versus DT5 combination which changed from -0.484 to -0.197. In this case, the majority

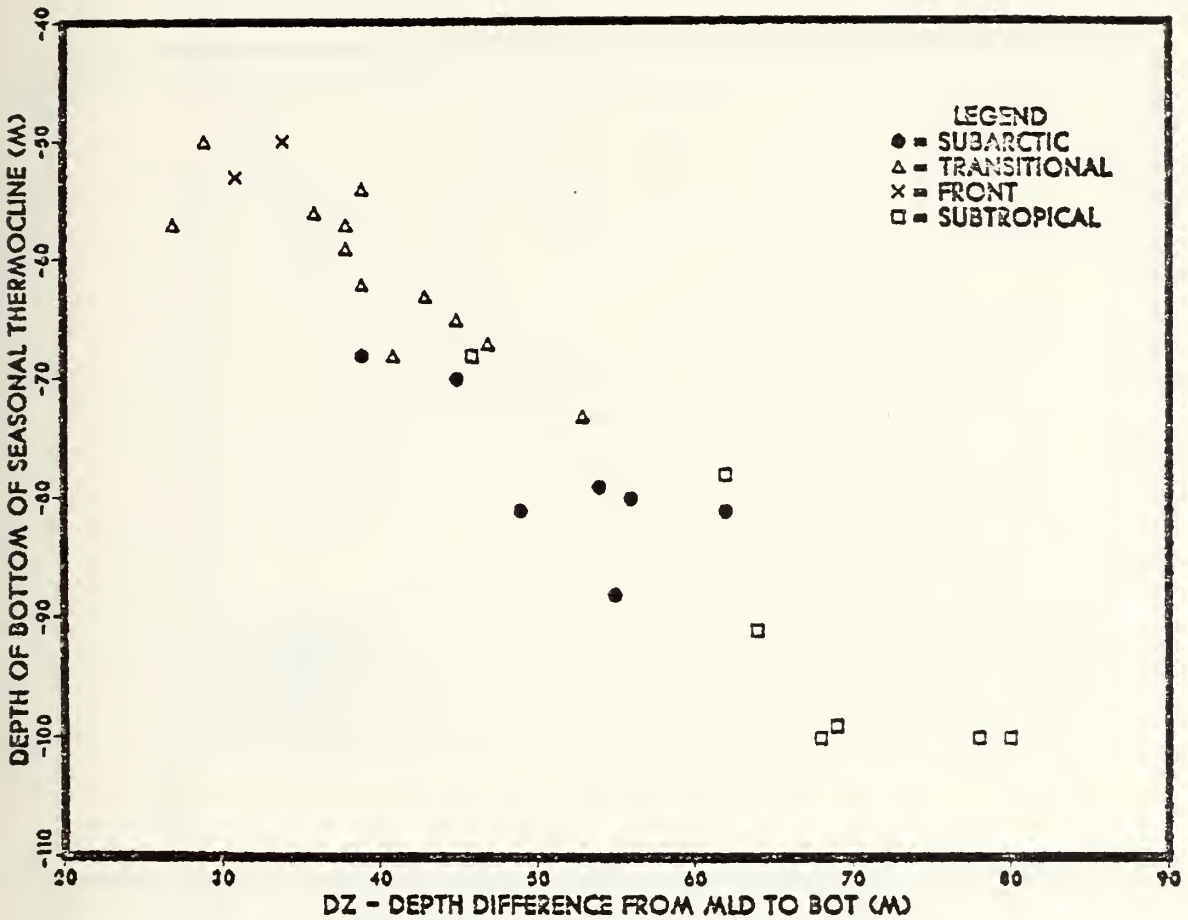

Figure 19. Regional Scatter Diagram - DZ Versus BOT.

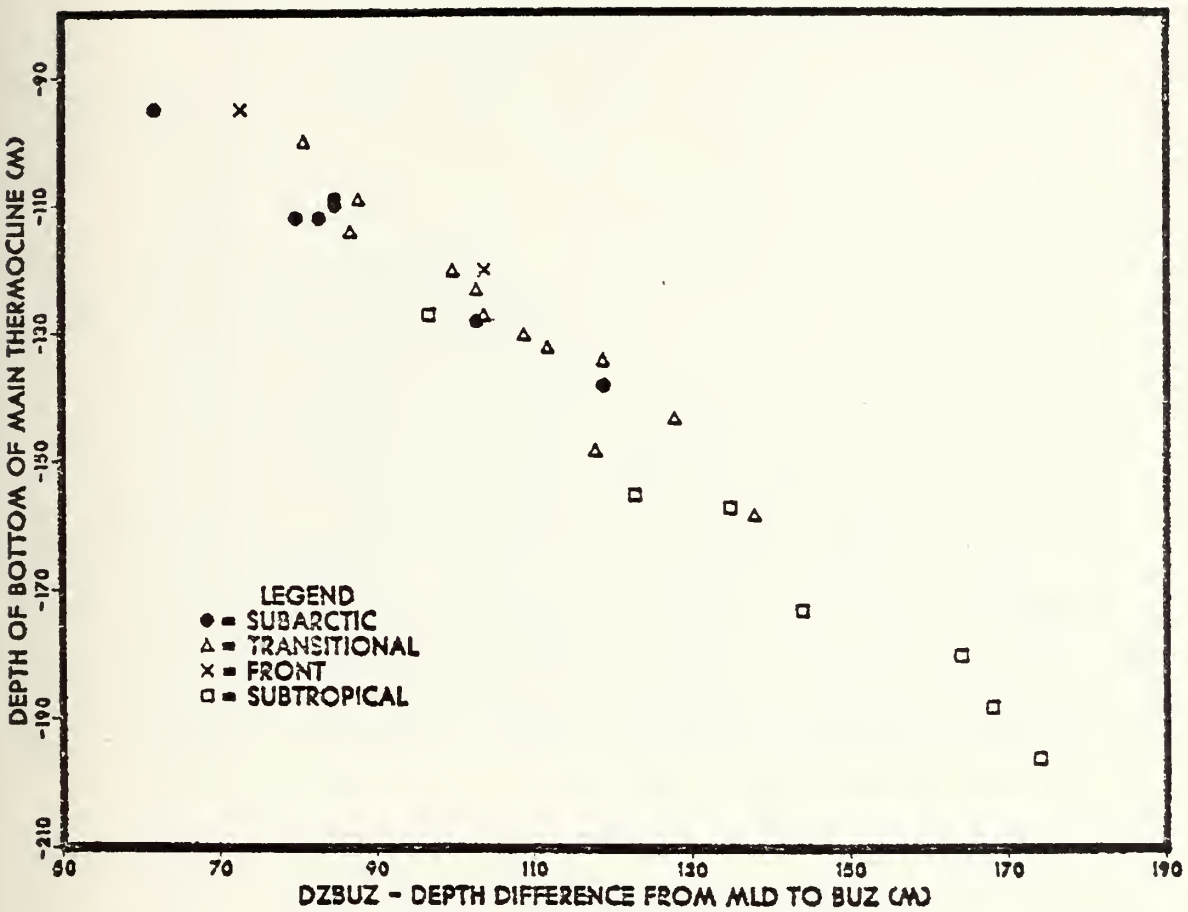

Figure 20. Regional Scatter Diagram - DZBUZ Versus BUZ.

TABLE V

Best-Fit Correlation Coefficients of Thermal Variables

MLD	MLD														
SST	.535′	SST													
DT5	-.197°	.271′	DT5												
DT15	.197′	.677′	-.063°	DT15											
DT50	.452′	.930′	-.435′	.+60°	DT50										
DT100	.495′	.905	-.289′	.385°	.926	DT100									
DT	.499′	.889′	-.497′	.511′	.952′	.846°	DT								
DZ	-.156	-.645′	.030°	-.228′	-.441′	-.559′	-.200	DZ							
BOT	.557′	.776′	-.255°	.256′	.594′	.725′	.410′	-.949	BOT						
TBOT	.480′	.944	-.199′	.225	.771′	.839′	.585°	-.772′	.873′	TBOT					
BUZ	-.307′	-.790′	.212′	.223′	-.239	-.496	-.566	-.643	.514	-.653	BUZ				
TBUZ	.622′	.949	-.379′	.354	.790′	.715°	.673°	-.624′	.831′	.878°	-.654	TBUZ			
DTBUZ	.436′	.960	-.304′	.357	.935′	.977′	.859°	-.503′	.650′	.841°	-.636	.698°	DTBUZ		
DZBUZ	.531′	.766′	.021	.120′	.221	.298°	.292°	.237°	.171°	.182°	-.983	.071°	.348°	DZBUZ	
DIS	.554′	.993	.407′	.646′	.917′	.922′	.885	-.633′	.775′	.931	-.668	.963	.934	.884	DIS
T460	.240	.831	.057	.276	.541	.599	.644	-.588	.598	.835	-.686	.882	.706	.6 3	.846

note: (′) indicates increased coefficients
(°) indicates decreased coefficients

of data points were grouped about the DT5 value of 0.4C per 5 m and a MLD value of -23 m. The attempt to capture the trend of the Transition Region was made by excluding the distant scattered points; however, this detracted from the overall trend and reduced the correlation coefficient.

A large number of correlation coefficients improved significantly by this method of data exclusion. Most noticeable is the variable SST, which, (except for the combination with DT5) increased all other coefficients to greater than 0.645 with six increasing above 0.900. The important correlations of SST with BOT and BUZ improved from -0.203 and -0.682 to 0.776 and -0.790, respectively. The correlation coefficient of SST versus BOT even reversed sign.

This increased strength in the various correlations between variables provided the confidence to infer that usable relationships exist in the vertical thermal profile. Since the variable SST had the greatest number of strong correlations with the other variables, the statistical method of deriving linear regression equations using only the input of SST appeared practical.

E. REGRESSION EQUATION ANALYSIS

From the best fit correlation coefficients of the variable SST in combination with the other variables, the following linear regression equations were derived:

$$MLD = (1.2001)\ SST - 43.300$$

$$DT5 = (0.03629)\ SST - 0.21573$$

$$DT15 = (0.18058)\ SST + 2.2271$$

$$DT50 = (0.48462)\ SST - 0.14105$$

$$DT100 = (0.48506)\ SST + 0.52999$$

$$BOT = (3.9611)\ SST - 133.08$$

$$TBOT = (0.61762)\ SST - 1.9317$$

$$DT = (0.41729)\ SST + 0.94677$$

$$DZ = (-2.7611)\ SST + 89.782$$

$$BUZ = (-7.5247)\ SST - 0.00793$$

$$TEUZ = (0.48510)\ SST - 0.66001$$

$$DTEUZ = (0.55345)\ SST - 0.42130$$

$$DZEUZ = (7.7697)\ SST - 27.820$$

To construct a complete vertical temperature profile, since the variables previously mentioned only defined the upper domain of the thermal structure, a new variable was needed from lower depths. The temperature at 460 m was chosen because it was the lowest datum point available from the XBT data provided along the track. This type of variable was not particularly desired as it relates a temperature to a specific depth rather than to a feature on the thermal profile. A better variable would be at a reference depth where the temperature gradient becomes isothermal in the deeper regions of the ocean. However, this was not available from the limited depth of the data and the T460 variable was established. The same methods of analysis were employed on this variable as were conducted on the others. When compared to the sea surface temperature, a correlation coefficient of 0.831 was computed along with a strong linear trend in the regional scatter diagram. Therefore, a linear regression equation could be used to determine the bottom point of the predicted temperature profiles at 460 meters from the variable SST. The linear regression equation for T460 was computed as:

$$T460 = (0.21834)\ SST + 1.3109$$

Two other important relationships which were derived by regression analysis, but they do not use SST as the independent variable:

$$DZ = (-0.85394)\ BOT - 12.693$$

$$DZBUZ = (-1.0359)\ BUZ - 27.892$$

These equations use the computed values of BOT and BUZ as determined from the SST to calculate the thickness of the seasonal and main thermoclines. The magnitude of these thicknesses (DZ, DZBUZ) when added to the BOT or BUZ, respectively, can then define the mixed layer depth.

Due to the relatively low correlation coefficient between SST and MLD for the SST-derived MLD equation (0.535), possibly a combination of equations which define MLD with higher correlations could improve the accuracy in determining the mixed layer depth. The regression equation for the SST-derived BUZ, with a correlation coefficient of -0.790 between the two variables, along with the BUZ-derived DZBUZ mentioned above with a correlation coefficient of -0.983, seemingly provide the strongest combination. Therefore, the group of equations used for the mixed layer depth determination were:

$$BUZ = (-7.5247)\ SST - 0.00793$$

$$DZBUZ = (-1.0359)\ BUZ - 27.892$$

$$MLD = BUZ + DZBUZ$$

Three other combinations of regression equations could have been used to determine the mixed layer depth, but were not chosen because of their lower correlation coefficients between variables. The equations and correlation coefficients (r) are listed below:

$$BOT = (3.9611)\ SST - 133.08 \qquad r = 0.776$$

$$DZ = (-2.7611)\ SST + 89.782 \qquad r = -0.645$$

$$MLD = BOT + DZ$$

$$BOT = (3.9611)\ SST - 133.08 \qquad r = 0.776$$

$$DZ = (-0.85394)\ BOT - 12.693 \qquad r = -0.949$$

$$MLD = BOT + DZ$$

BUZ = (-7.5247) SST - 0.00793 r = -0.790

DZBUZ = (7.7697) SST - 27.820 r = 0.766

MLD = BUZ + DZBUZ

With the MLD determined, the temperature at this depth was needed to provide the fundamental temperature from which the thermocline could be computed. A variable TMLD was added to represent the temperature at the mixed layer depth and was defined as the sum of TBUZ and DTBUZ. Since both temperature-dependent variables had very high correlations with the SST, 0.949 and 0.960 respectively, strong confidence could be placed in the resulting variable, TMLD.

An additional feature in calculating TMLD by this method was to allow for a slight negative temperature gradient to occur in the mixed layer. Many ocean thermal structure models assume that this upper layer will be isothermal when actually a realistic profile often includes a temperature gradient.

The four thermal gradient variables DT5, DT15, DT50 and DT100, as determined from the SST, were subtracted from the temperature and depth of the mixed layer to form the thermocline. This structure, along with the SST and mixed layer

depth values, provided the upper portion of the vertical temperature profile.

In the region below the seasonal thermocline the temperature-dependent variables, TBOT and TBUZ, and depth-dependent variables, BOT and BUZ, were computed directly from the input of SST and applied to the temperature profile. Several times during the plotting of these points in the testing and comparison phase of the thesis, the location of the DT100 variable would occur below both the BOT and BUZ or between them. In these cases it was simple to adjust the sequence of points to allow the proper construction of the temperature profile.

Finally, in the generation of the temperature profiles, the variable T460 was used to provide the lower base of the structure. Since T460 was an artificially-generated variable, defined at a constant depth, the characteristic small temperature variations at that depth should still be accurately reflected.

A total of nine points were used to define the entire vertical temperature profile. These were plotted on a TEKTRONIX 618 graphic display system and connected with a rational spline method that allows some curvature between

points. This was done to portray the temperature profiles of the region more realistically.

F. THERMAL PROFILE TEST AND COMPARISON ANALYSIS

1. TEST 1

The first type of comparison test was conducted with the original track of data used in the generation of the predicted thermal profiles. The XBT temperature-depth profiles of the Subarctic Water and Transition Zone were compared with the computed temperature profiles which utilized the sea surface temperature of the actual XBT trace as the only input. Fig. 21 shows the comparison between the observed and predicted thermal structures for the northernmost XBT station on the track. Appendix F lists the remaining twenty profile comparisons for the northern regions excluding the Subtropic Water.

The comparisons generally illustrated a strong similarity in the upper layers. The mixed layer depth along with the slight negative temperature gradient in the layer were realistically predicted for a majority of cases; internal wave motions are assumed responsible for the largest variation from the predicted profiles. The upper thermocline region closely approximated the strong thermal

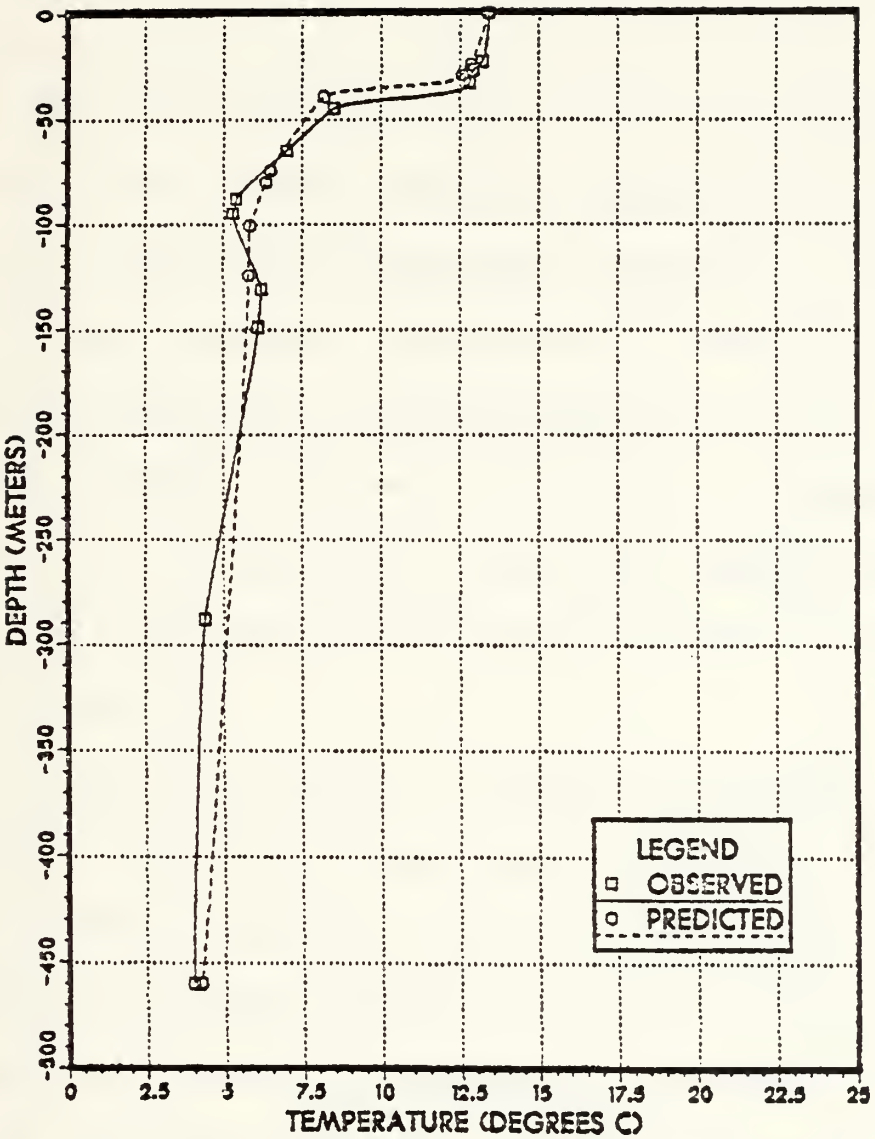

Figure 21. Observed and Predicted Thermal Profiles - XBT Station 339.

gradient measured by the XBTs. In the lower thermocline, greater variability occurred, assumed due to internal waves and thermal advection, resulting in poor comparisons as shown in Figs. F.2, F.11 and F.12 for XBT stations 341, 350 and 351.

The predicted lower regions were not as precise when compared to the observed profiles usually due to the existence of a significant temperature inversion. Lack of a model for this feature, which was not attempted, clearly affected the profiles at depths greater than 130 m. Several predicted profiles, however, did attempt to reproduce this structure with the placement of the DT100 variable below the BUZ. This was shown in XBT stations 343-346 and 348 (Figs. F.4 - F.7 and F.9).

Between the bottom of the main thermocline and 460 m, several predicted profiles completely failed to approximate the observed structure. This was caused by the lack of variables in the lower layers as well as the computer-generated curvature between data points. When the variables DT100 and BUZ were very close together, as shown for XBT stations 348 and 349 (Figs. F.9 and F.10), the profile would bulge with a positive or negative gradient.

Utilizing only nine points to define the predicted thermal profile obviously smooths the fine structure within the thermocline and mixed layer. However, due to the small size and transient nature of these features, their removal would not severely limit the usefulness of the predicted structures.

In this initial test, since the predicted temperature structures were generated and compared with the same XBT data from the meridional track, the comparisons should be relatively close. The predicted profiles would actually represent the average of all the observed thermal structures as the variables reflect the trends along the track.

2. TEST 2

A more stringent and realistic test was attempted that defines the spatial limitations of this thermal prediction method. Test 2 consists of comparing observed and predicted temperature profiles which occurred during the same time period as the data generation, but spatially removed. A possible indication as to a limit in the effective distance would be the observation that the predicted profile begins to diverge greatly from the actual temperature profile.

The test XBT data were obtained from Fleet Numerical Oceanography Center by a computer search for all available XBT drops which occurred in September from 1965 to 1980 in a ten degree wide strip of longitude which surrounds the original track. Inexplicably, the data received were limited to the area south of 44N, excluding the Subarctic Water. Lack of time prevented an attempt to acquire these data which would be useful, but not entirely necessary, for analysis. The temperature-depth data were then selected by noting the positions relative to the original data. To provide an effective test, a variety of locations in the Transitional Zone were chosen. However, these positions were constrained by the availability of data in the region and appeared as a zonal belt perpendicular to the original track. Fig. 22 shows the location of original and test XBT drops.

The temperature-depth points provided by FNOC were then plotted and connected on the computer graphical display with the same amount of curvature applied to the profile as before. Both observed and predicted profiles were plotted together again for analysis and comparison purposes.

Five vertical temperature profiles from the 10-11 September period were compared with the predicted profiles

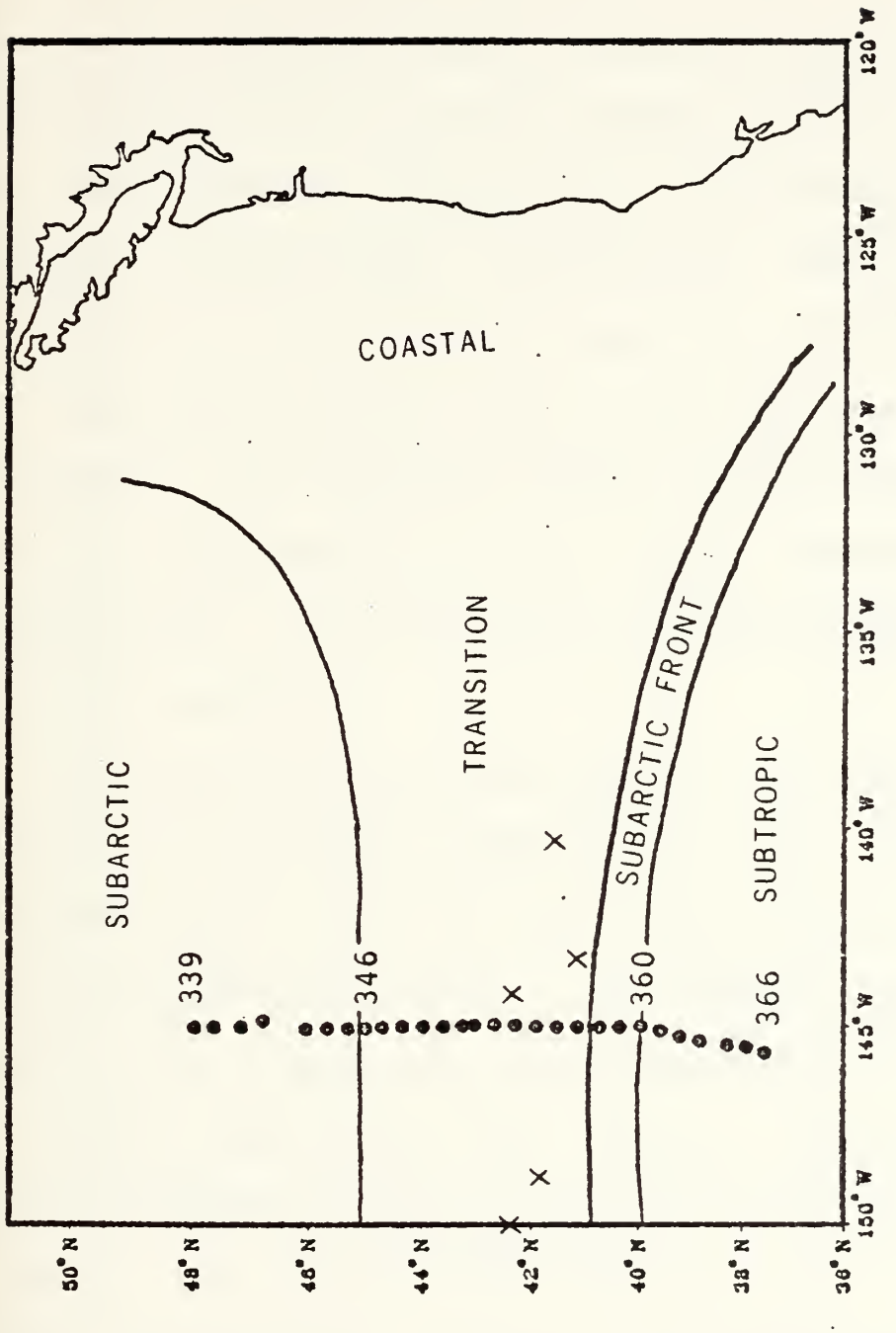

Figure 22. Location of Original (•) and Test 2 (X) XBT Drops.

as generated from the sea surface temperature of the observed profiles. The test produced varied results with several features of the computed temperature profiles comparing favorably with the actual thermal structure. The largest differences were noted for the two profiles located the greatest distance from the meridional track at 145W. Figs. 23 and 24 illustrate the comparisons at these locations, approximately 400 km east and west from the original track of data. The mixed layer depth and upper thermocline regions of the predicted profile closely resembled the observed profile, but both structures displayed differences in the lower regions.

The eastern most observed profile had a thin, strong thermocline which gradually weakened with depth. This contrasted markedly with the strong and sharply-defined thermocline of the predicted profile. The regions below 150 m displayed similar temperature gradients for both profiles.

For the western most test profile, the only region to differ significantly from the predicted structure was the lower domain below 130 m. The location of the two close variables, BUZ and DT100, along with the computer-generated curvature forced the predicted profile to diverge from the weak temperature inversions.

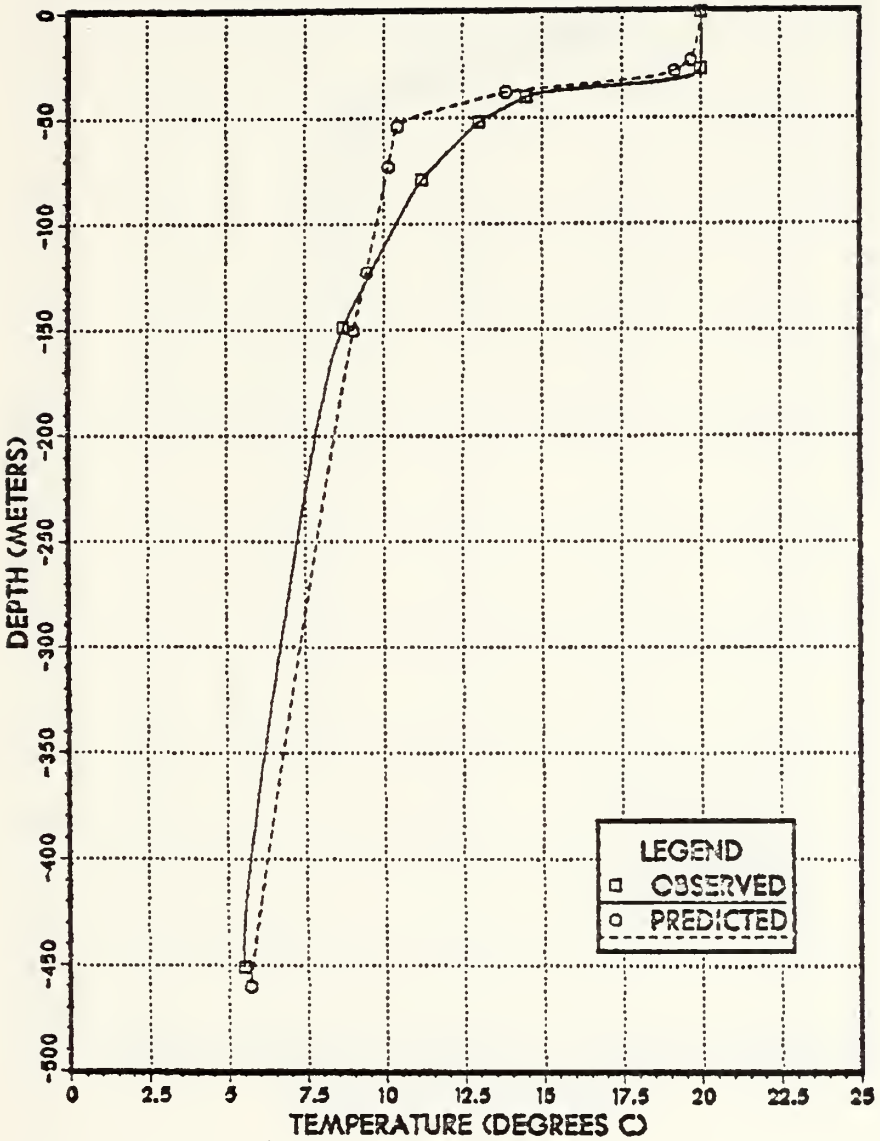

Figure 23. Observed and Predicted Thermal Profiles at 41.5N, 140.3W For 101200Z SEP 77.

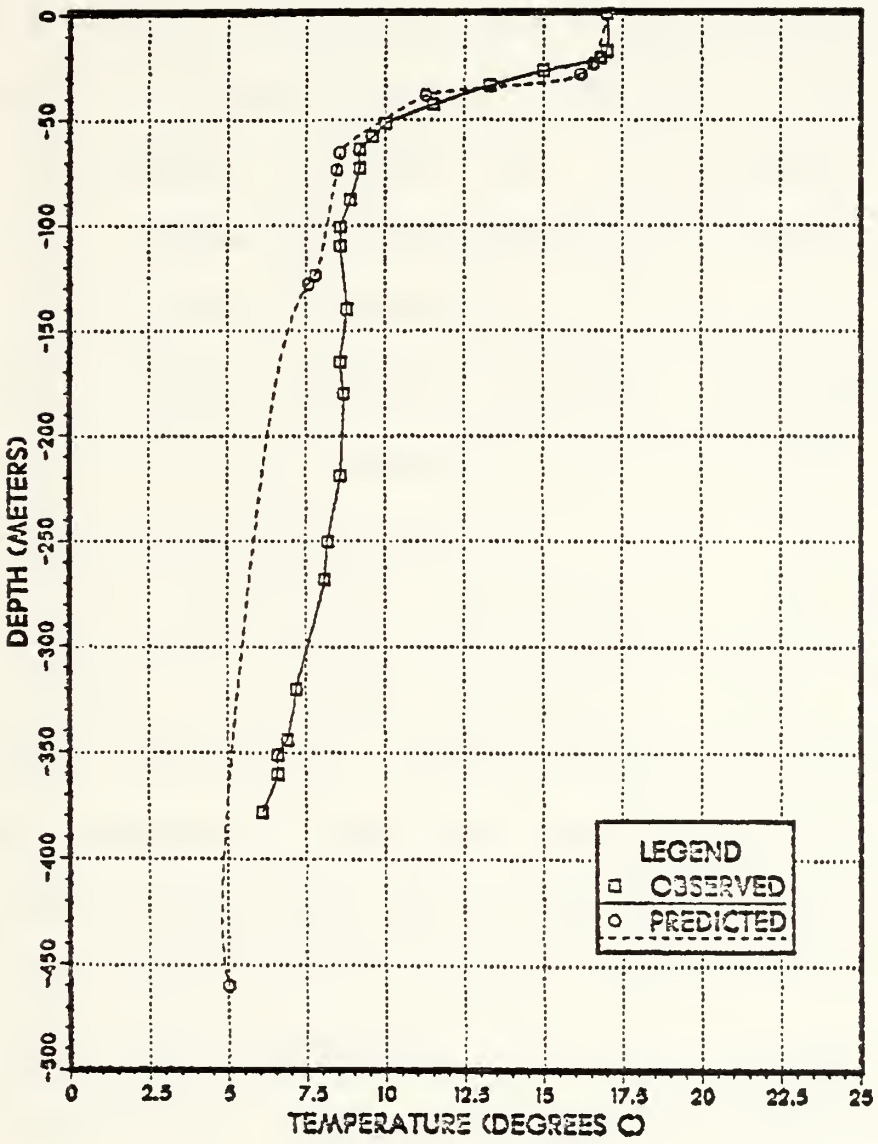

Figure 24. Observed and Predicted Thermal Profiles at 42.3N, 150.0W For 110059Z SEP 77.

The three other test cases, shown in Figs. 25, 26 and 27, which were located closer to the original track, all displayed strong similarities between the observed and predicted profiles. Except for the fine structure and possible effects of internal waves on the depth of the thermocline, the computed profiles were very accurate. The unusual shape of the observed temperature profile at the bottom of the seasonal thermocline, in Fig. 27, and close approximation by the predicted profile, illustrates the strong ability of this statistical method to produce thermal features unique to a certain region.

To test the spatial limitations of this empirical method further, a vertical temperature profile taken at Ocean Weather Station "P" during the data-generation time period was examined. Since the location of the northern most XBT drop on the track was two degrees of latitude south of OWS-P, the results should indicate the reliability of the method outside the test region. Fig. 28 displays the comparison between the observed and predicted profiles for OWS-P.

From the surface to the middle of the thermocline, the two profiles were very similar, with the mixed layer

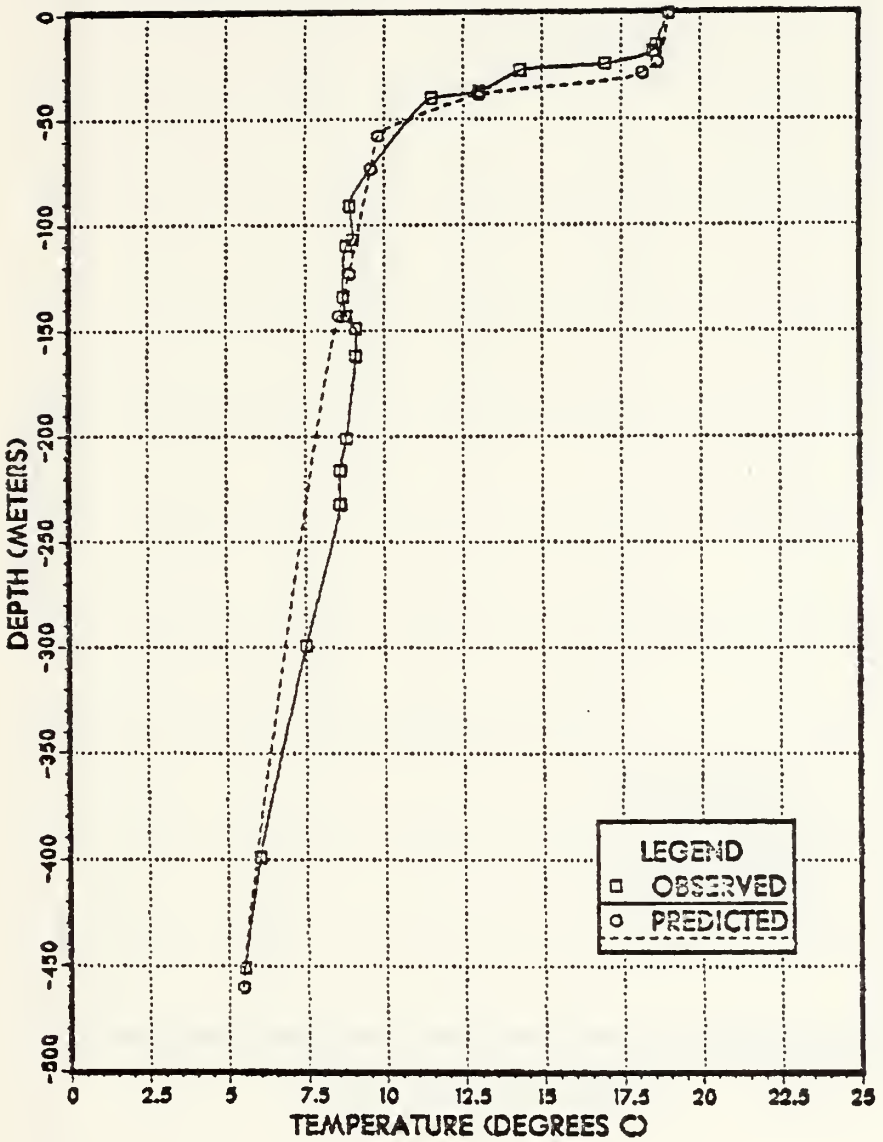

Figure 25. Observed and Predicted Thermal Profiles at 41.9N, 148.7W For 101200Z SEP 77.

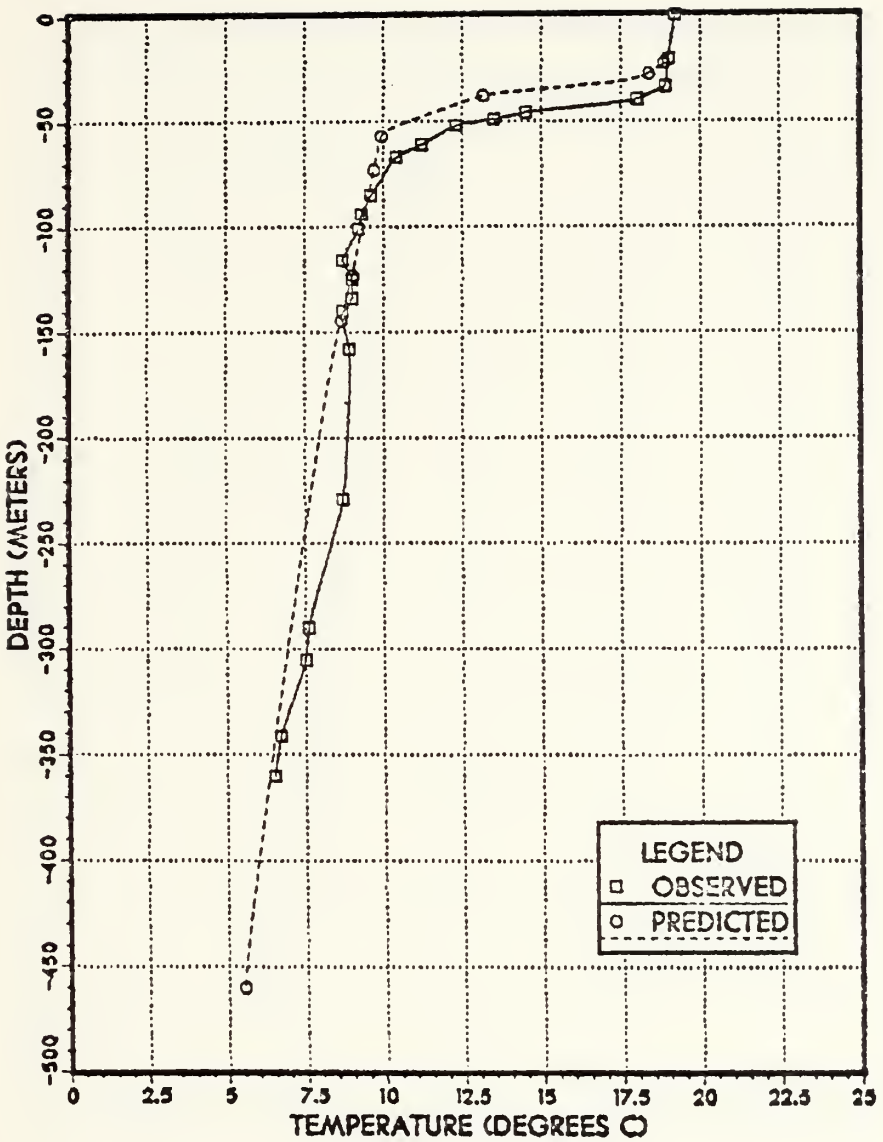

Figure 26. Observed and Predicted Thermal Profiles at 42.3N, 144.0W For 102115Z SEP 77.

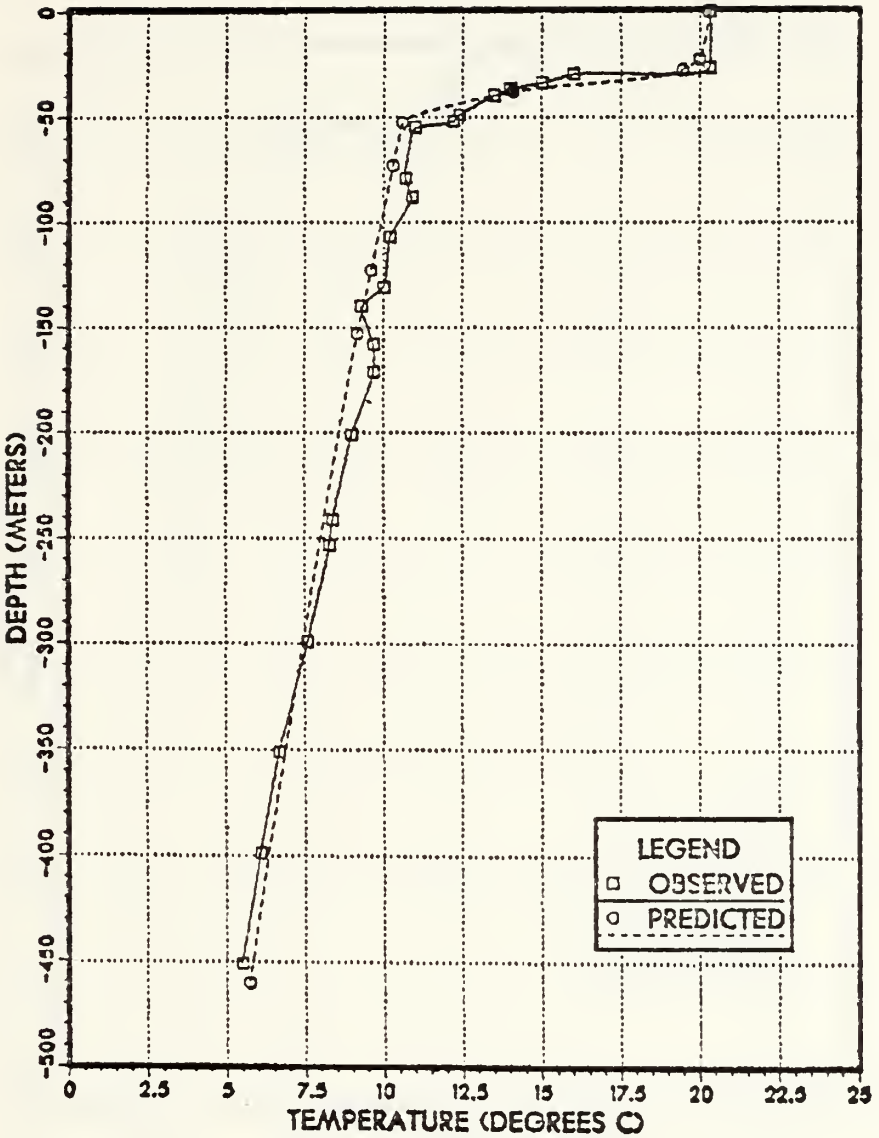

Figure 27. Observed and Predicted Thermal Profiles at 41.1N, 143.2W For 110000Z SEP 77.

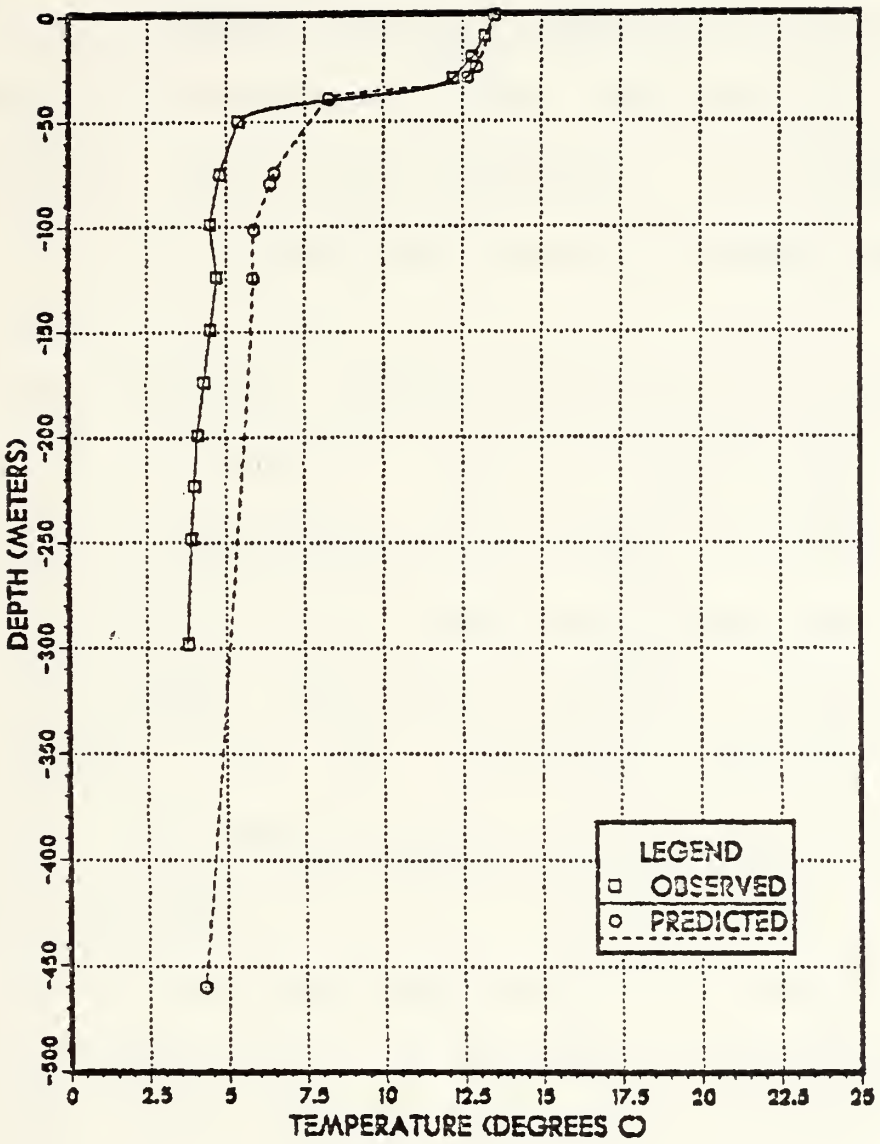

Figure 28. Observed and Predicted Thermal Profiles at OWS-P for 110318Z SEP 77.

depth accurately depicted. However, the lower segment of the two profiles differed by 2.0C. With the actual vertical temperature profile being considerably cooler than predicted, a different regime must have been encountered. Tabata (1961) suggests from his observations in the region that horizontal transport of colder water from the vicinity of the Alaskan Gyre, lying northwest of the station, may cause a decrease in temperature during the summer months.

3. TEST 3

The third test included both spatial and time differences in an attempt to forecast the vertical thermal structure up to three weeks in the future. The only available XBT test data in the Transitional Region were located within three degrees longitude to the west of the original track as shown in Fig. 29. Vertical temperature profiles were chosen at weekly intervals and compared with the predicted structures.

At the end of the first week, the observed thermal profile, as shown in Fig. 30, displays a deeper mixed layer to a depth of 40 m overlying an extremely strong negative temperature gradient. This feature was not represented well by the predicted profile as the computed MLD and thermocline

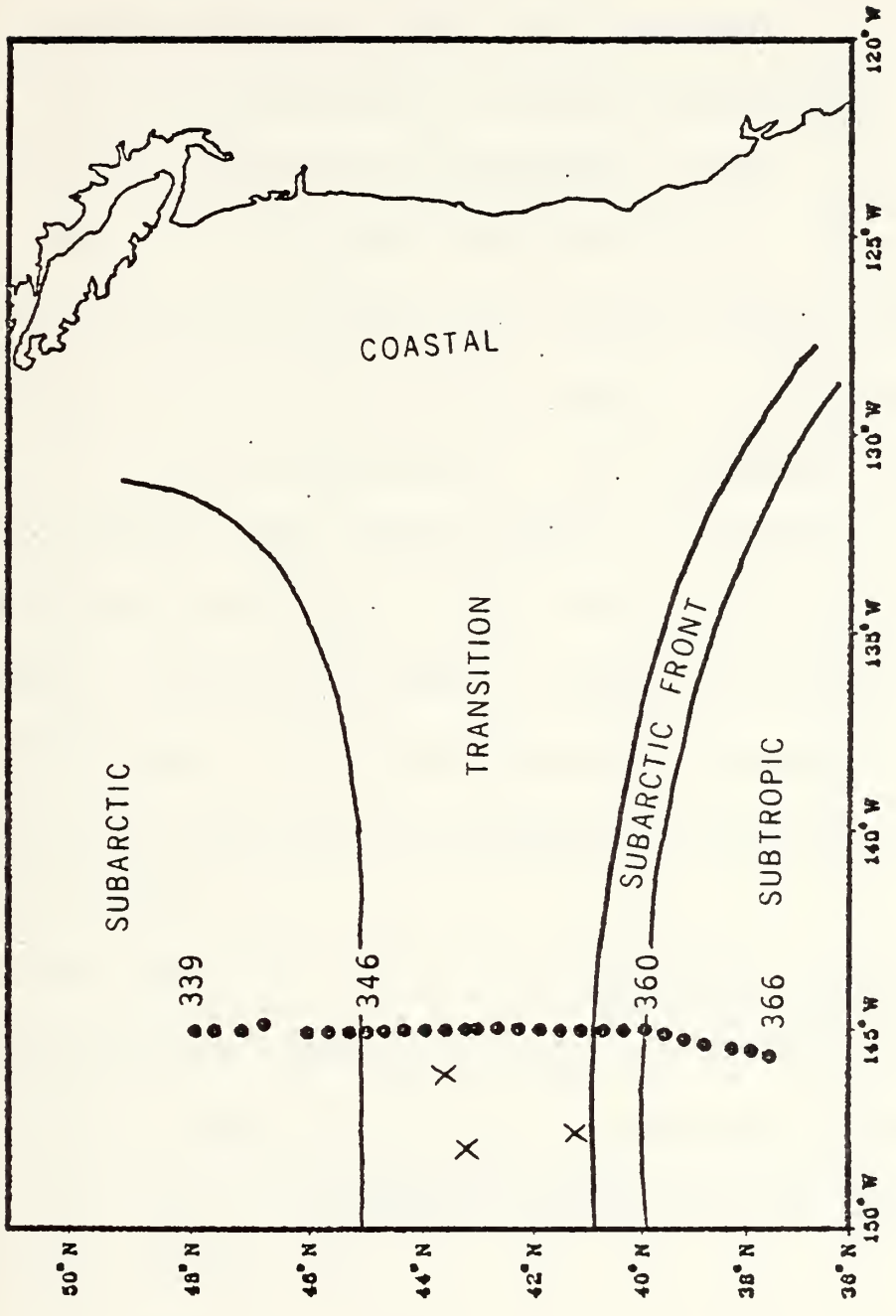

Figure 29. Location of Original (•) and Test 3 (X) XBT Data.

variables were shallower in depth. The shape of the observed mixed layer infers strong wind and convective mixing, so surface weather charts for the period of 11-18 September 1977 in the Northeast Pacific were checked for the occurrence of a significant atmospheric event. On 17 September 1977, a cold front associated with a low pressure system in the Gulf of Alaska had quickly passed through the test region with rain and 35 knot winds. The weather during the period of data acquisition, 8-11 September 1977, as described before, was mostly cloudy with periods of light winds and scattered showers (FNOC, 1977). These contrasting atmospheric situations suggest a major limitation in the statistical model, as weather effects on the upper vertical temperature structure must be properly accounted for in the predicted profile.

The lower half of the thermocline on the predicted temperature profile closely followed the observed structure down to 170 m. Except for the weak temperature inversion at 200 m, which was not included in the empirical model, the lower domain behaved well.

The next test profile was taken on 24 September 1977, thirteen days after the data generation for the

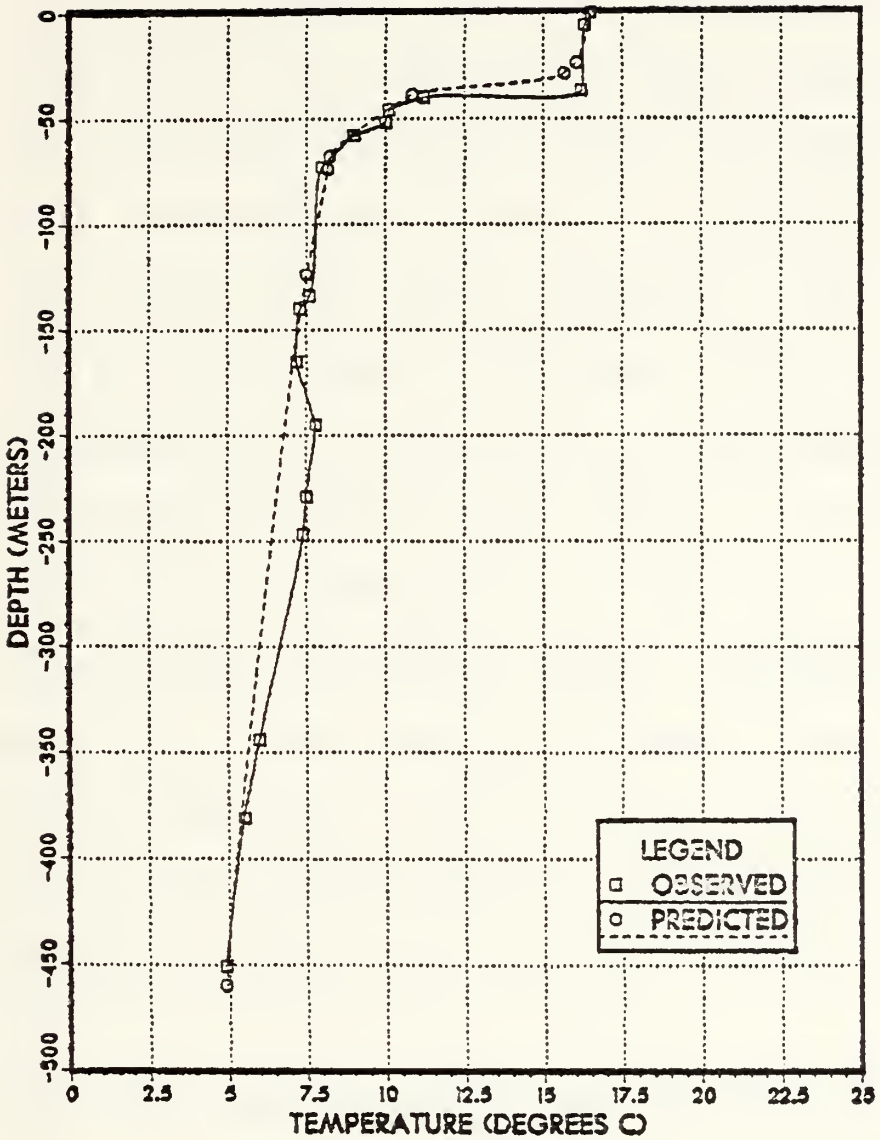

Figure 30. Observed and Predicted Thermal Profiles for 182030Z SEP 77 at 43.7N, 146.1W.

predicted structure. Location of this test XBT was on the southern boundary of the Transitional Zone approximately 200 km west of the original track. The predicted temperature profile in Fig. 31 clearly resembled the observed vertical thermal structure, but with slightly cooler temperatures. Due to the strong winds from the storm a week earlier, the observed MLD remained deep. However, a transient at 30 m depth had formed with a 0.5C increase in sea surface temperature as the weather in the region during the second week was dominated by a strong high pressure system. The observed profile's thermocline also deepened by about 10 m, which may be due to internal waves, or it may have been caused by warm advection from the south. Immediately below the thermocline, the two profiles differed slightly because of the fine structure in the region. The predicted temperature at 460 m depth remained accurate when compared to the observed temperature throughout all the temporal tests.

The final test forecast was conducted for an XBT location 209 km to the west of the north-south track on 30 September 1977, nearly two weeks after the basic data were acquired. Another cold front associated with a low pressure

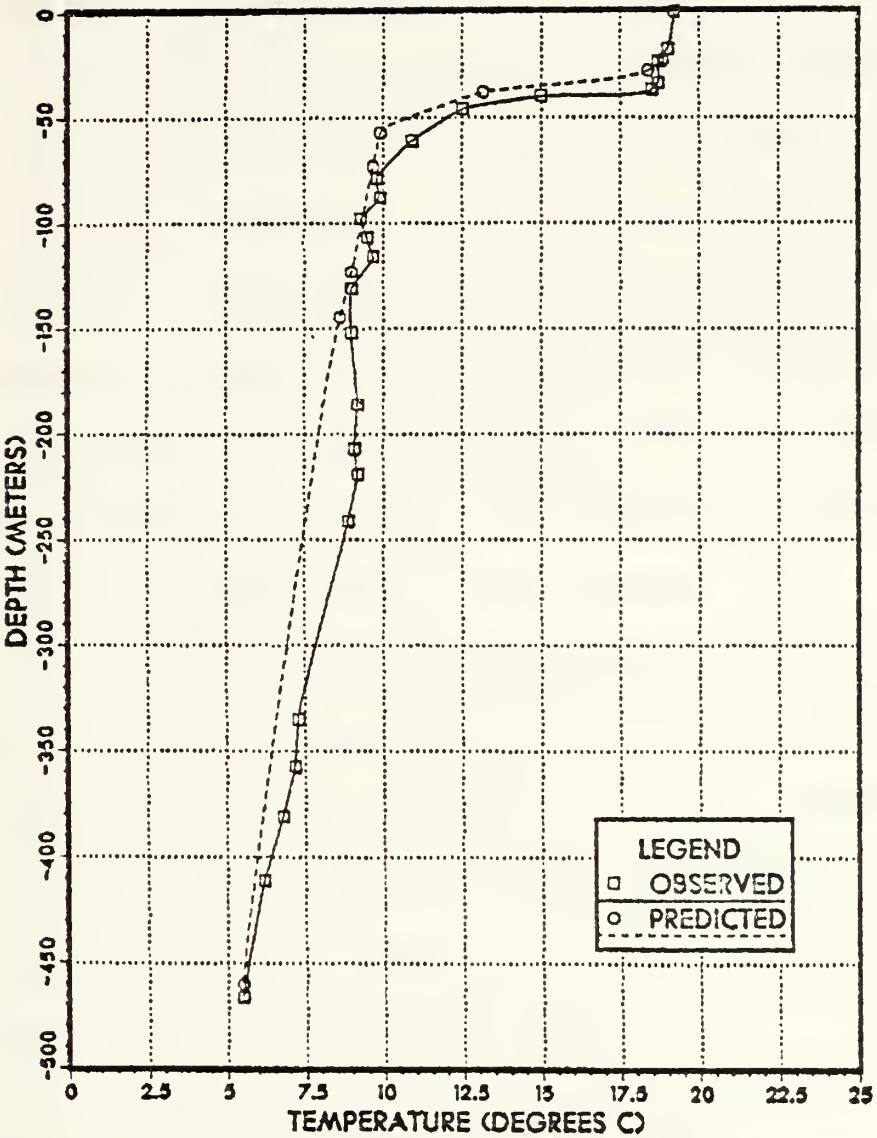

Figure 31. Observed and Predicted Thermal Profiles for 240000Z SEP 77 at 41.2N, 147.5W.

system moved through the area on 25-26 September 1977 and was immediately followed by a high pressure ridge. The storm, with maximum winds of 40 knots, maintained the 40 m thick isothermal mixed layer as shown in Fig. 32. The wind mixing had increased and deepened the negative temperature gradient of the thermocline to a level approximately 10 m below the predicted profile. In the lower domain of the thermal structure a large difference was noted due to the slight temperature inversion of the observed profile and to the close location of the two variables, BUZ and DT100, at 130 m on the predicted profile. The profiles coincided at the 460 m depth as determined by the variable T460.

The accuracy of the predicted profile after three weeks from the time of data acquisition for the statistical analysis shows an overall degradation. However, considering that two storm systems passed through the region and the summer heating season was approaching its end, the forecasted profile was not excessively poor.

G. REVIEW OF PREDICTED THERMAL PROFILE RESULTS

The underlying requirement of the statistical approach in predicting the vertical temperature profile is to acquire accurate data that reflects the mean thermal conditions for

a particular season and region. Besides the acquisition techniques, the importance in precisely defining the regional boundaries is essential. Both temperature and salinity should be used to establish the limits of usable data when applying correlation and regression analyses. Results of the predicted thermal profiles located outside the data generation area, as defined by a certain region, displayed a marked degradation in the lower thermocline and lower domain regions. The predicted profiles located near the area generally portrayed the observed temperature profiles realistically within the spatial limits of 455 km about the original data.

The results of the temporal accuracy of the predicted profiles indicate a favorable ability to forecast the thermal structure with certain limitations. The main limiting factor was the weather which must be included in the analysis. Clearly, when high winds pass through a region after the vertical temperature data is acquired, the upper thermal structure will be altered. Two regions of the thermal profile that will be affected are the depth of the mixed layer and strength of the thermocline. For short periods of about one week, this upper domain in the water column will

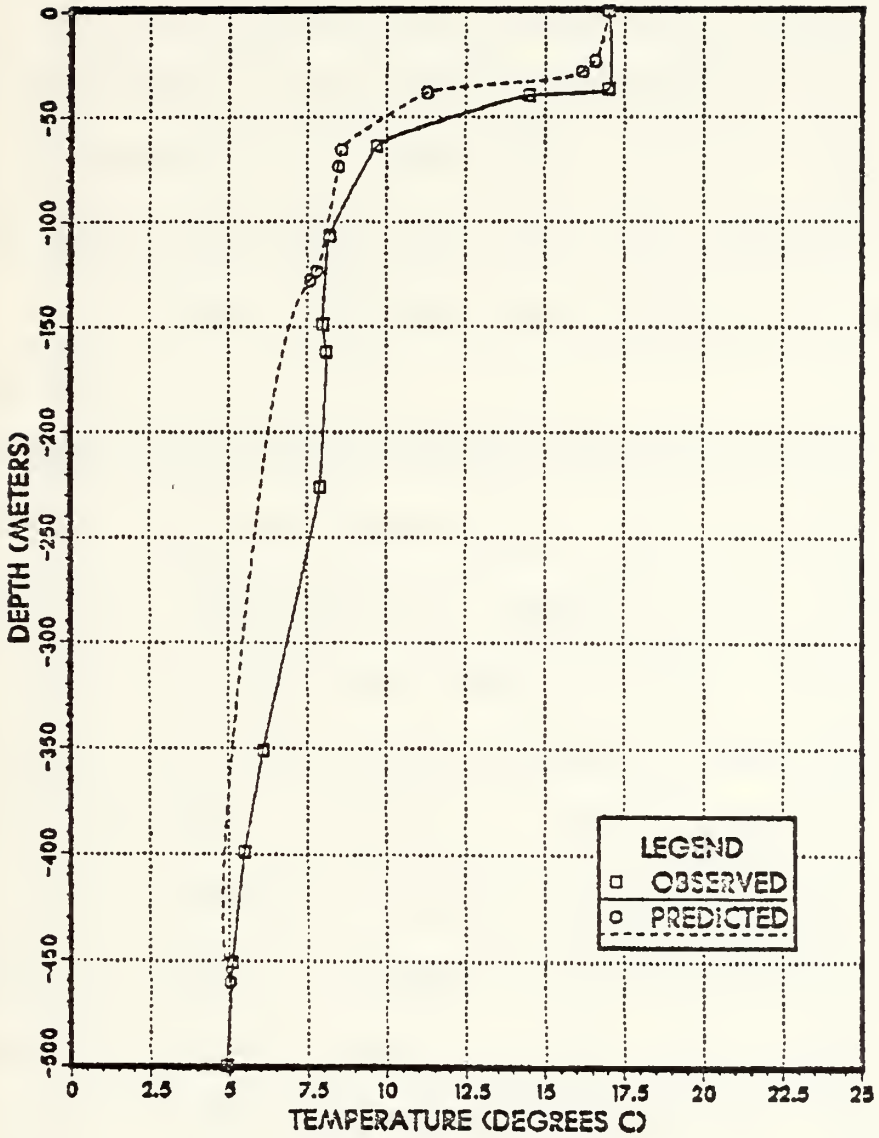

Figure 32. Observed and Predicted Thermal Profiles for 300000Z SEP 77 at 43.3N, 147.7W.

primarily reflect changes due to the wind and free convective mixing. For time scales of greater than a week, an occasional thermal intrusion from the Subarctic or Subtropic Region may be an additional factor that could alter the thermal structure. Such advective processes would be difficult to forecast by the statistical method in regions where large meanders and eddies occur, but they should not greatly affect a relatively quiescent area such as in the Transitional Zone.

An example of another problem encountered by this method of thermal structure prediction from the sea surface temperature is the process of heating at the ocean's surface, called the "afternoon effect." Fig. 33 illustrates the difference in the predicted profile's structure with the observed "afternoon effect." Since the sea surface temperature determines the thermal profile in this statistical model, an error is imposed in the subsurface structure, throughout the entire depth. With the surface heating removed, the predicted profile would closely resemble the observed profile. The "afternoon effect" would greatly hinder the ability of remote sensing to determine the subsurface thermal structure by this method.

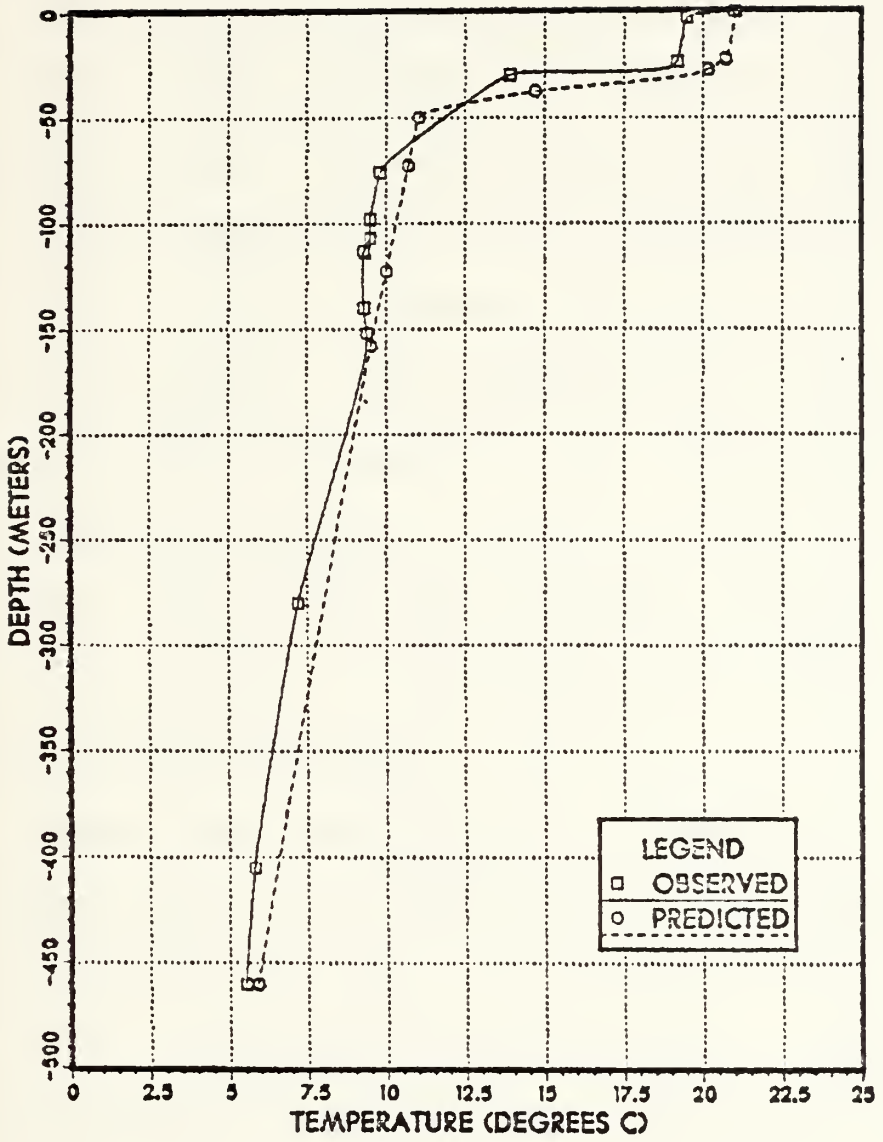

Figure 33. Example Predicted Profile Error Due to "Afternoon Effect".

The method of determining mixed layer depth was reviewed to ensure that the best possible value was computed and used in the empirical scheme. As discussed earlier, the MLD provides a base for the variables DT5, DT15, DT50, DT100, DT, DZ, DTBUZ and DZBUZ to define their values in the predicted temperature profile. The other variables BOT, TBOT, BUZ and TBUZ, besides contributing to the construction of the profile, provide a check to maintain continuity with the MLD-determined variables. The technique used in this thesis to compute MLD caused no problems in the determination of the thermal profile; however a comparison test of computing mixed layer depth by the five different methods, defined earlier in Chapter IV, was conducted to ascertain which method is the most accurate.

All methods were provided with the same SST values from the original data of the north-south track and compared with the actual mixed layer depth. The computed depths were then correlated to determine the best technique. Results from the test indicated all methods were surprisingly equal. The method used was chosen because of the higher correlations between variables. However, the simplist method, which was the SST-derived mixed layer depth, with a correlation coefficient of 0.535, could have been used with equal success.

V. CONCLUSIONS AND RECOMMENDATIONS

A. CONCLUSIONS

The sea surface temperature reflects many of the physical processes that govern the oceans. Use of remote sensing to map the surface thermal structure of the world's oceans accurately and rapidly presently exists, but the determination of precise subsurface vertical temperature structure from these surface signatures is unrealized. Possibly only in selected ocean regions can insight be gained into determining quantitative relationships for directly inferring the subsurface features from the sea surface temperature. In relatively quiet locations with uniformly changing properties, such as in the Transitional Zone of the Northeast Pacific, many strong correlations can be observed within the thermal structure.

The results of the statistical analysis indicated that the strongest relationships within the vertical temperature profile occurred with the thermally-dependent variables (TBOT, DT, TBUZ, DTBUZ) as they varied with SST. The depth-related variables (MLD, BOT, DZ, BUZ, DZBUZ) displayed

weaker correlations with the surface temperature, but trends still could be observed through the thermal structure. The use of scatter diagrams to assist in the correlation analysis of variables was necessary to establish regional boundaries and the best fit points for the derivation of regression equations.

An important region within the vertical temperature profile is the thermocline. In practical terms, its depth, strength and gradient strongly influence the propagation of underwater sound. The prediction of this structure by use of only sea surface temperature would greatly enhance ASW capability. Normally, within the Northeast Pacific, the correlation between SST and thermocline depth is not very high; however, in the Transition Zone with uniformly changing structure a reasonable predictability can be obtained. The thermocline variables (DT5, DT15, DT50, DT100) all provided trends from which SST-related values were computed to define the thermal structure. Overall, the most precisely predicted region of the temperature profile was the thermocline. The depth may have varied due to internal waves, but the negative temperature gradient was accurate and realistic when compared to the observed structure.

B. RECOMMENDATIONS

In future research of this method, an expanded set of vertical temperature data from parallel or bisecting tracks should be established as the data base for statistical analysis. The addition of an east-west track of data would provide latitudinal trends which could also be used in the predicted temperature profiles. As in any data aquisition, a consideration as to the minimum amount of data points to determine the thermal structure statistically should be made. Meanwhile, a number of no less than 20 profiles over a distance of 1000 km with spacing between points not to exceed 50 km is recommended.

Other suggestions for model improvement include adding dynamical and thermodynamical variables such as wind speed, direction and duration, air temperature, radiation flux, and other atmospheric effects which could alter the ocean thermal structure. Most of these factors can be determined by remote sensing; data from other satellite sensors, such as an altimeter, SAR and Coastal Zone Color Scanner which can measure sea surface signatures, should also be included.

To determine the limitation of accuracy for the statistically-determined profile method, more stringent tests

should be conducted which increase the spatial and time factors. In certain ocean regions one could possibly maintain reasonable accuracies within hundreds of kilometers and several weeks duration from the acquisition of thermal data. Different ocean locations should be analyzed and tested to determine the possible regions where the thermal profiles vary in an orderly fashion which can be easily modeled. Areas where mesoscale features, such as eddies and fronts, are constantly altering the water column by advective processes would be poor candidates for this method.

Another recommendation is to test in other seasons of the year to determine if the statistical approach would apply. The difference in the vertical thermal structure from the heating to cooling season is so great that possibly there could be only a certain window of time that allows the sea surface temperature to define the subsurface structure.

Finally, a method for determining the occurrence of large temperature inversions in the Subarctic and Transition Regions is needed. This important thermal feature, because of its variation in magnitude, depth and location, affects greatly the propagation of sound by forming a sound channel immediately below the thermocline. If this structure can be

predicted then the full potential of the statistical method of determining subsurface thermal structure from sea surface temperature would be realized.

APPENDIX A

THERMAL VARIABLES VERSUS LATITUDE/DISTANCE ALONG TRACK

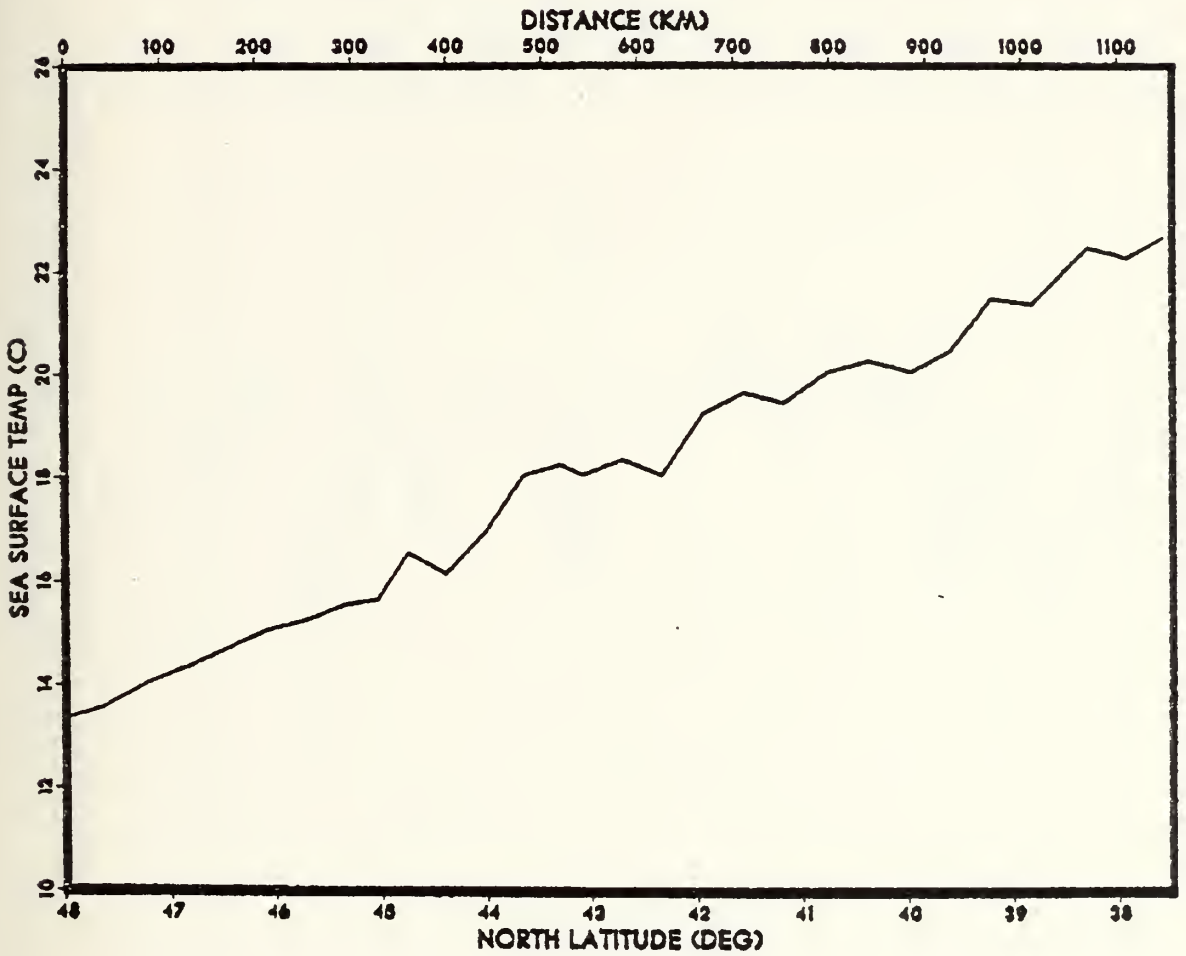

Figure A.1. SST Versus Latitude/Distance.

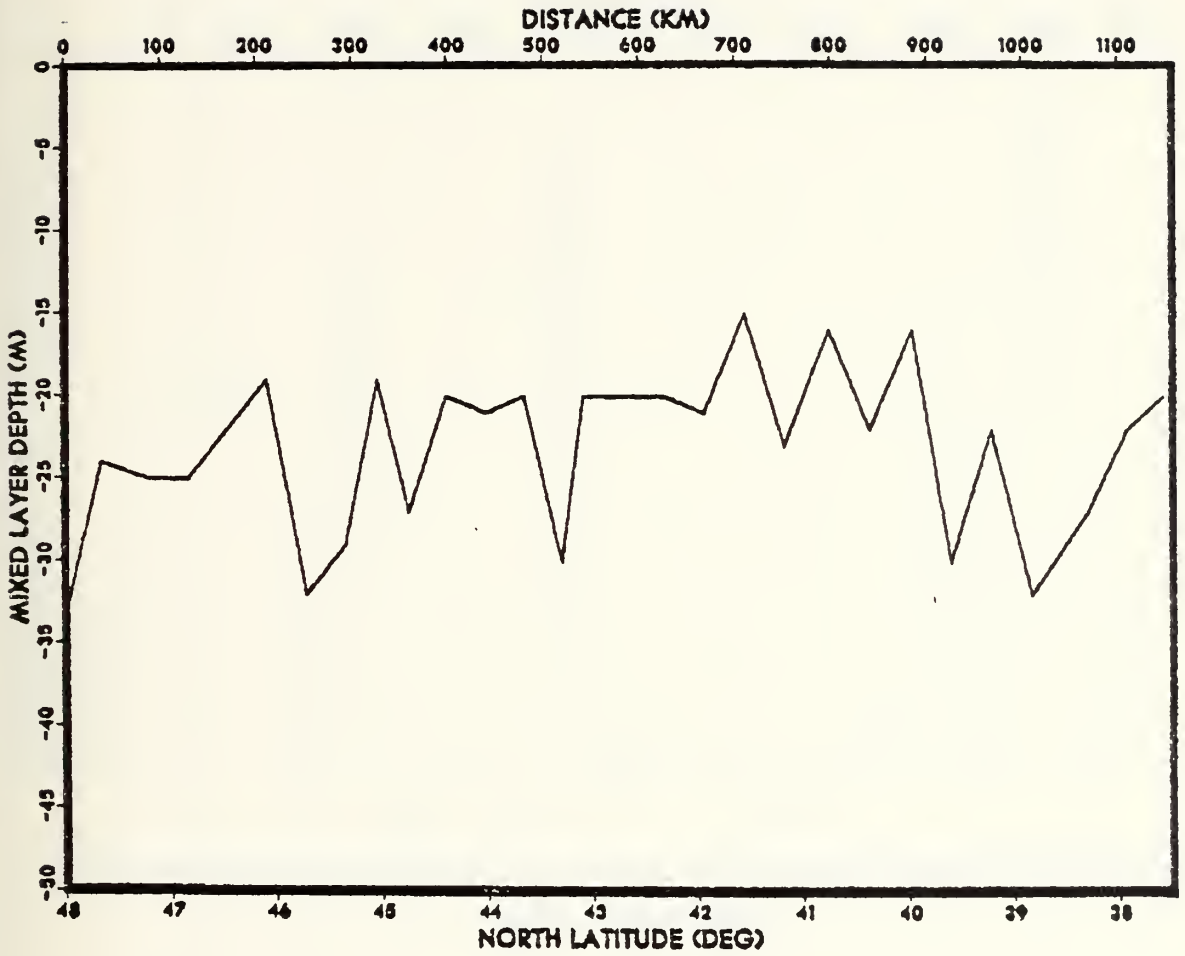

Figure A.2. MLD Versus Latitude/Distance.

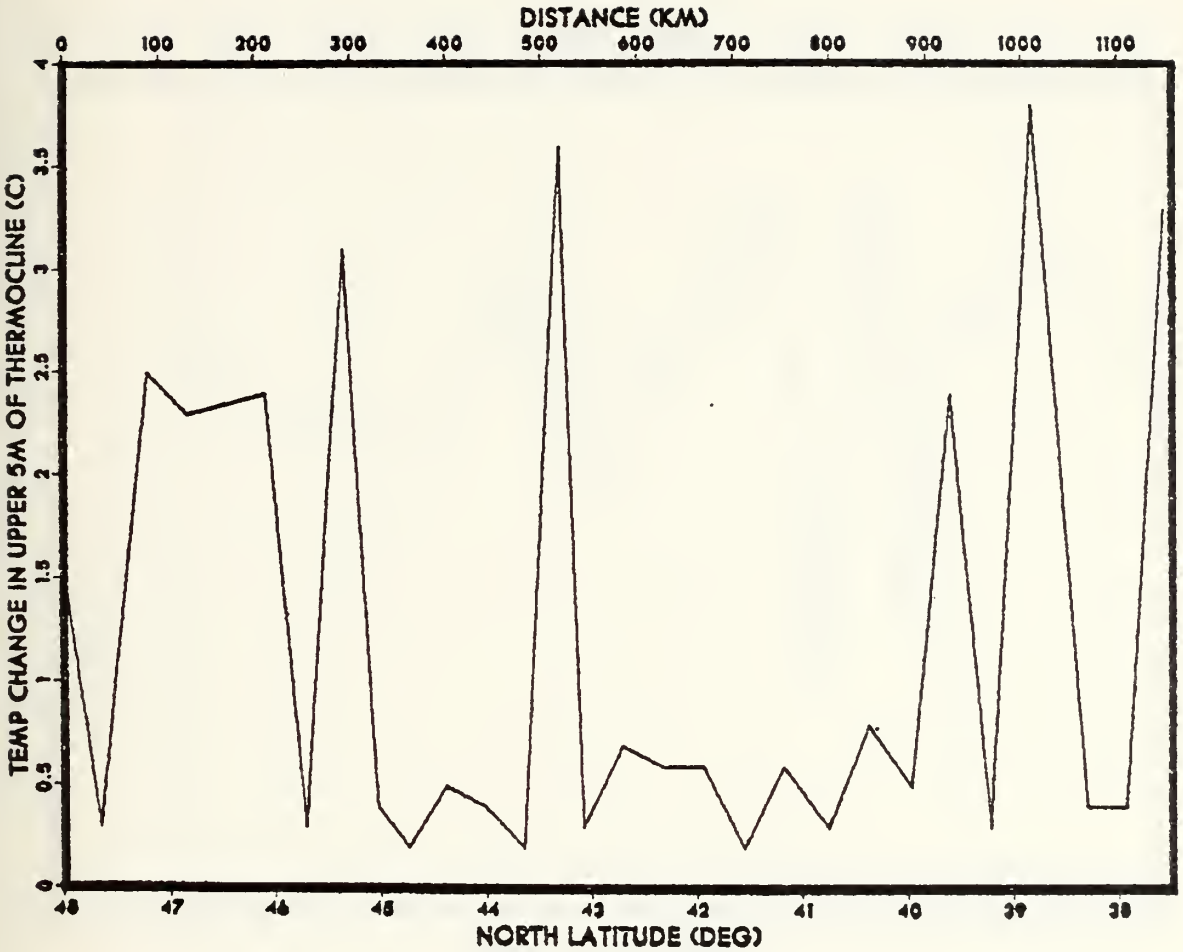

Figure A.3. DT5 Versus Latitude/Distance.

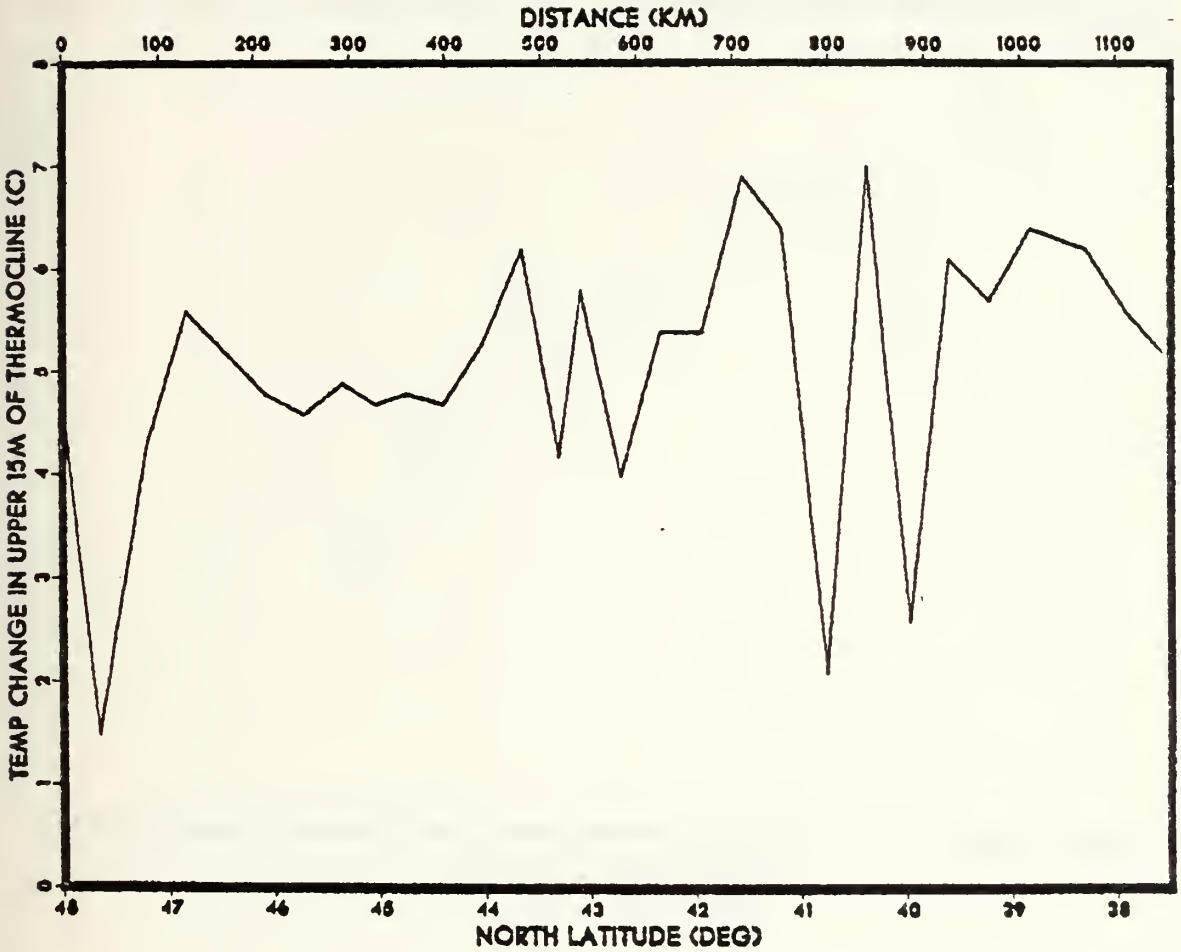

Figure A.4. DT15 Versus Latitude/Distance.

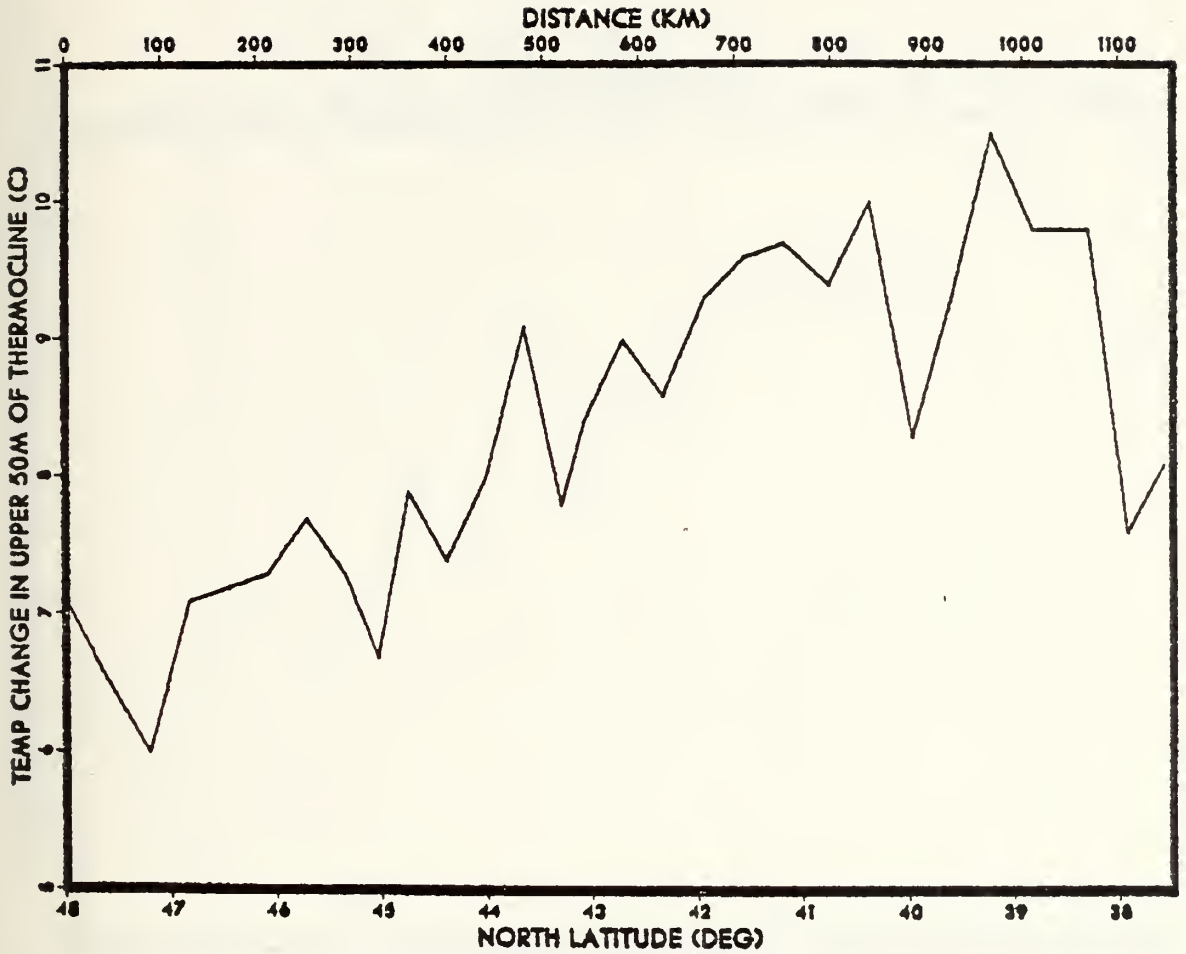

Figure A.5. DT50 Versus Latitude/Distance.

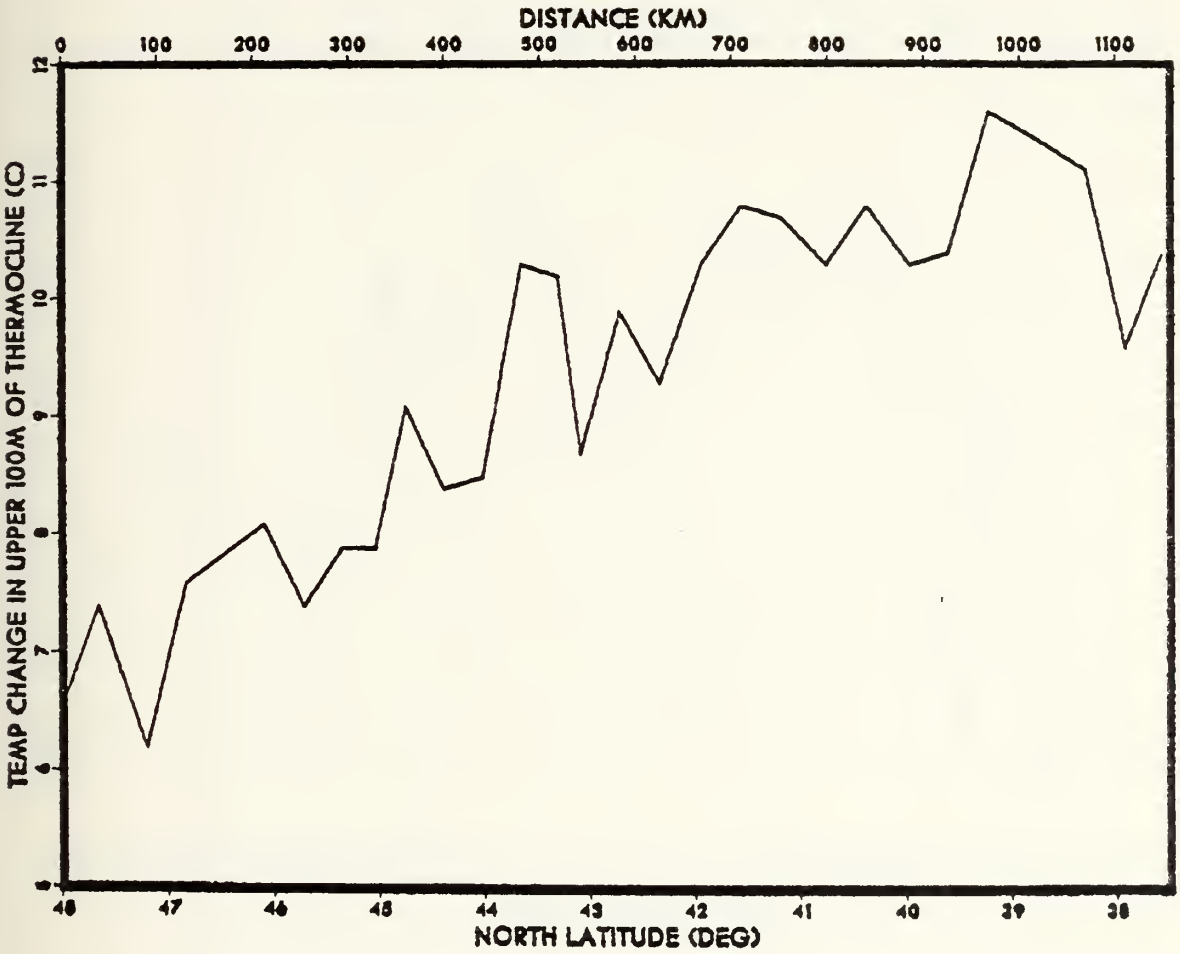

Figure A.6. DT100 Versus Latitude/Distance.

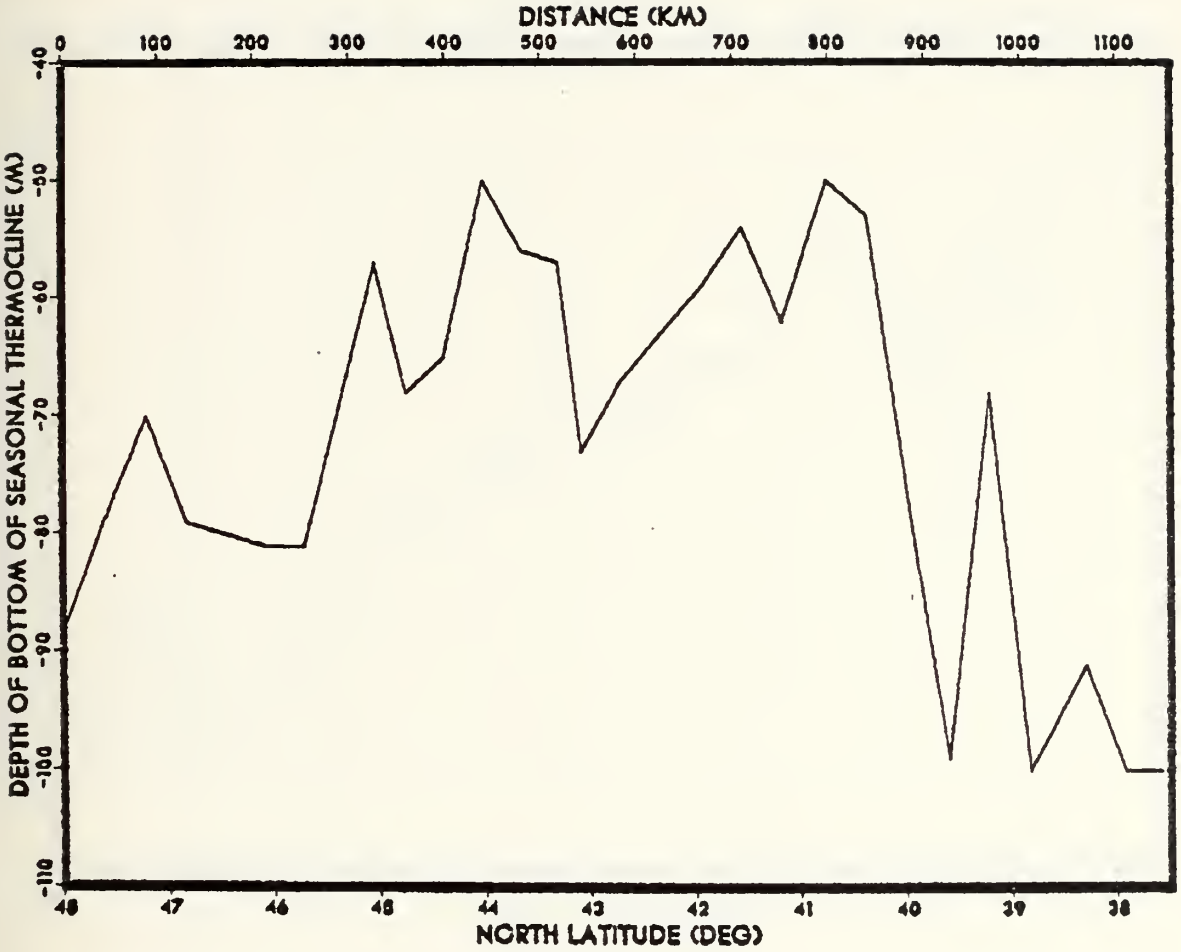

Figure A.7. BOT Versus Latitude/Distance.

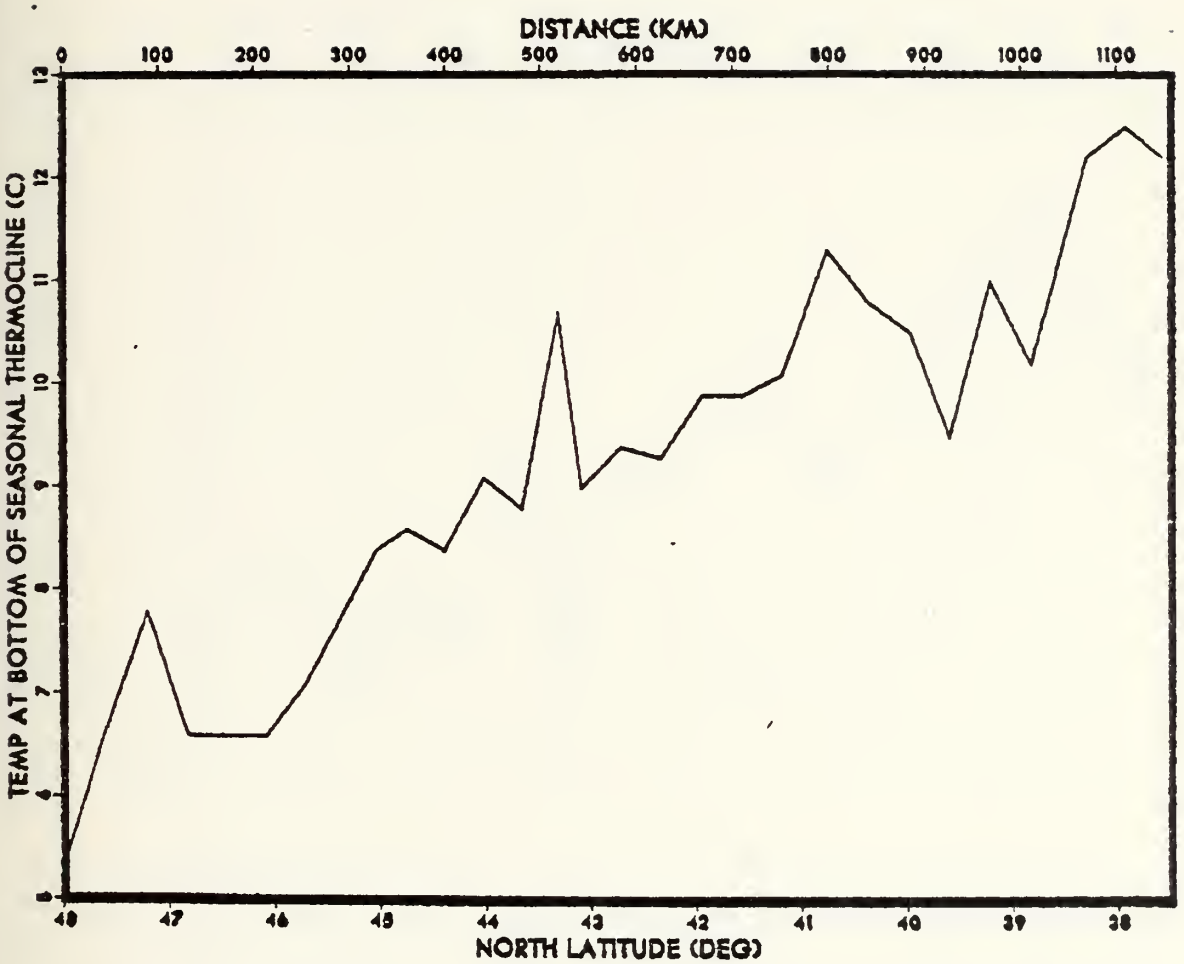

Figure A.8. TBCT Versus Latitude/Distance.

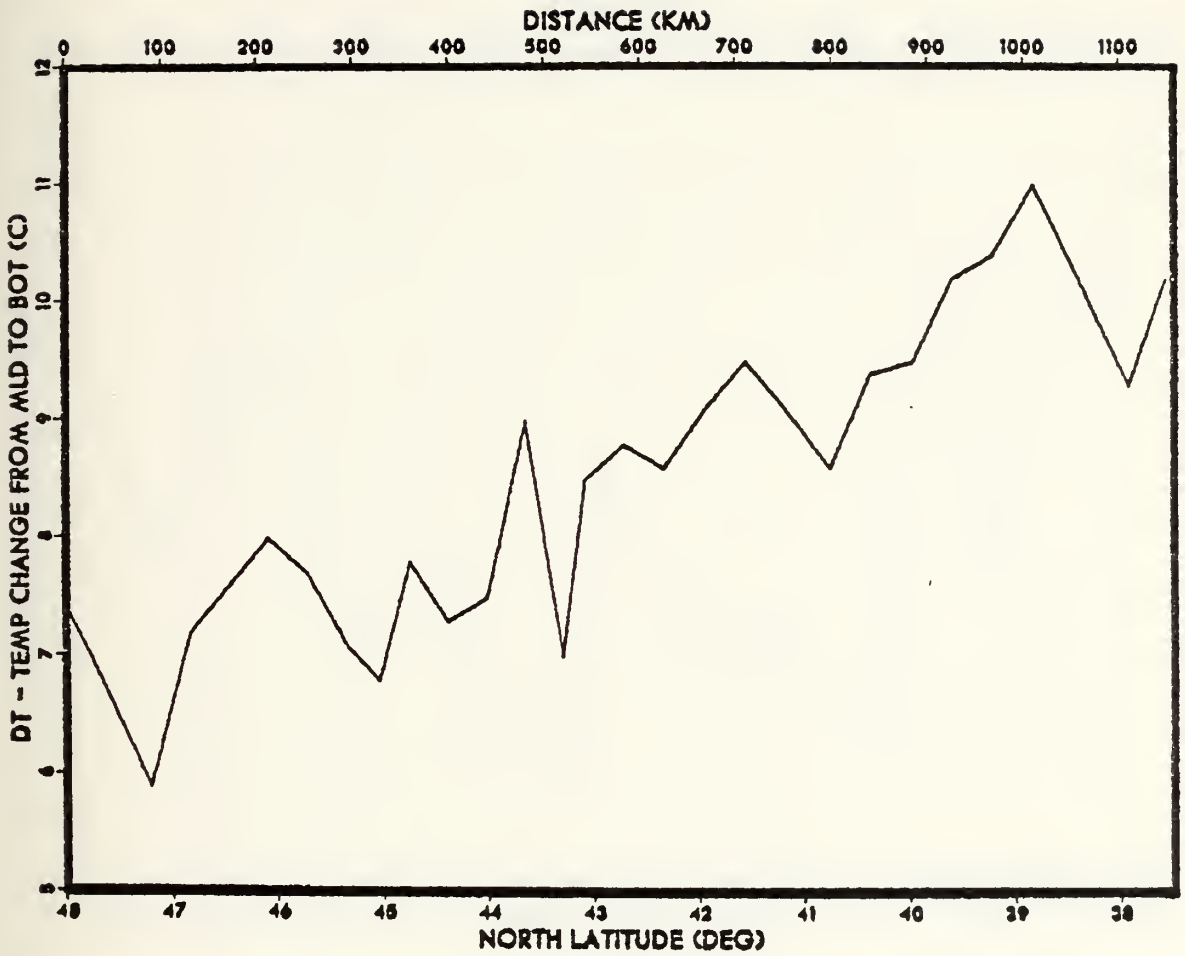

Figure A.9. DT Versus Latitude/Distance.

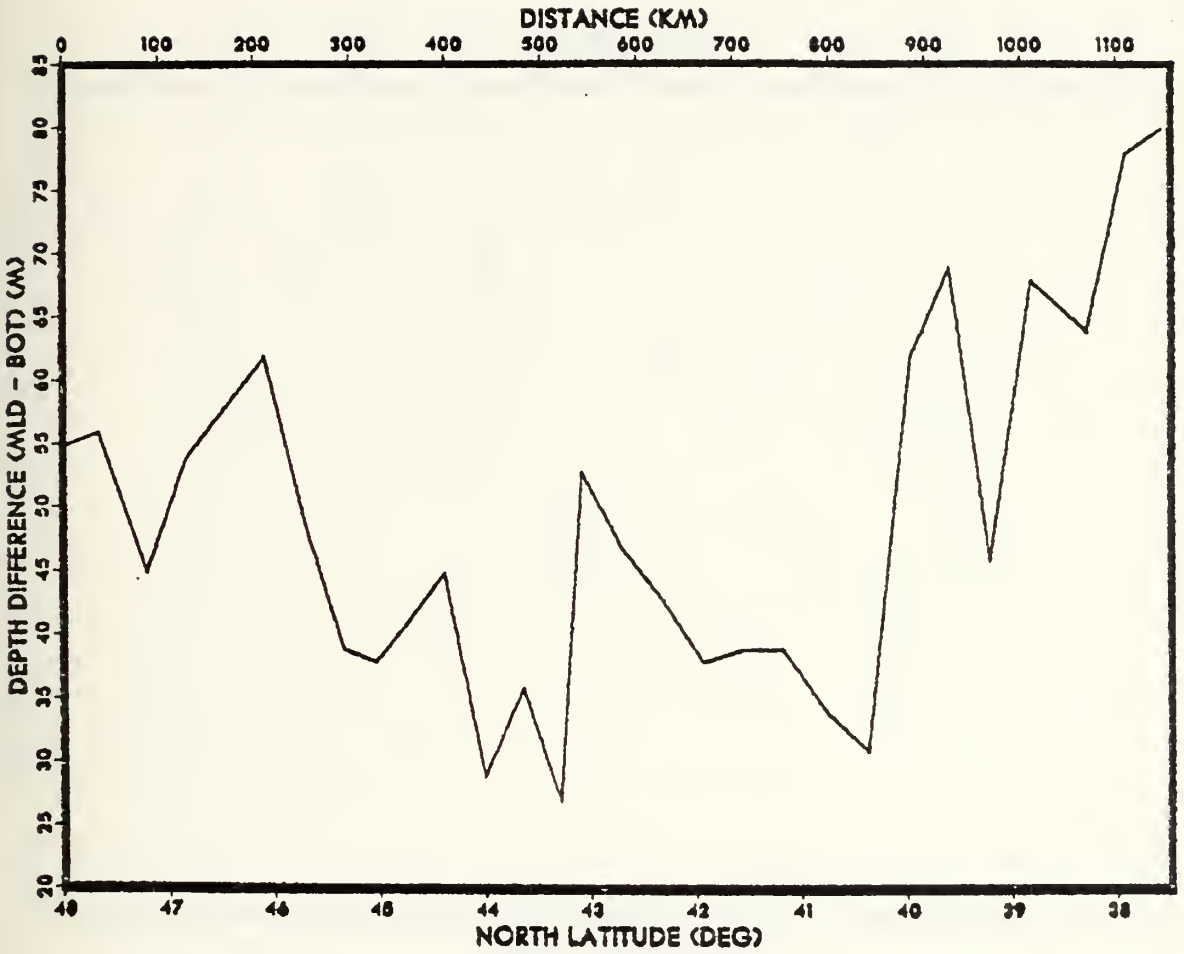

Figure A.10. DZ Versus Latitude/Distance.

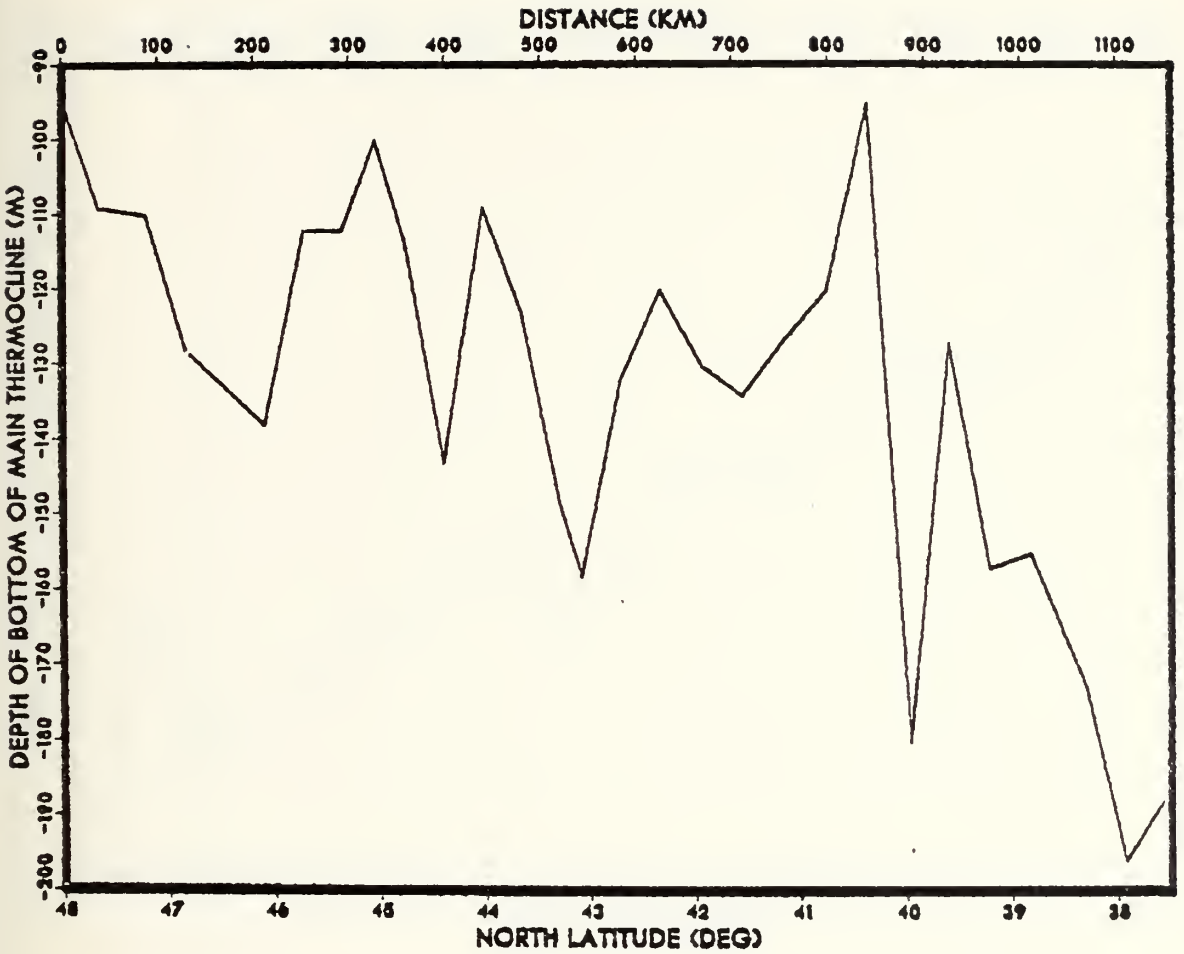

Figure A.11. BUZ Versus Latitude/Distance.

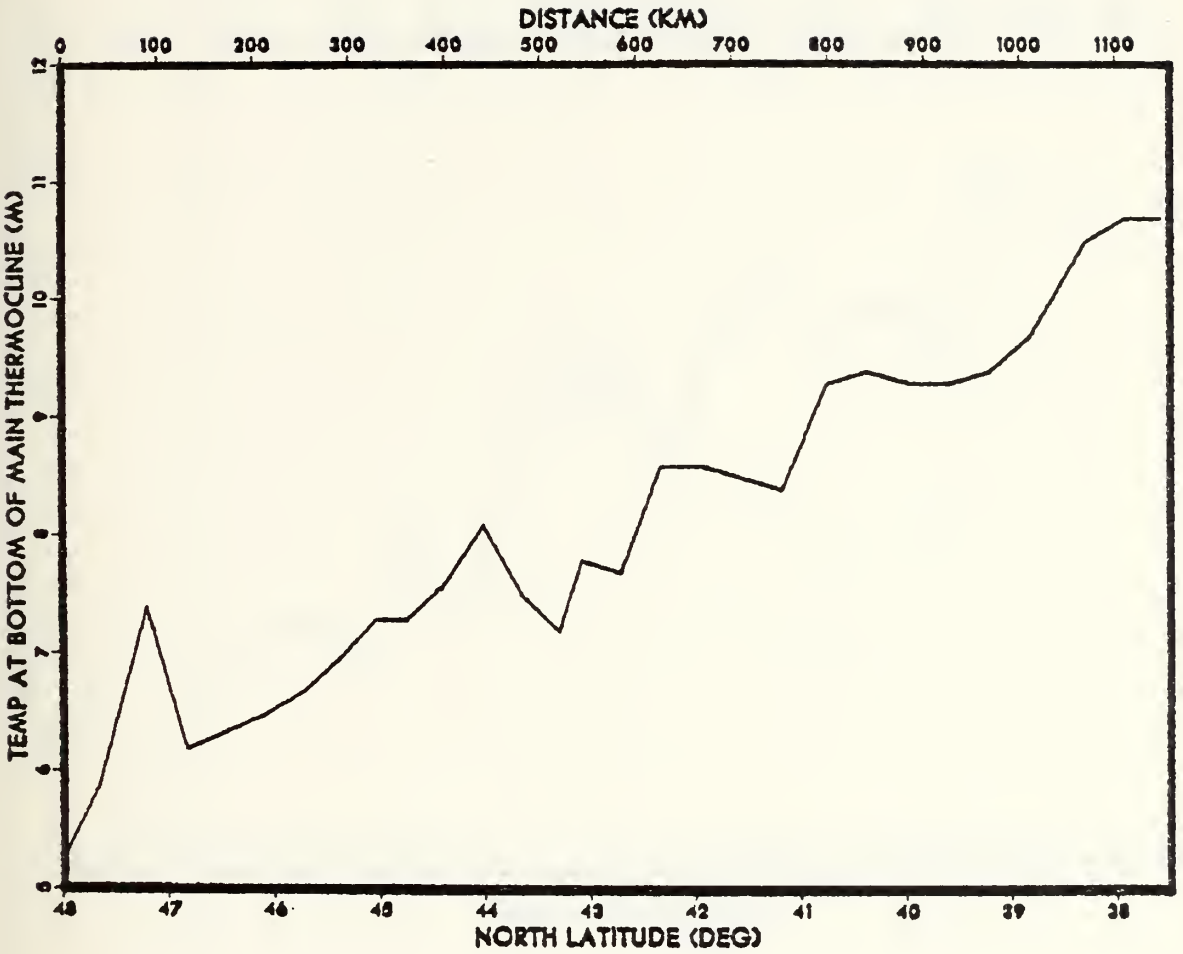

Figure A.12. TBUZ Versus Latitude/Distance.

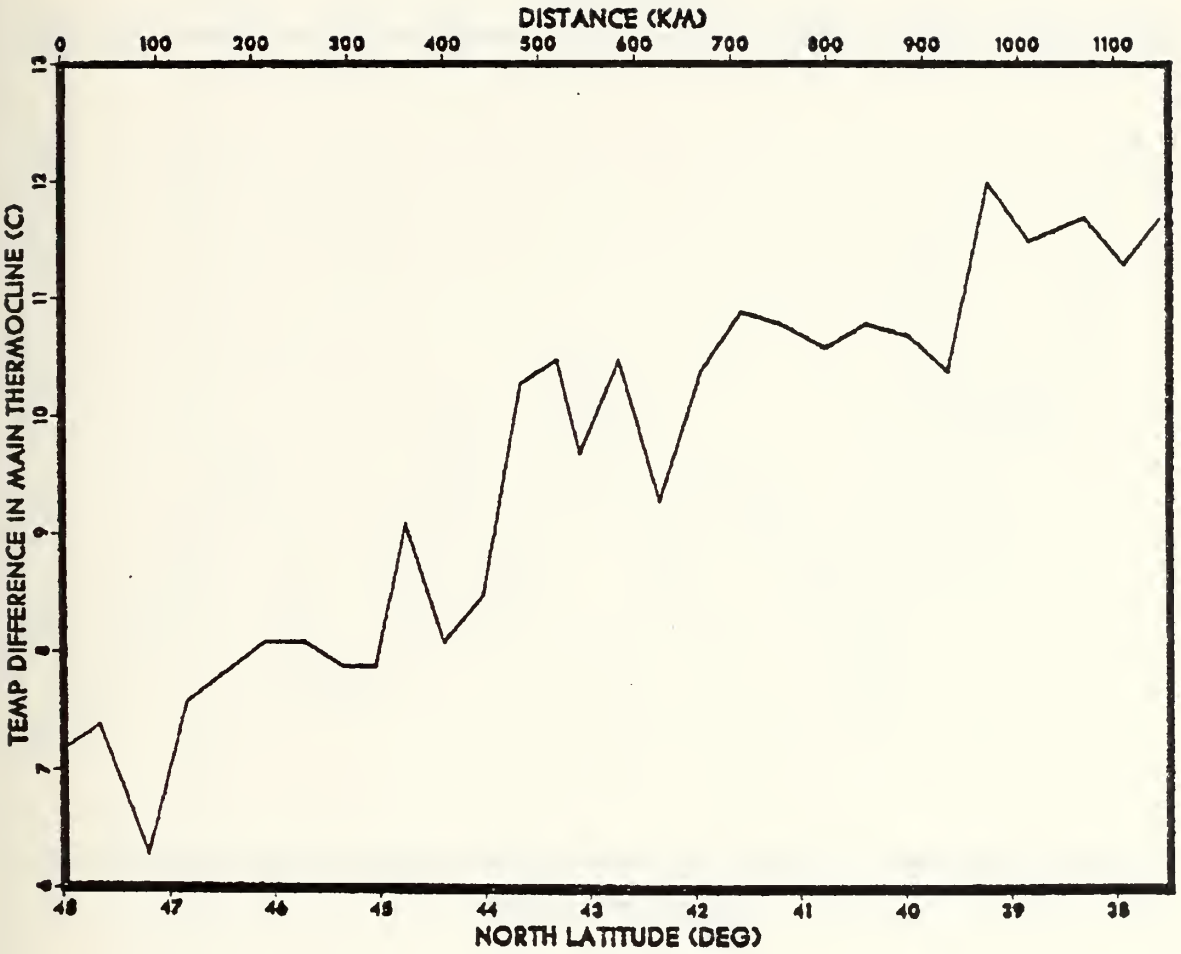

Figure A.13. DTBUZ Versus Latitude/Distance.

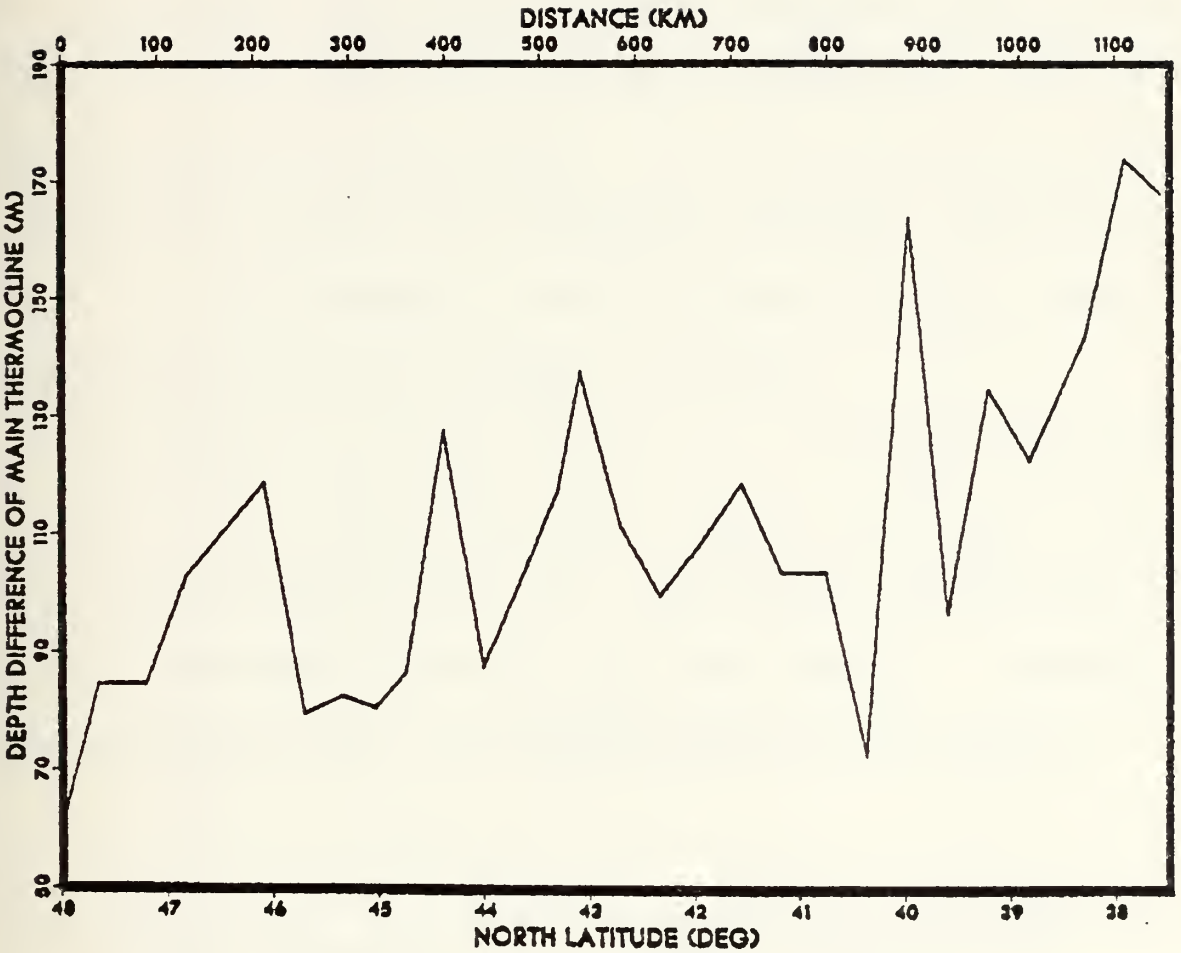

Figure A.14. DZBUZ Versus Latitude/Distance.

APPENDIX B

BIOMEDICAL COMPUTER PROGRAMS (DIXON AND BROWN, 1979)

The BIOMED statistical computer programs were utilized because of the simple and flexible programming it provided in analyzing the thermal data. In constructing the vertical temperature profiles, the statistical analysis required correlation and regression equation computation and scatter diagram plotting of the thermal variables.

The program initially selected was 'Stepwise Regression - P2R.' This program computes simple statistics, i.e., mean, standard deviation, etc., correlation coefficients and linear regression equations for any number of variables. The statistics used in the computations are defined as:

- mean $\bar{X} = \sum X_j / N$
- standard deviation $S = \left[\sum (X_j - \bar{X})^2 / (N-1) \right]^{1/2}$
- the correlation coefficient between two variables

$$r = \frac{\sum (X_j - \bar{X})(y_j - \bar{y})}{\left[\sum (X_j - \bar{X})^2 \sum (y_j - \bar{y})^2 \right]^{1/2}}$$

In simple linear regression analysis, where there is only one independent variable, the coefficients are determined by a least squares method. The form of the equations are:

$y = A + Bx$ (where A and B are the linear coefficients)

The BIOMED computer program used to print the regional scatter diagrams is titled 'Bivariate (Scatter) Plots - P6D.' Regression equations for regressing variable x on y and y on x can be requested along with the intersections of the regression lines with the axis of the plot. This was useful in analyzing the data to determine the best fit for the various regions.

APPENDIX C

REGIONAL SCATTER DIAGRAMS - SST VERSUS THERMAL VARIABLES

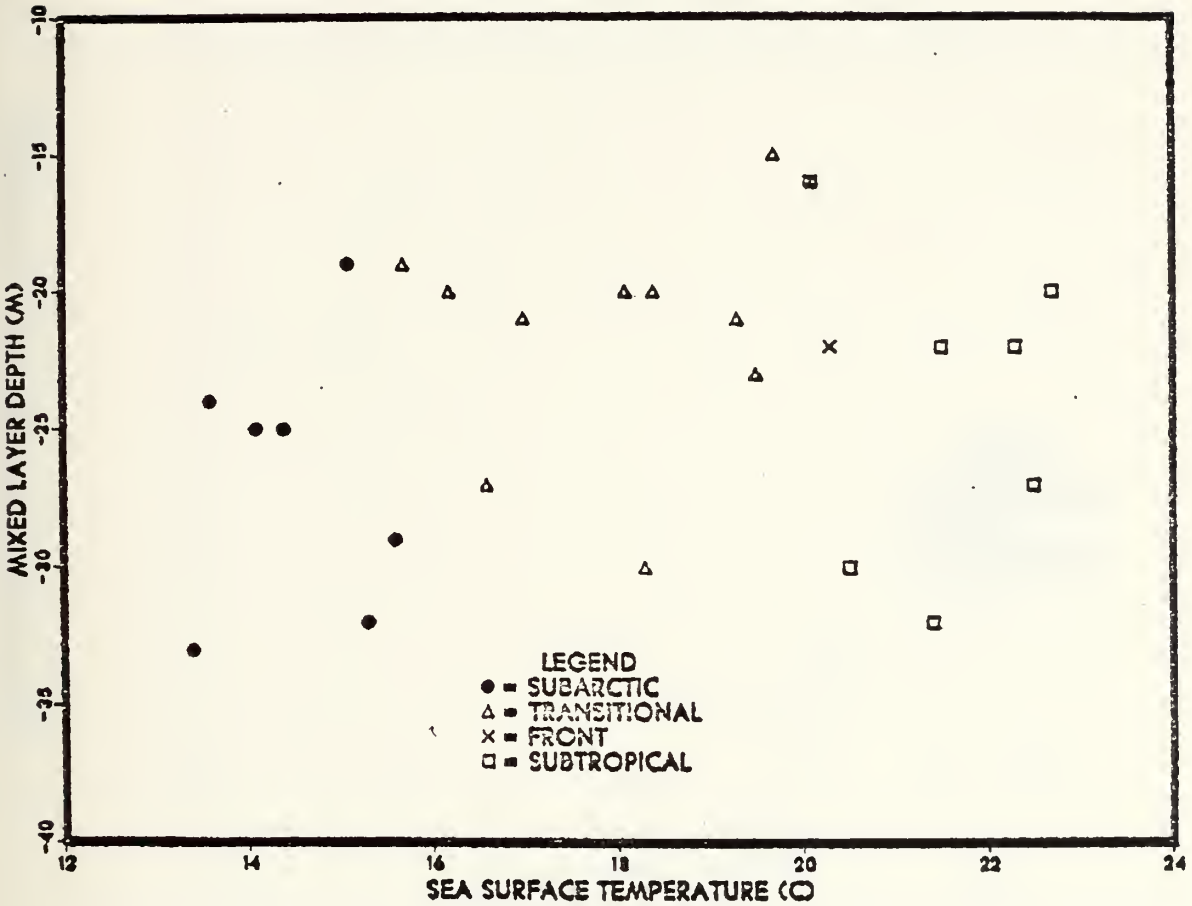

Figure C.1. Regional Scatter Diagram - SST Versus MLD.

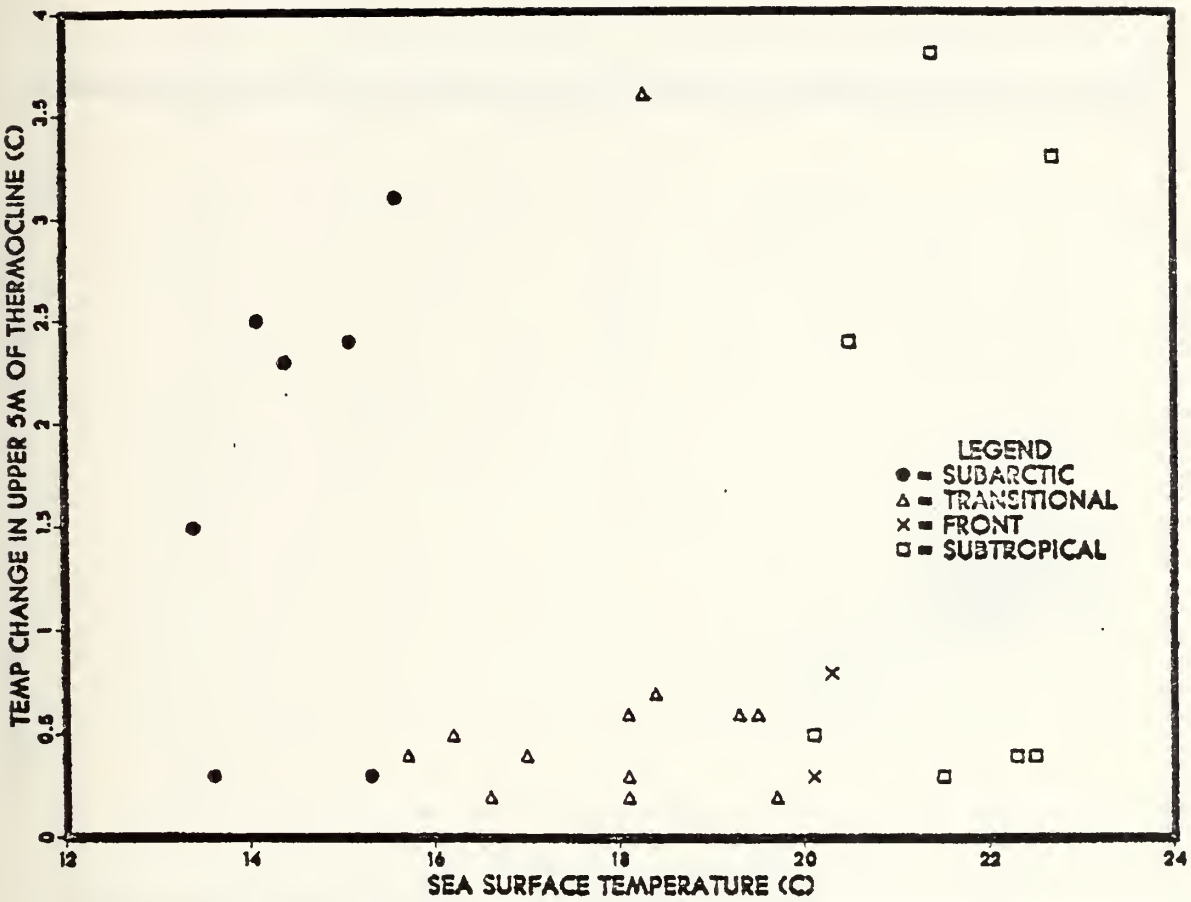

Figure C.2. Regional Scatter Diagram - SST Versus DT5.

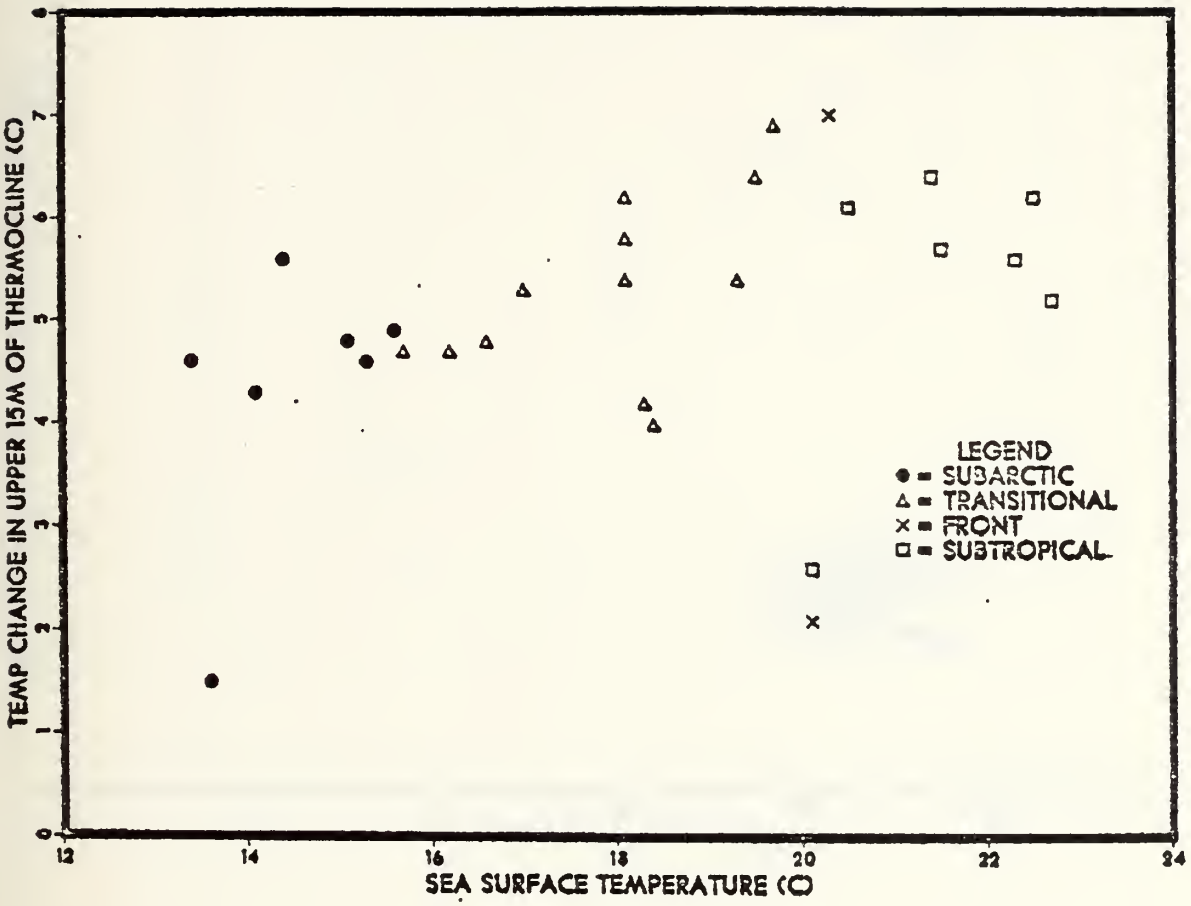

Figure C.3. Regional Scatter Diagram - SST Versus DT15.

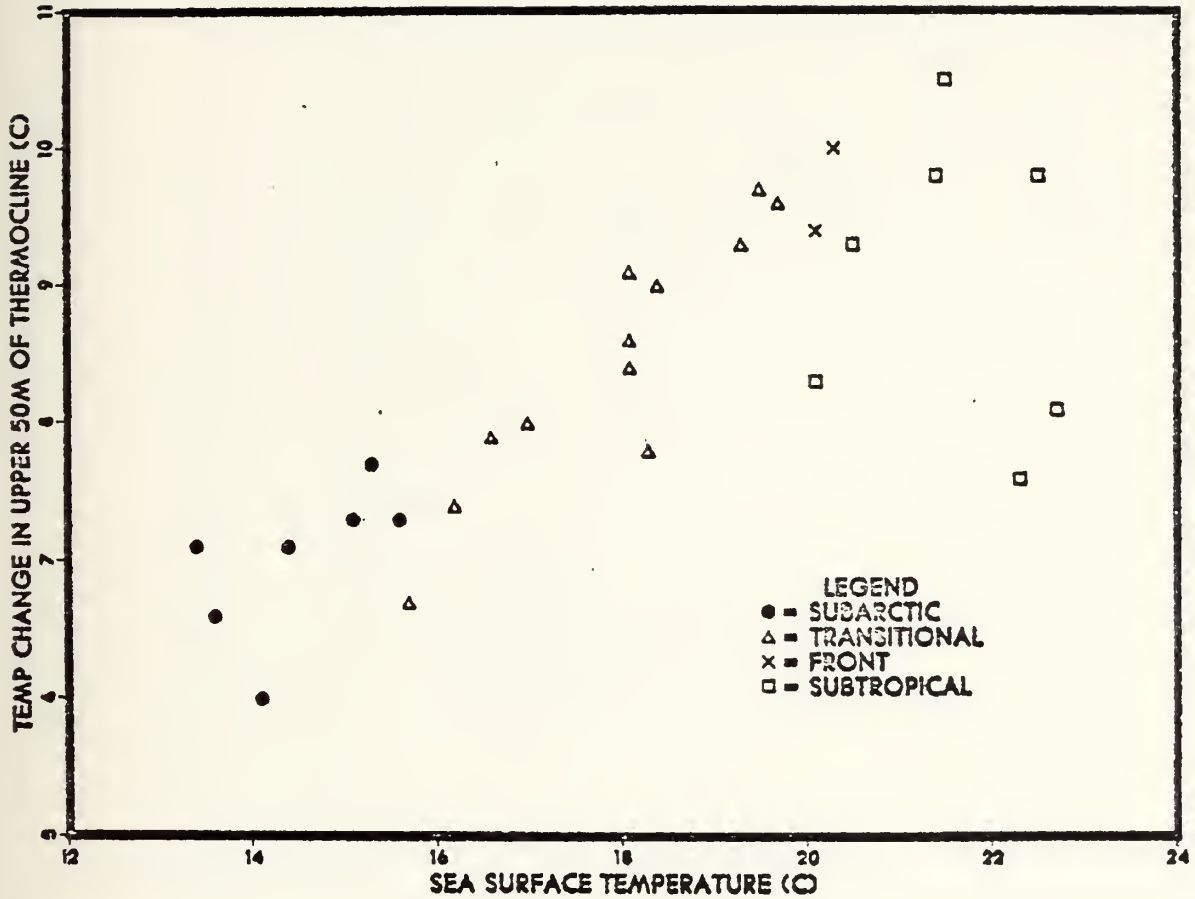

Figure C.4. Regional Scatter Diagram - SST Versus DT50.

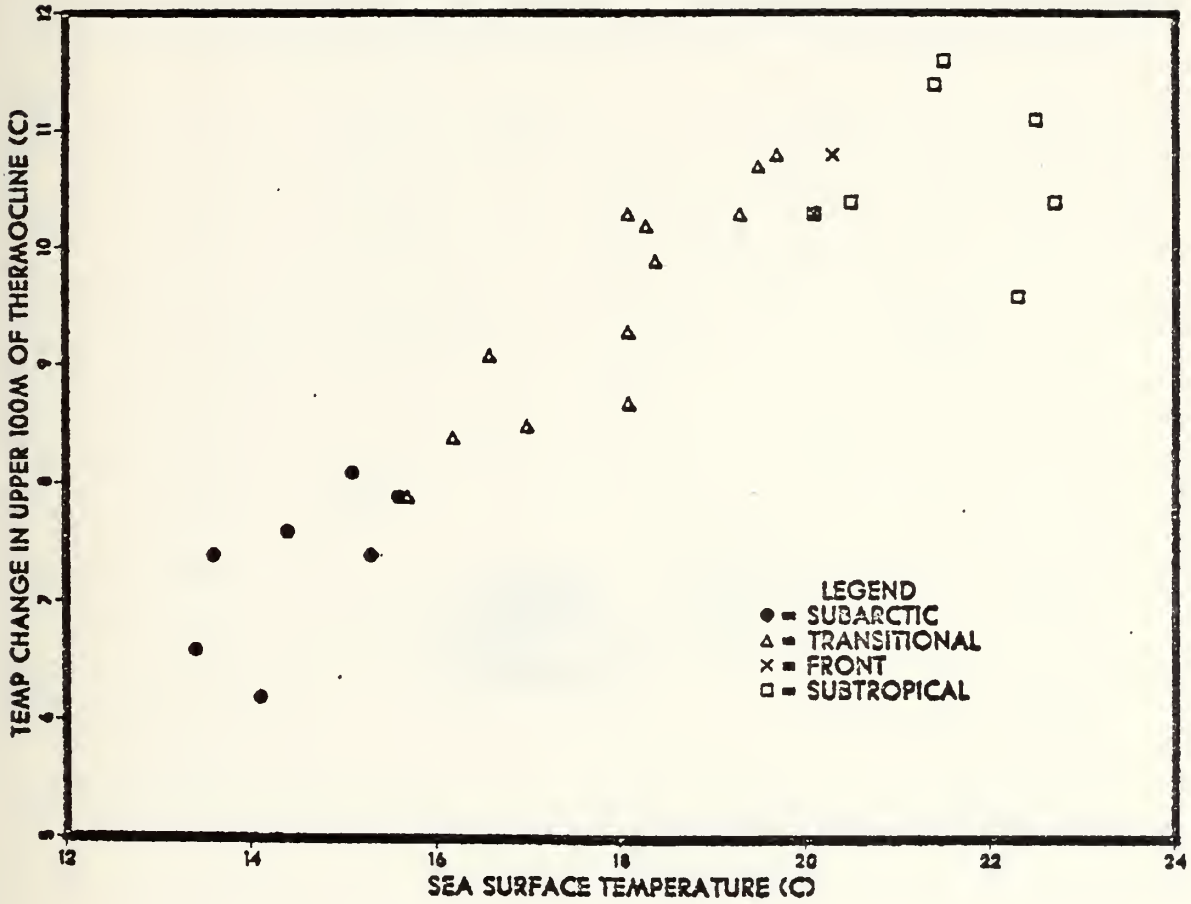

Figure C.5. Regional Scatter Diagram - SST Versus DT100.

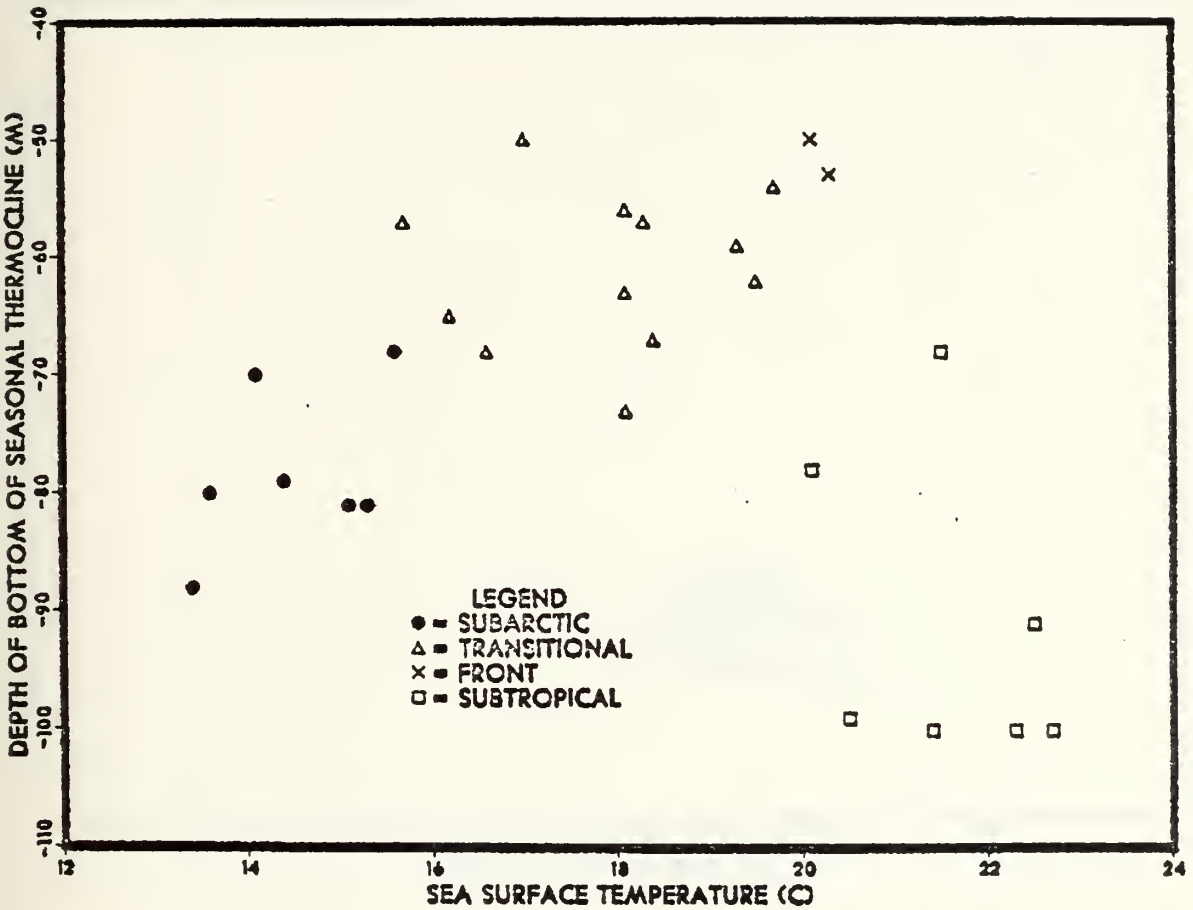

Figure C.6. Regional Scatter Diagram - SST Versus BOT.

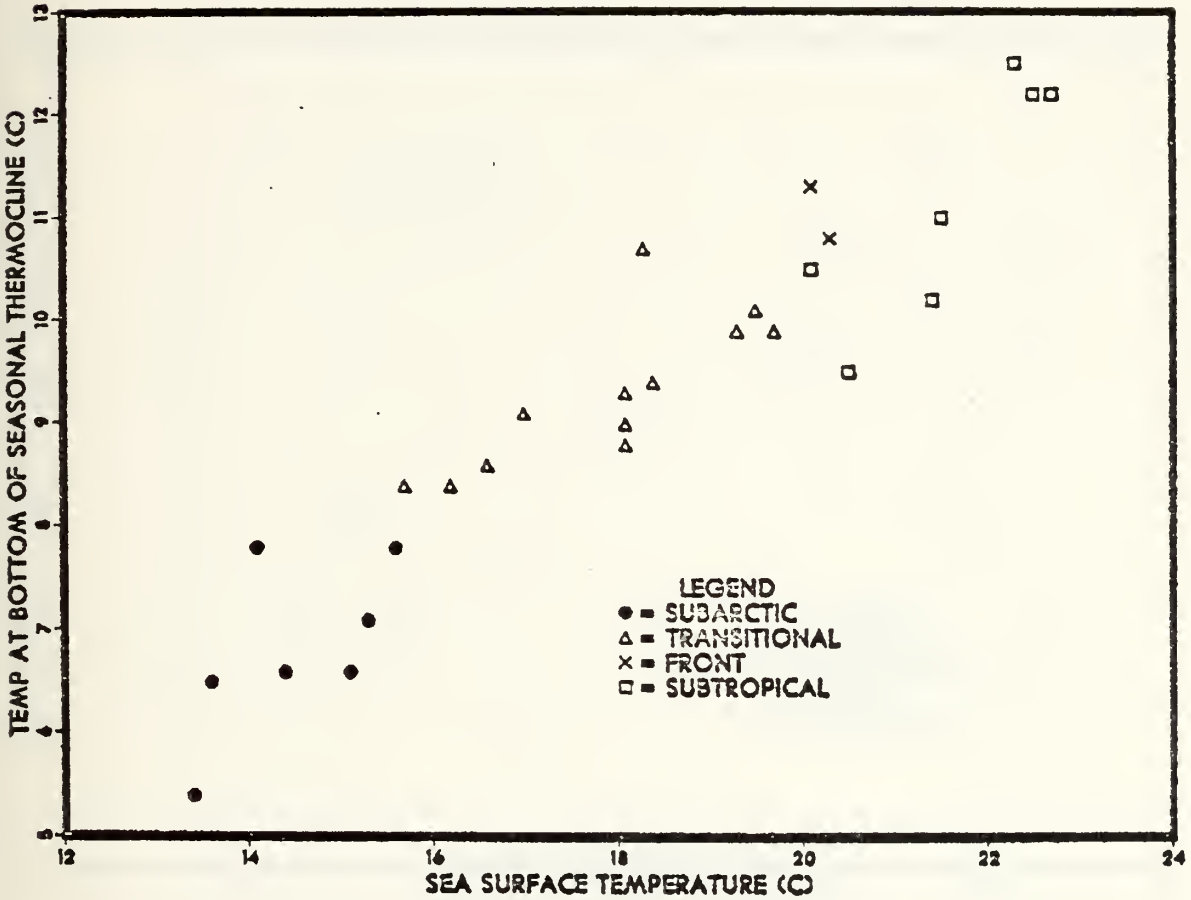

Figure C.7. Regional Scatter Diagram - SST Versus TBOT.

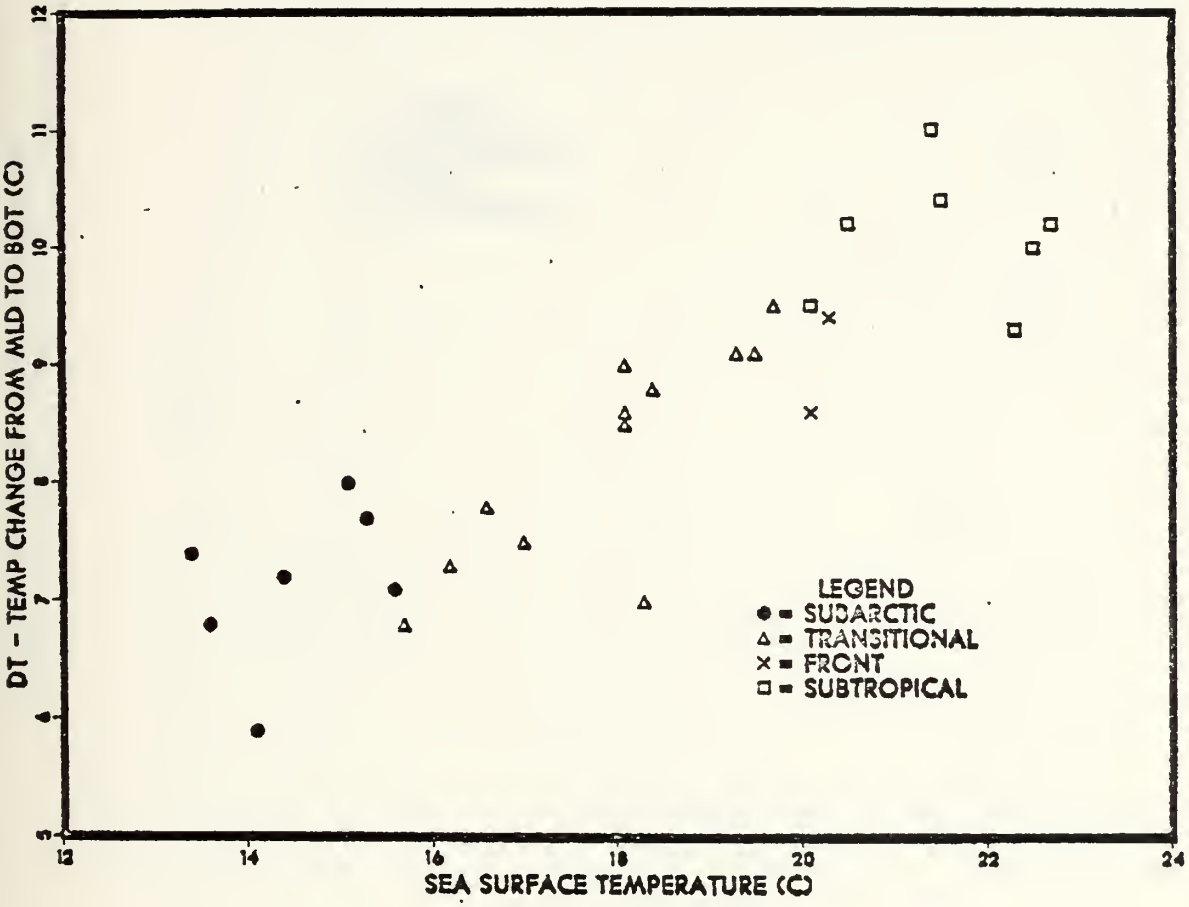

Figure C.8. Regional Scatter Diagram - SST Versus DT.

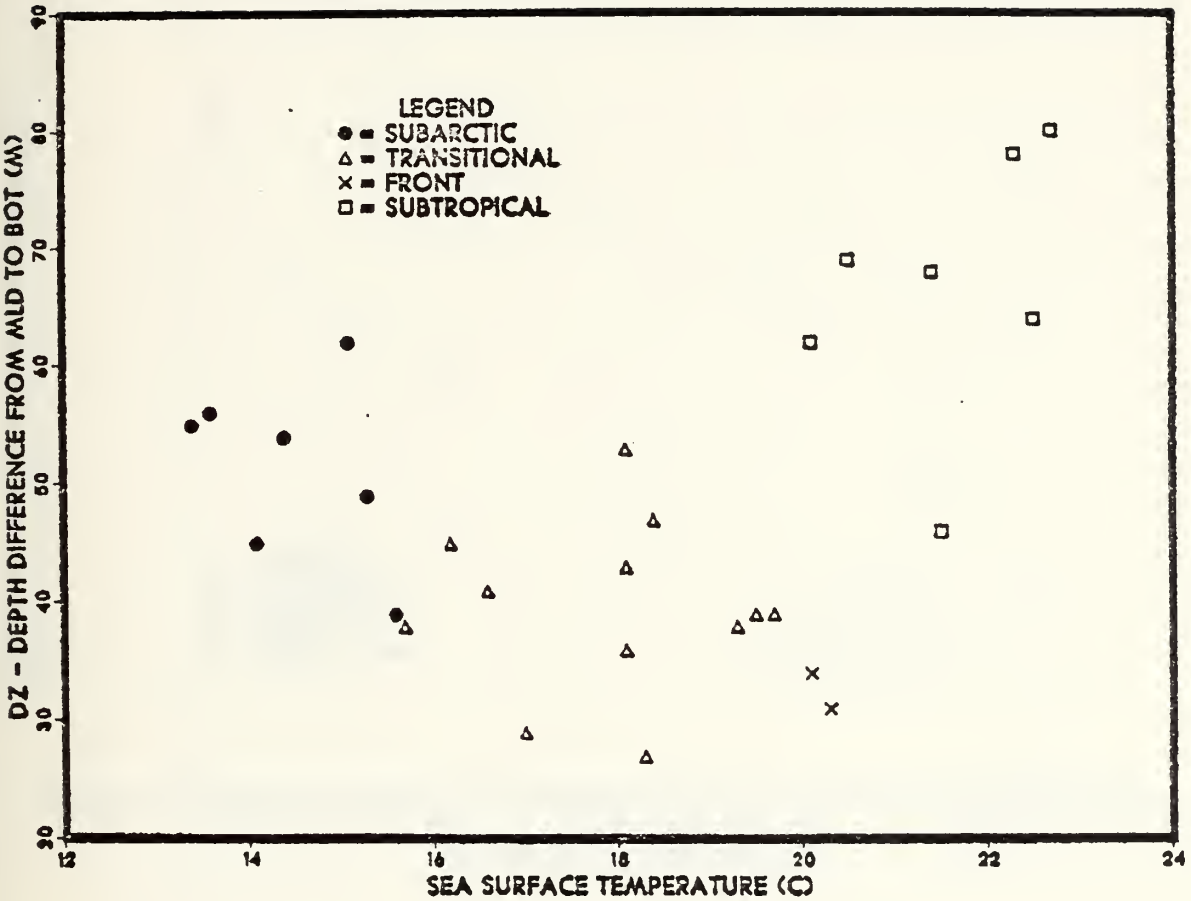

Figure C.9. Regional Scatter Diagram - SST Versus DZ.

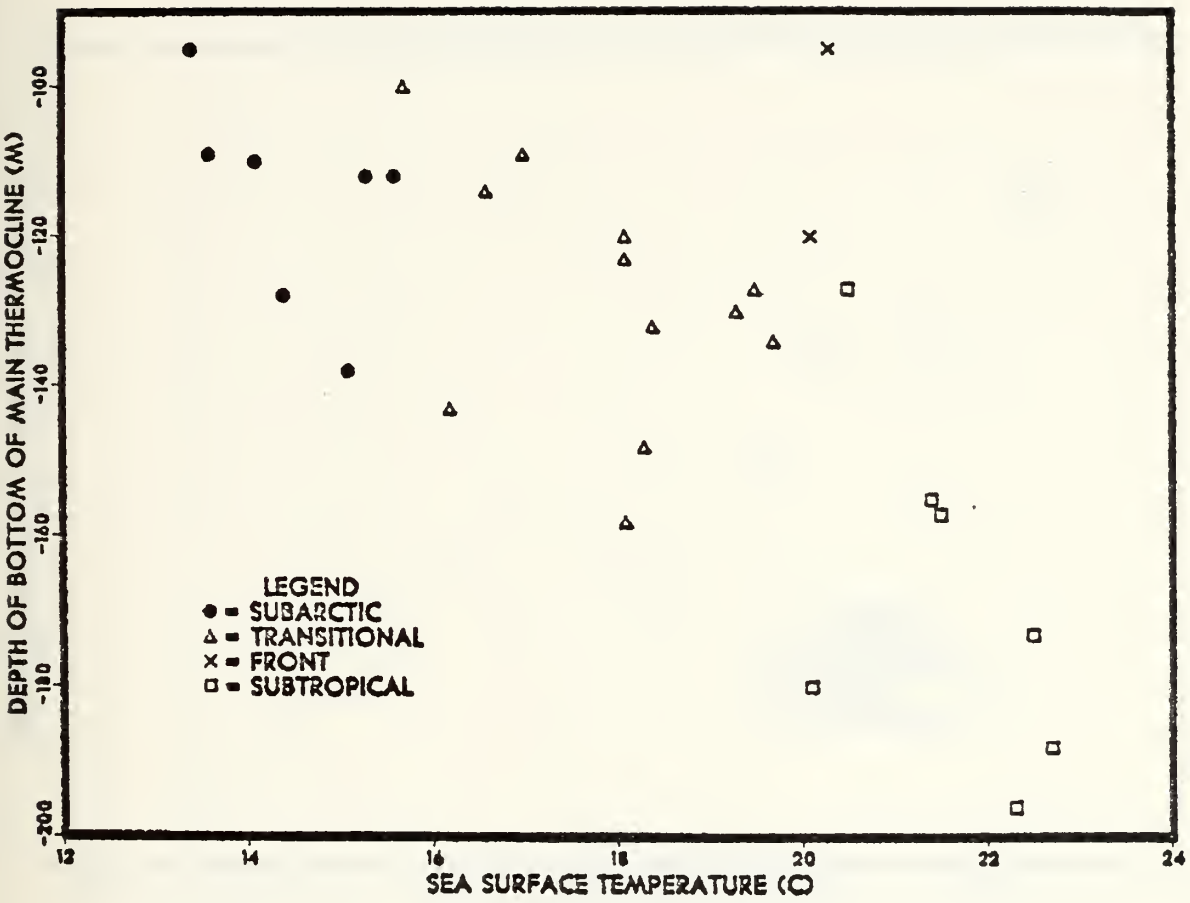

Figure C.10. Regional Scatter Diagram - SST Versus BUZ.

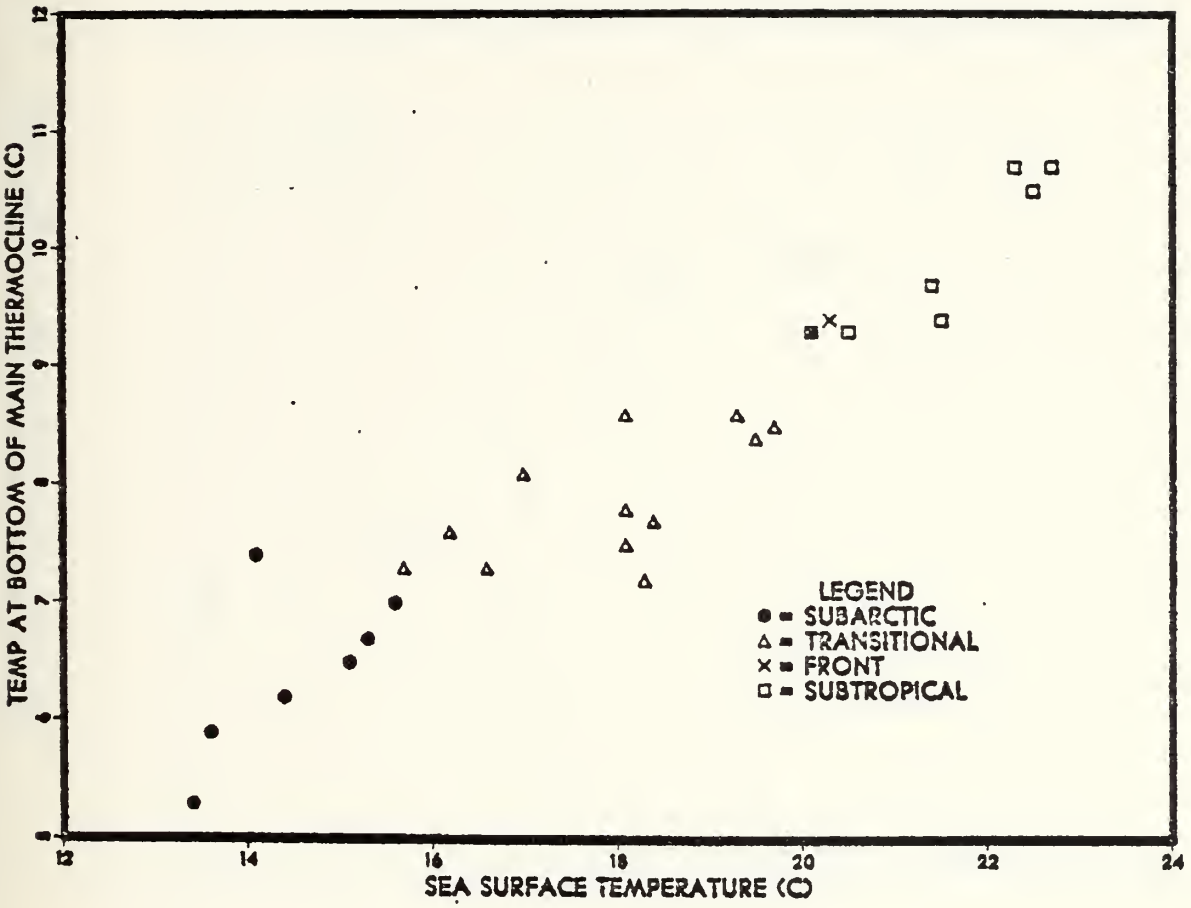

Figure C.11. Regional Scatter Diagram - SST Versus TBUZ.

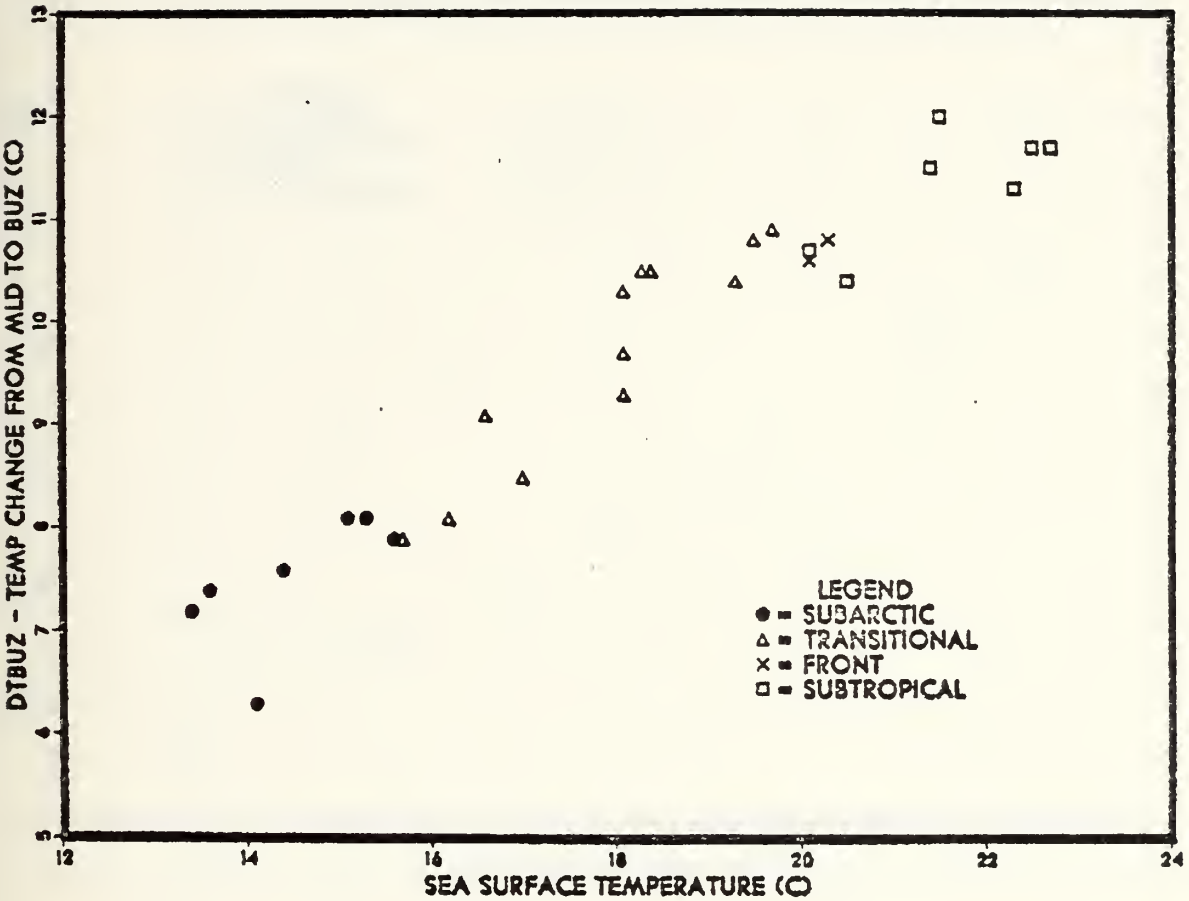

Figure C.12. Regional Scatter Diagram - SST Versus DTBUZ.

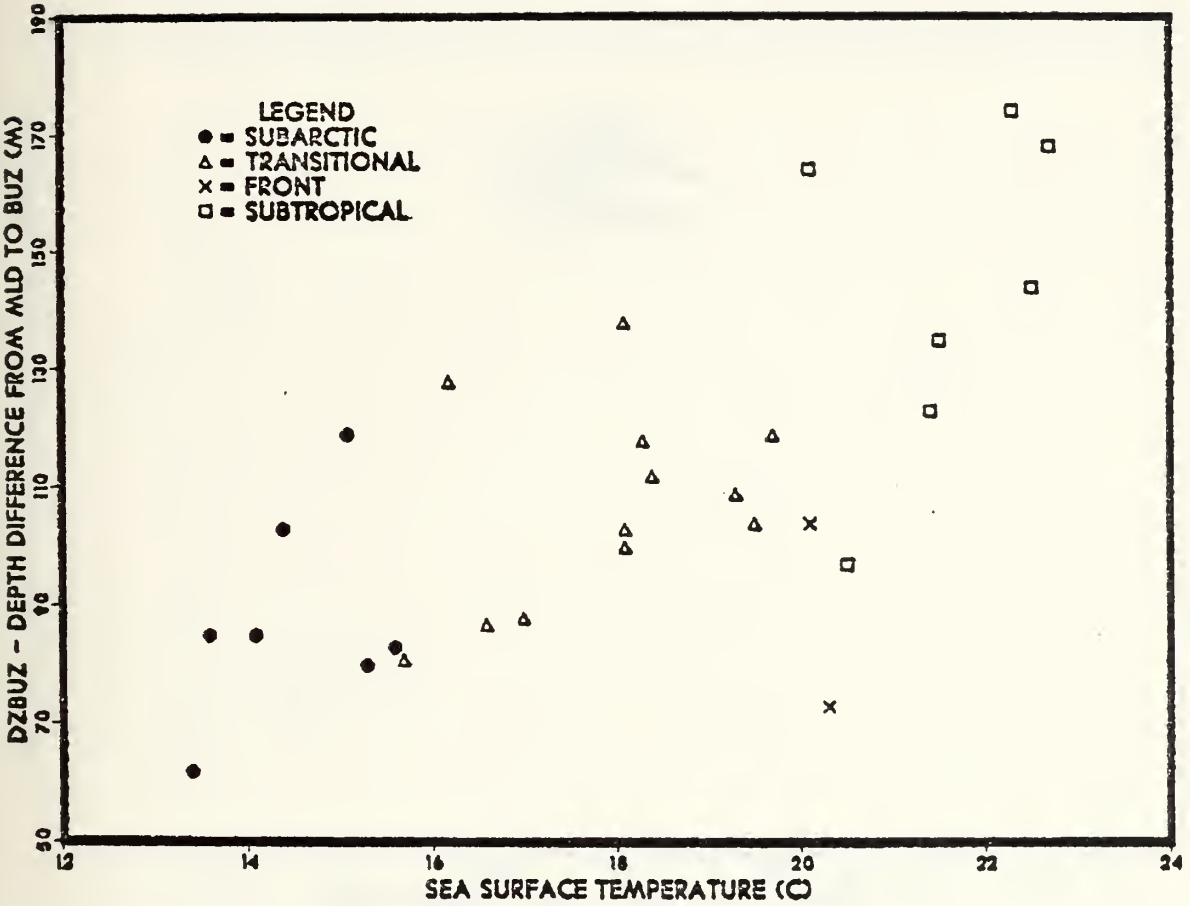

Figure C.13. Regional Scatter Diagram - SST Versus DZBUZ.

APPENDIX D

REGIONAL SCATTER DIAGRAMS - BOT VERSUS THERMAL VARIABLES

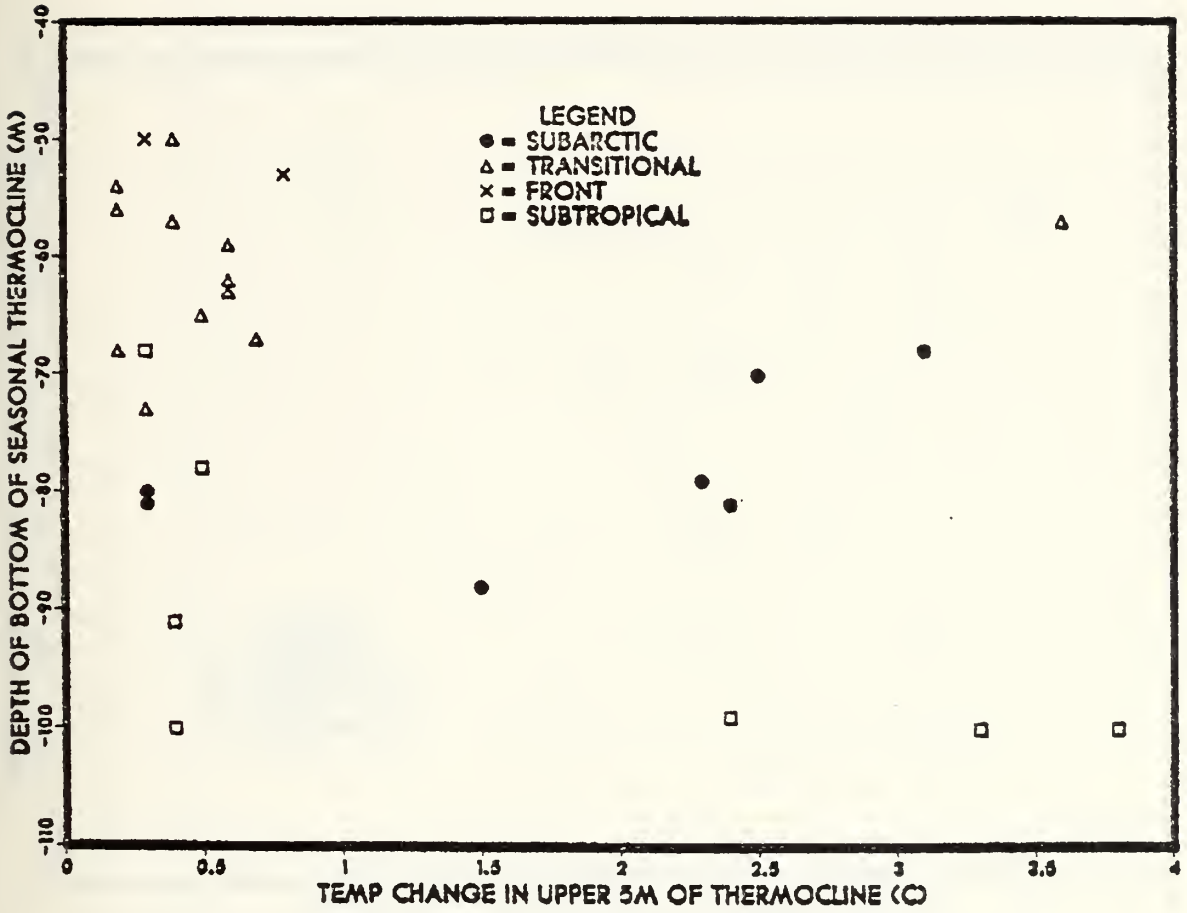

Figure D.1. Regional Scatter Diagram - BOT Versus DT5.

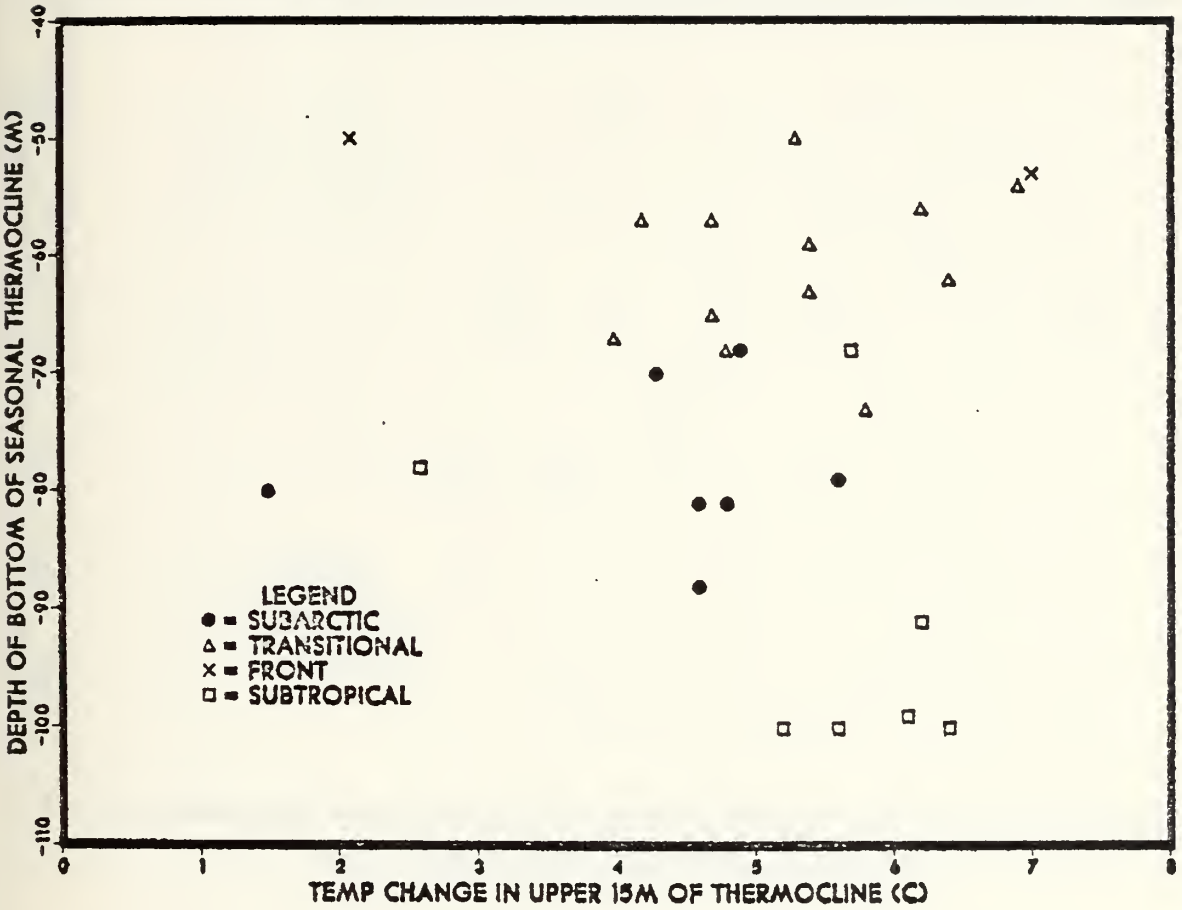

Figure D.2. Regional Scatter Diagram - BOT Versus DT15.

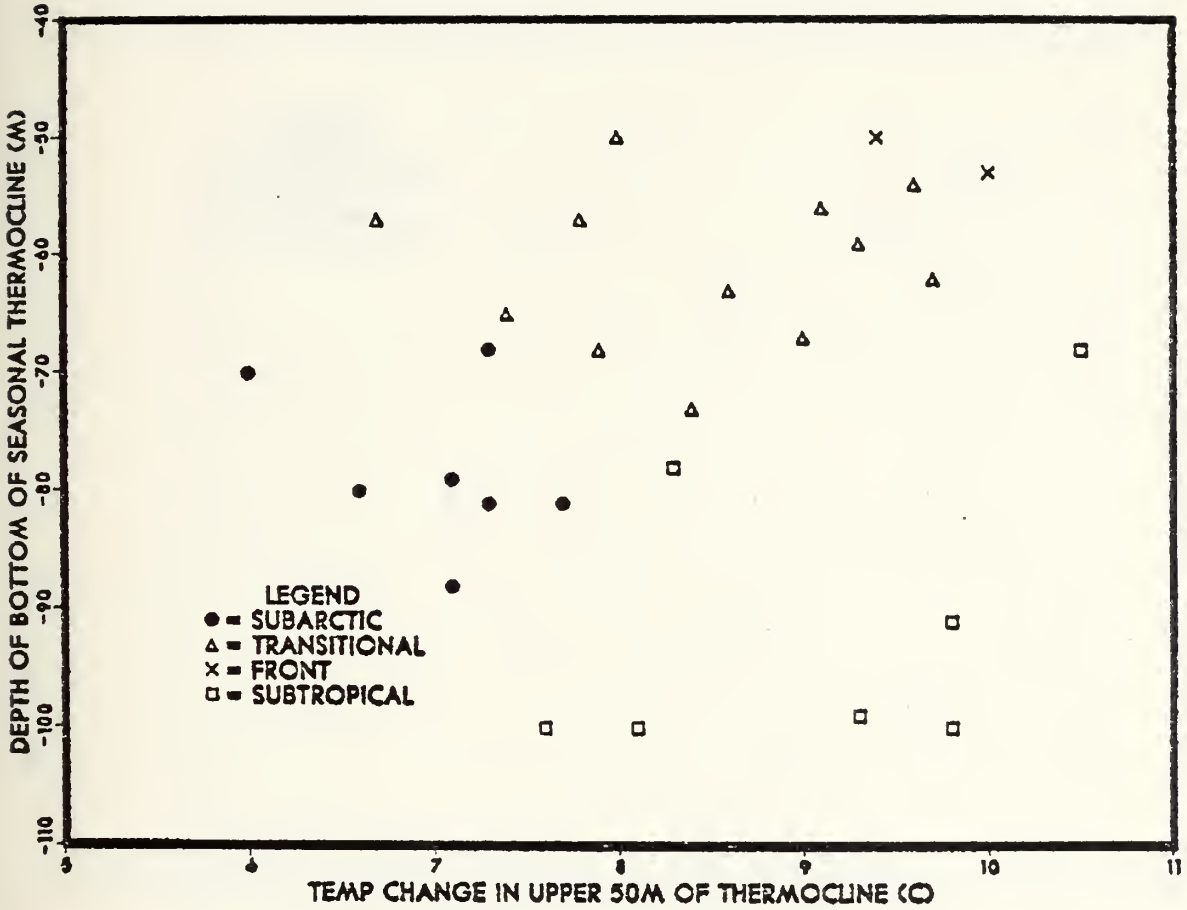

Figure D.3. Regional Scatter Diagram - BOT Versus DT50.

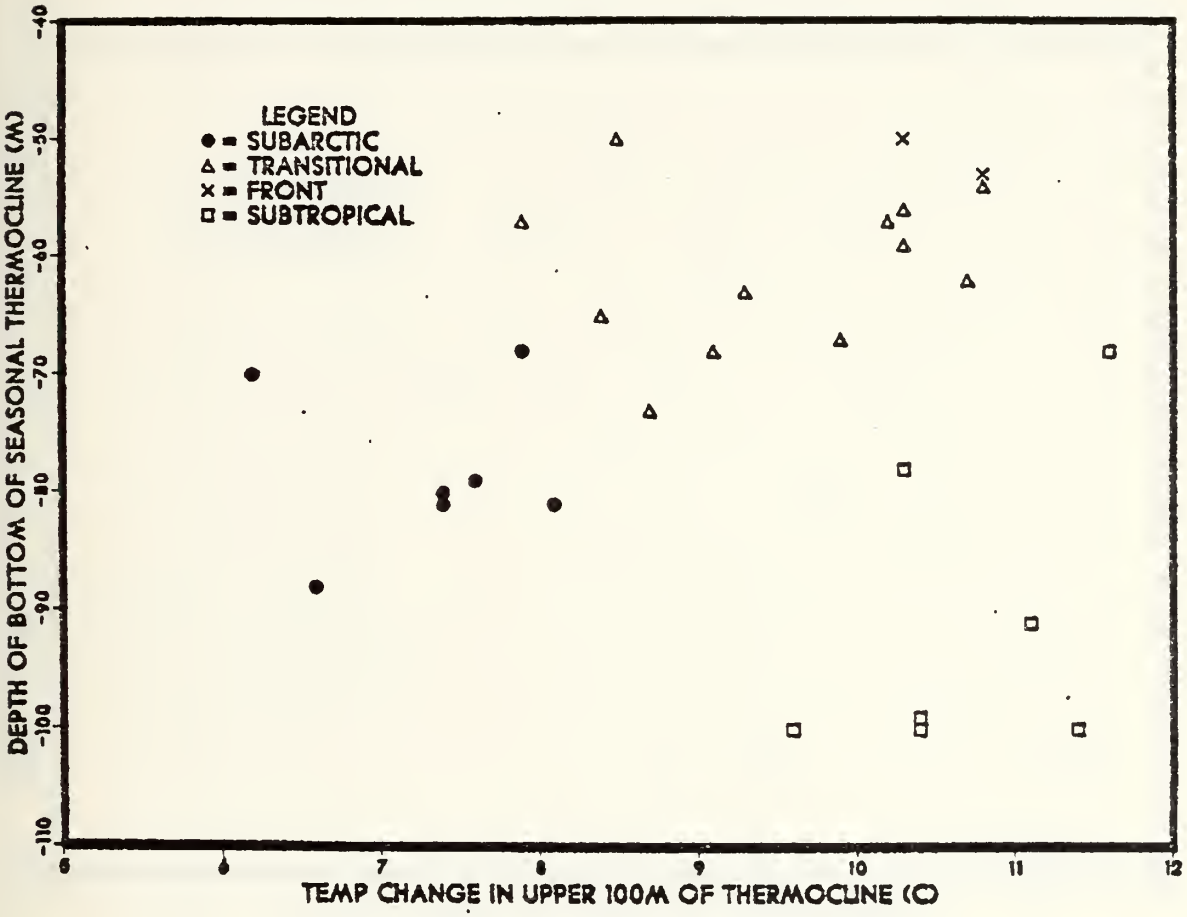

Figure D.4. Regional Scatter Diagram - BOT Versus DT100.

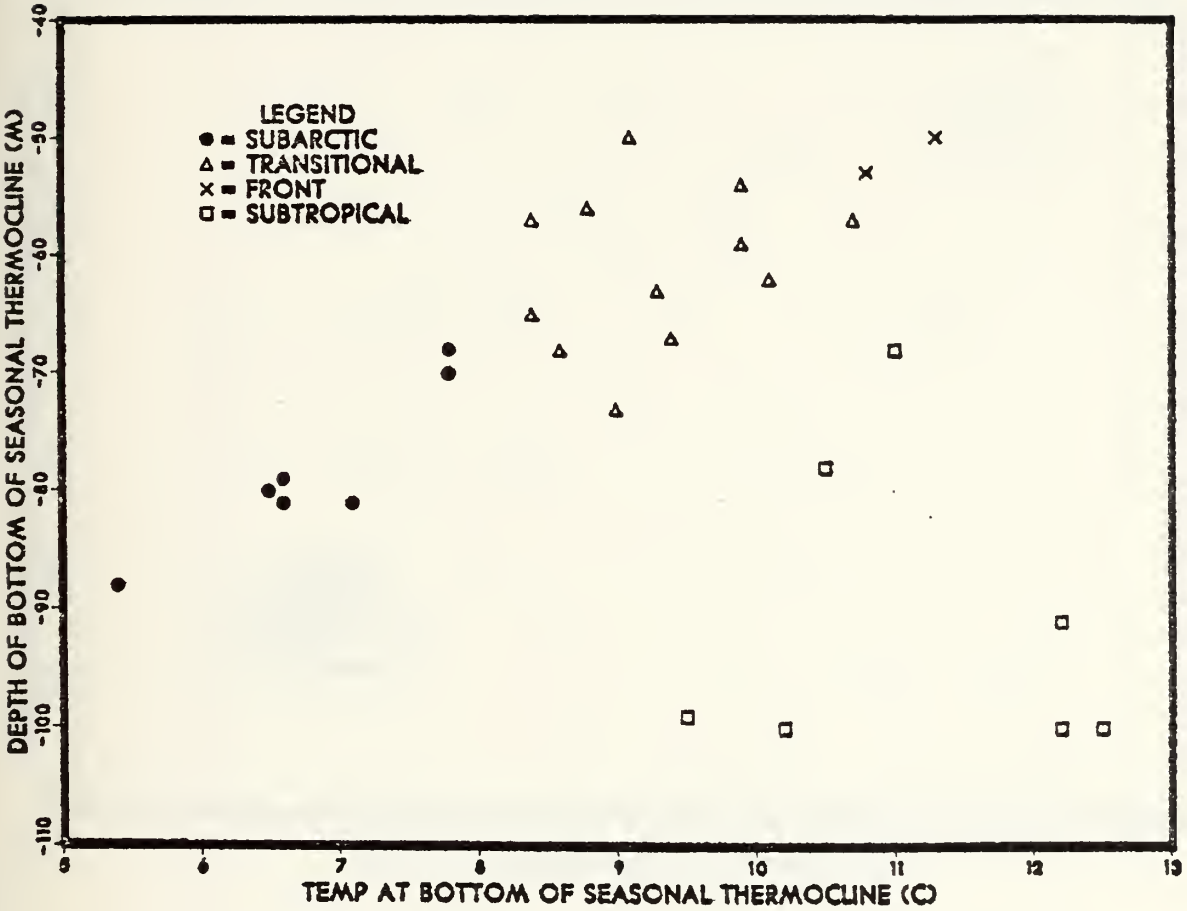

Figure D.5. Regional Scatter Diagram - BOT Versus TBOT.

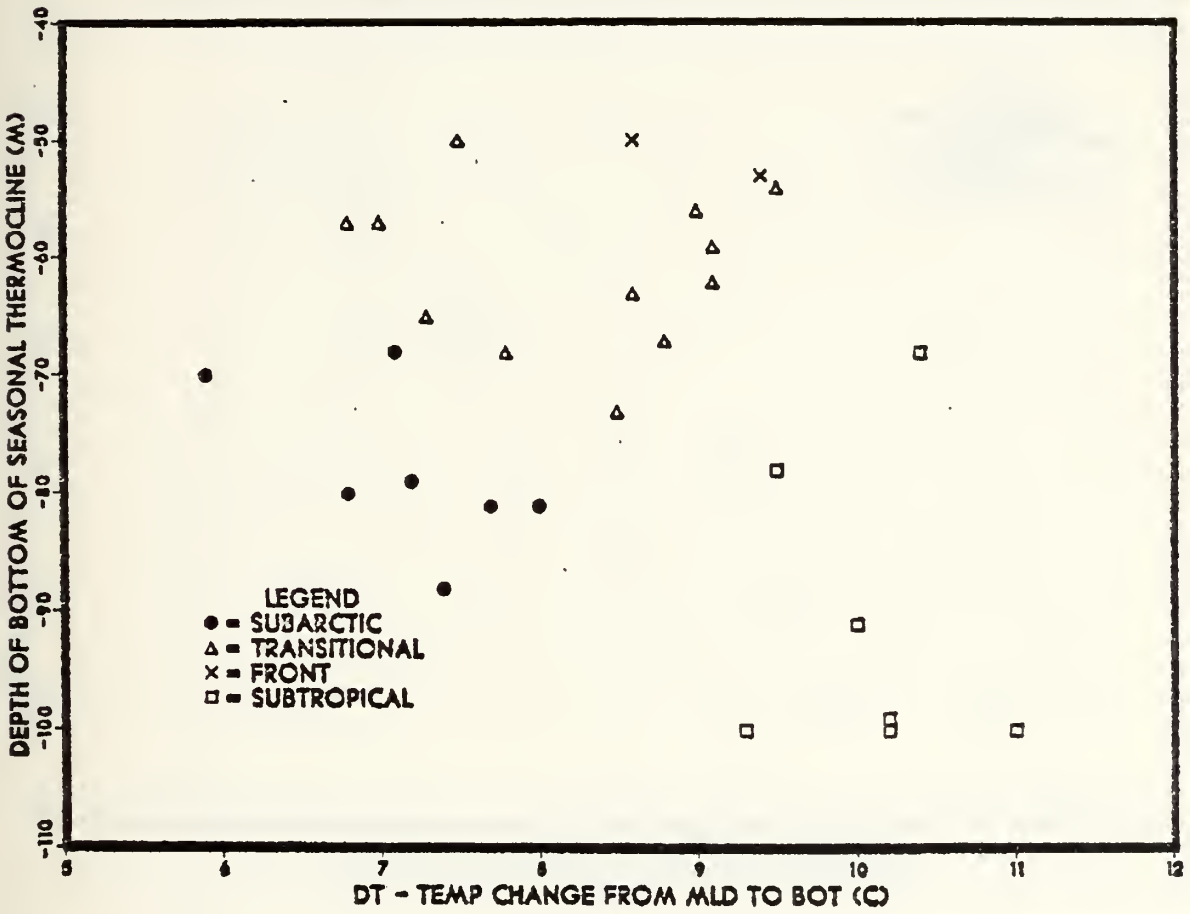

Figure D.6. Regional Scatter Diagram - BOT Versus DT.

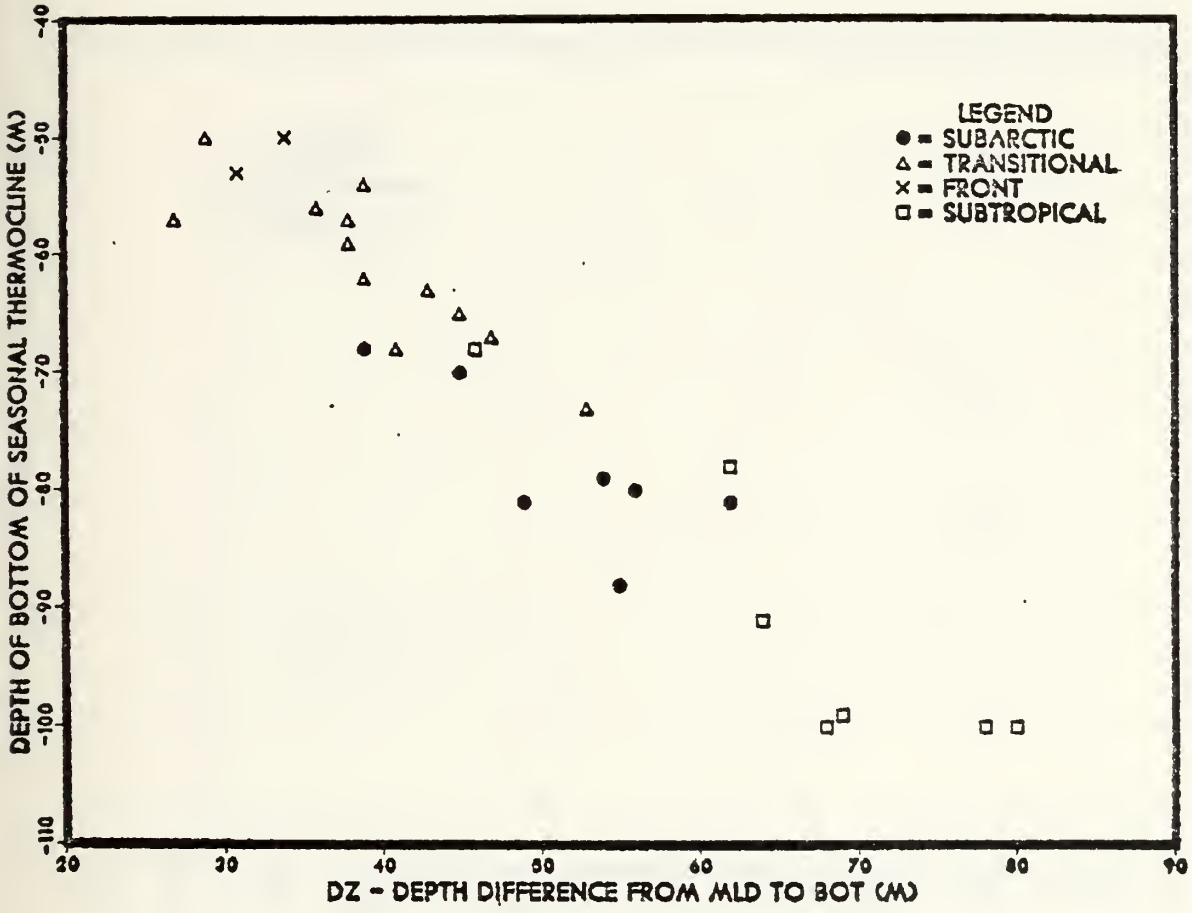

Figure D.7. Regional Scatter Diagram - BOT Versus DZ.

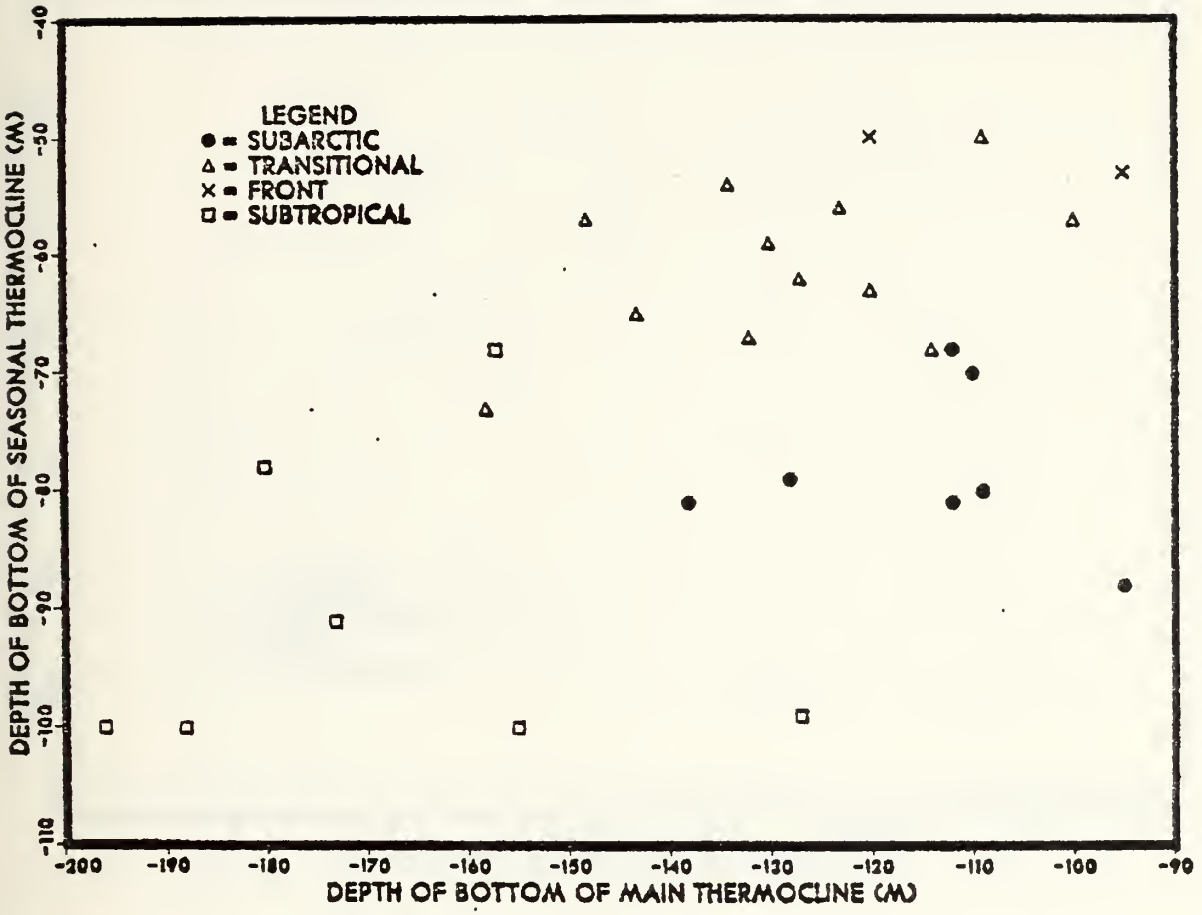

Figure D.8. Regional Scatter Diagram - BOT Versus BUZ.

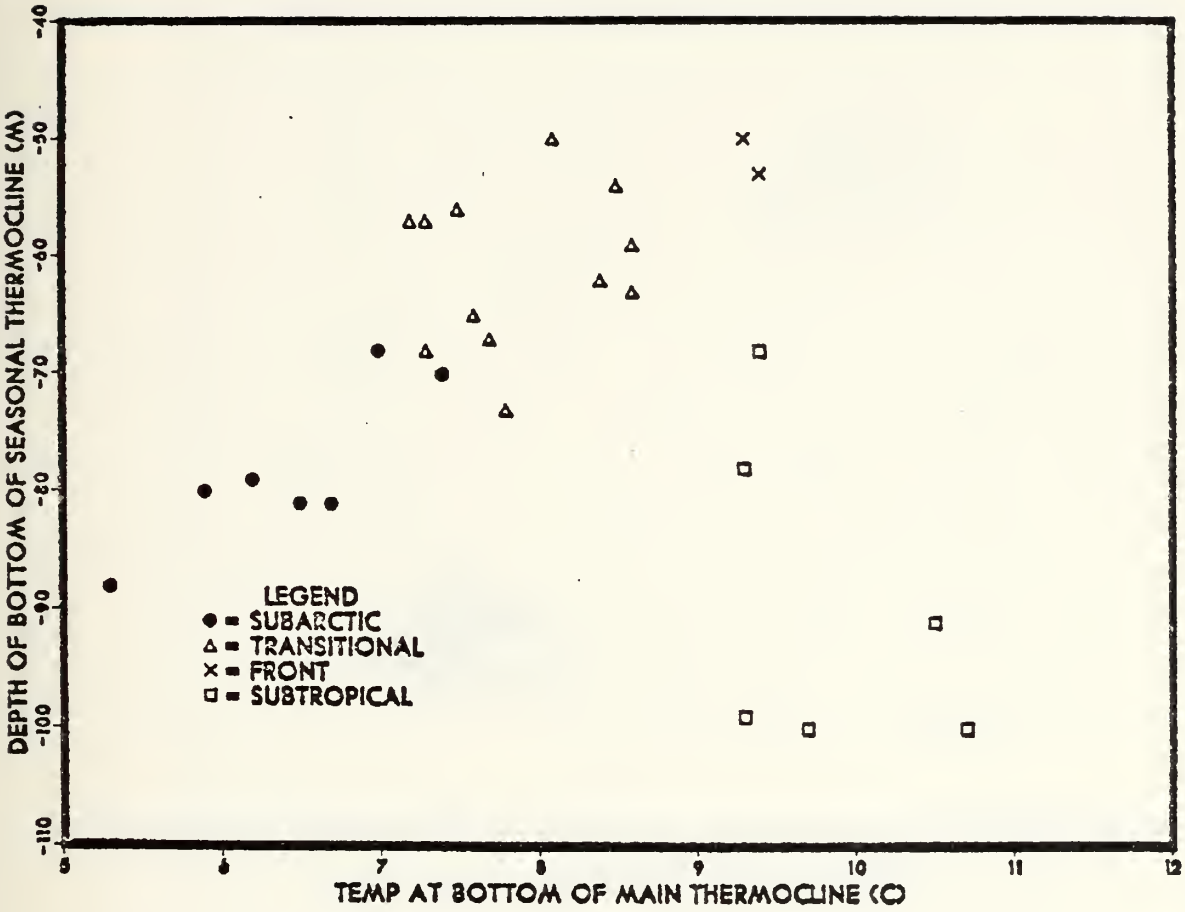

Figure D.9. Regional Scatter Diagram - BOT Versus TBUZ.

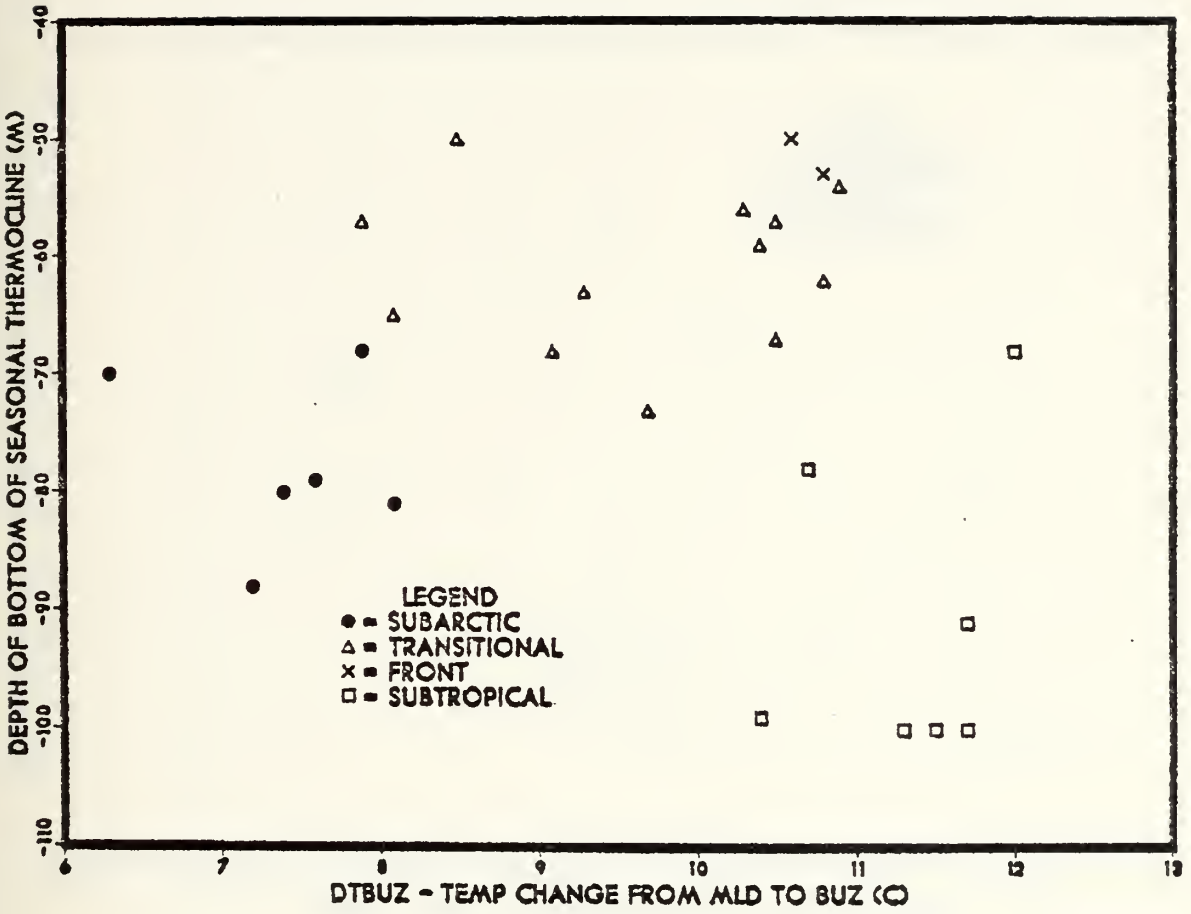

Figure D.10. Regional Scatter Diagram - BOT Versus DTBUZ.

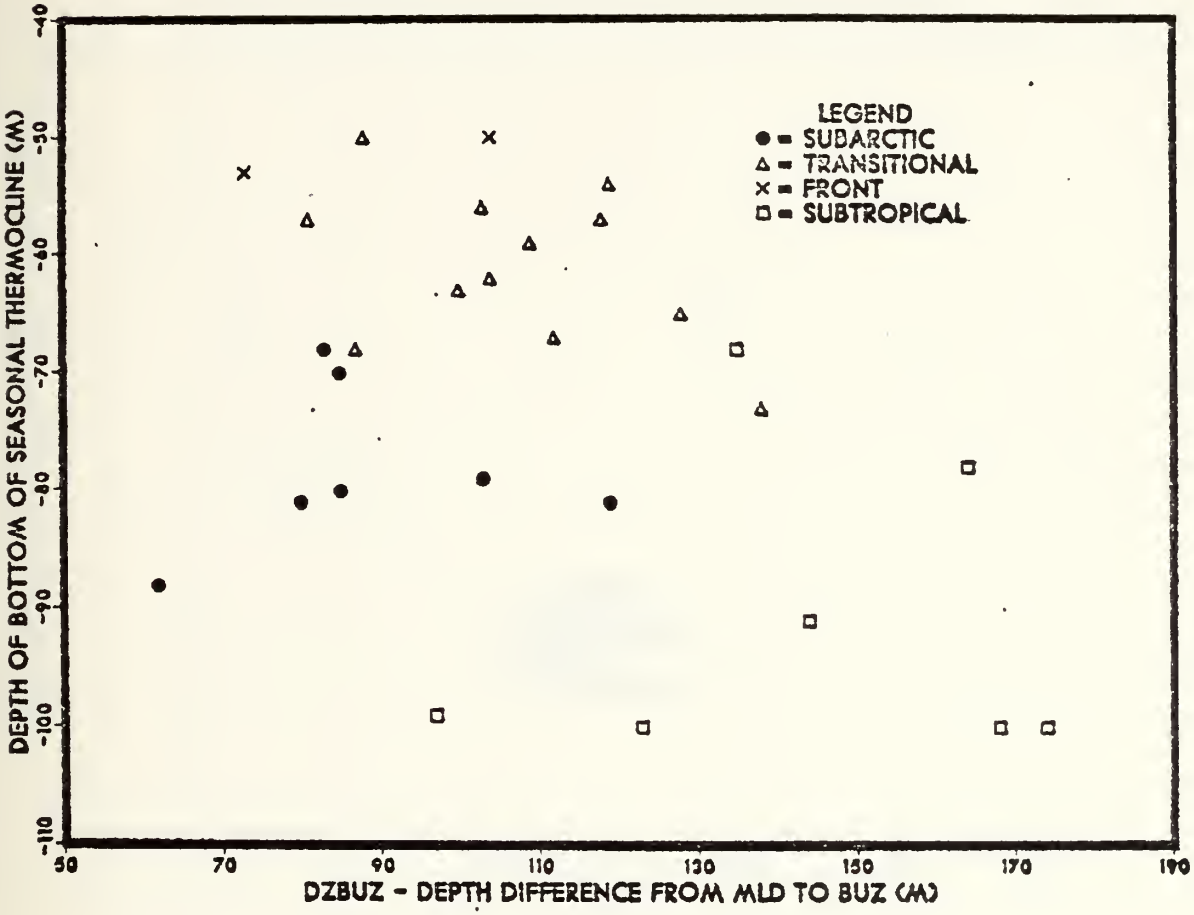

Figure D.11. Regional Scatter Diagram - BOT Versus DZBUZ.

APPENDIX E

REGIONAL SCATTER DIAGRAMS - BUZ VERSUS THERMAL VARIABLES

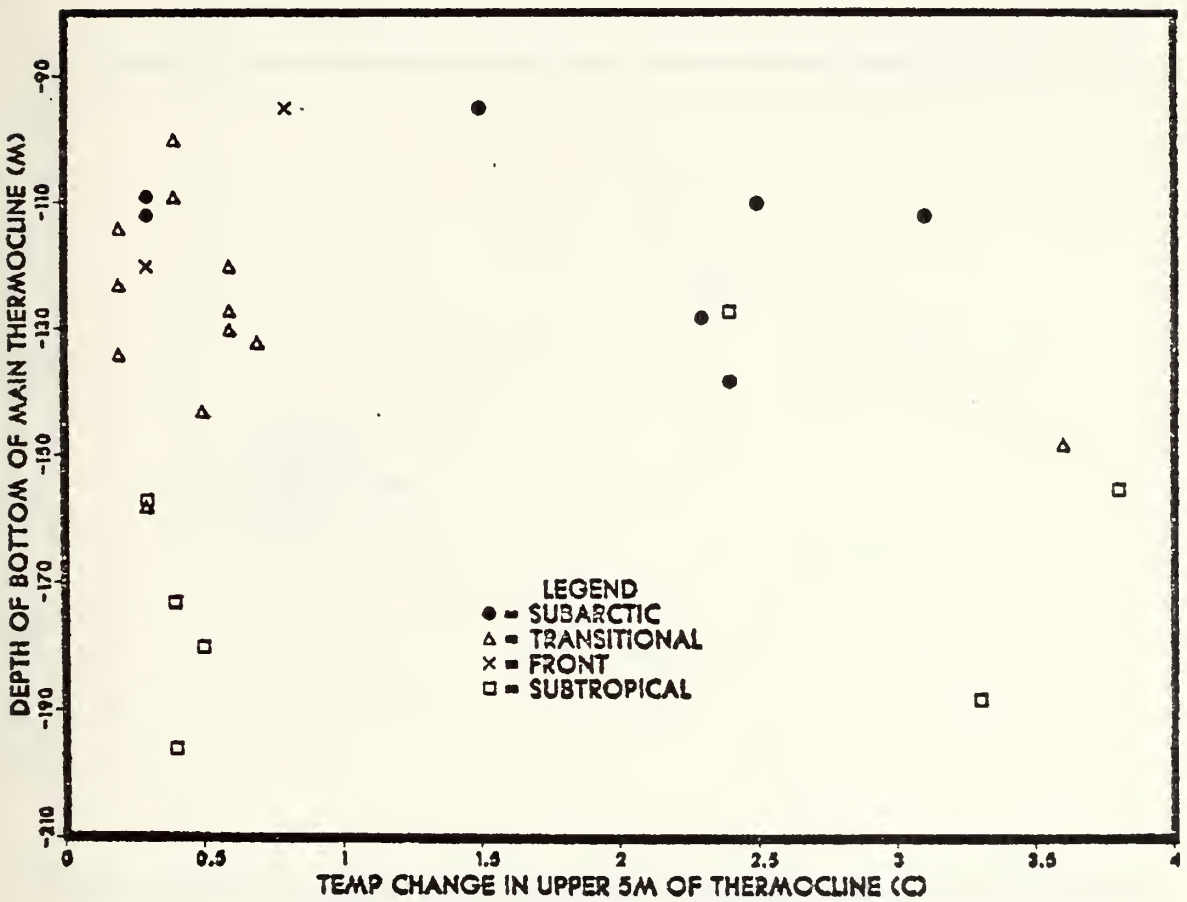

Figure E.1. Regional Scatter Diagram - BUZ Versus DT5.

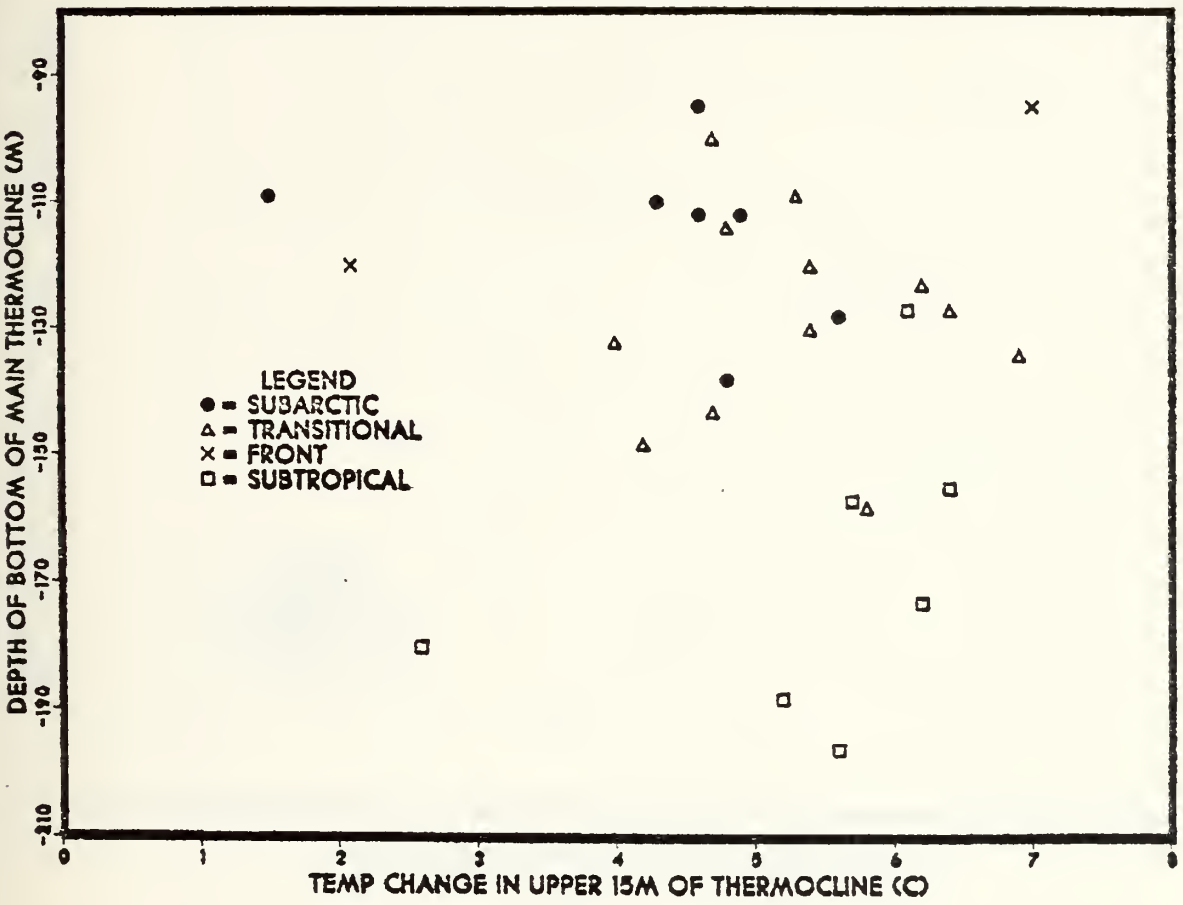

Figure E.2. Regional Scatter Diagram - BUZ Versus DT15.

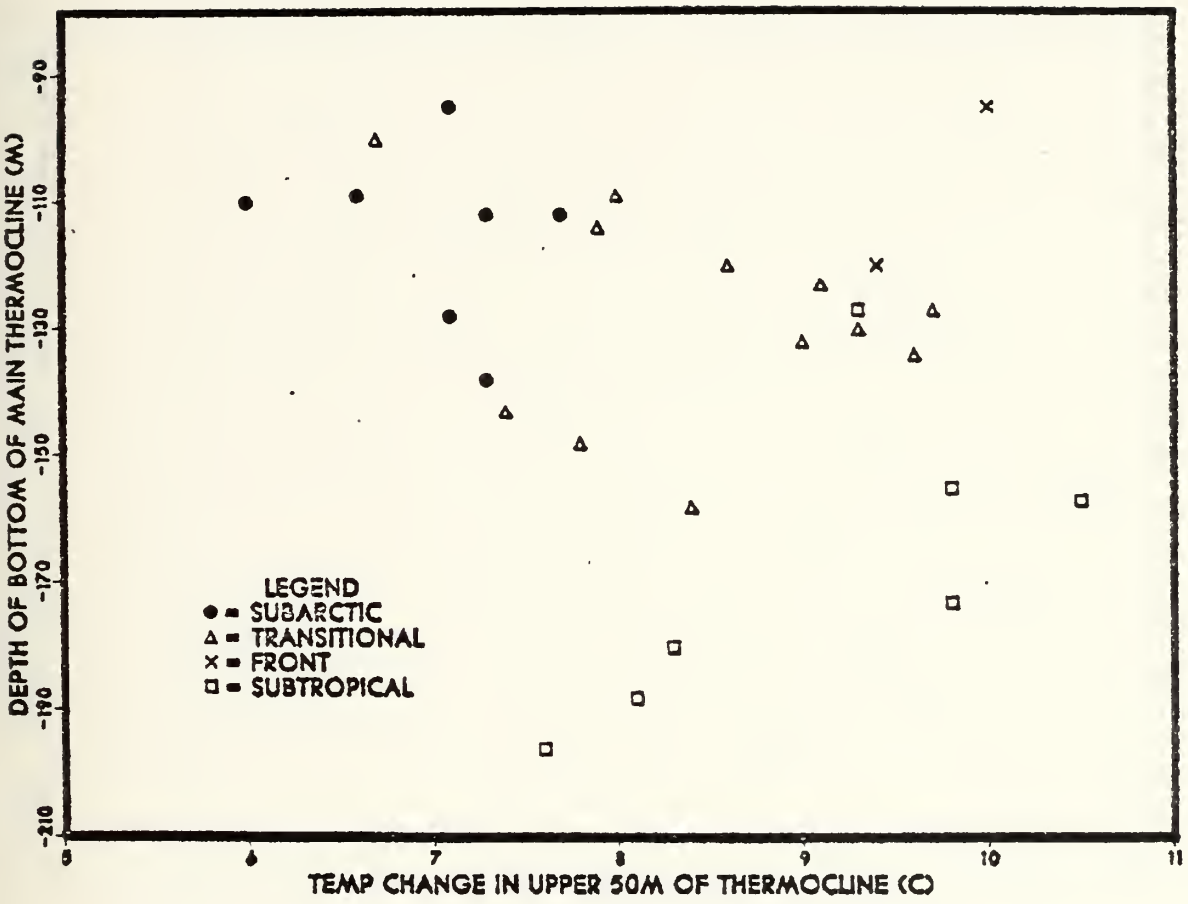

Figure E.3. Regional Scatter Diagram - BUZ Versus DT50.

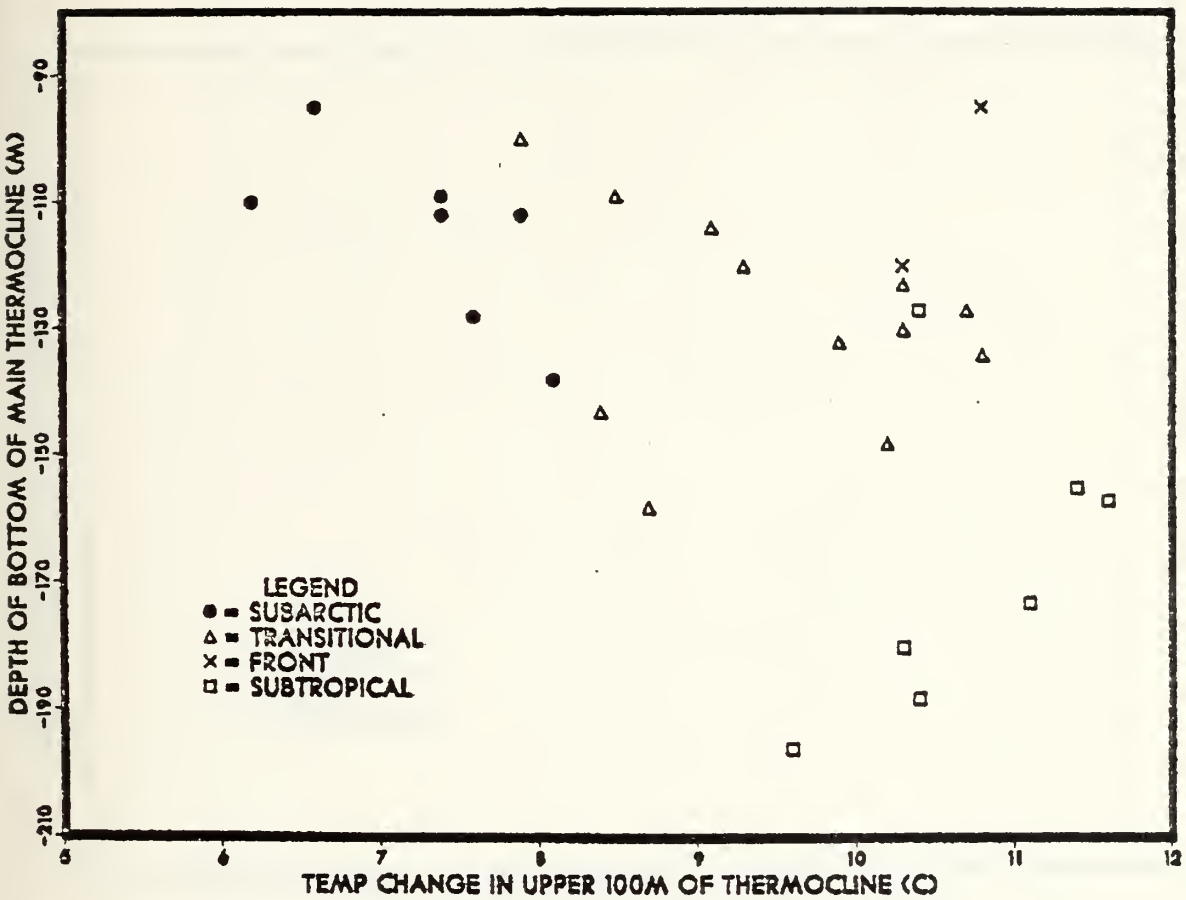

Figure E.4. Regional Scatter Diagram - BUZ Versus DT100.

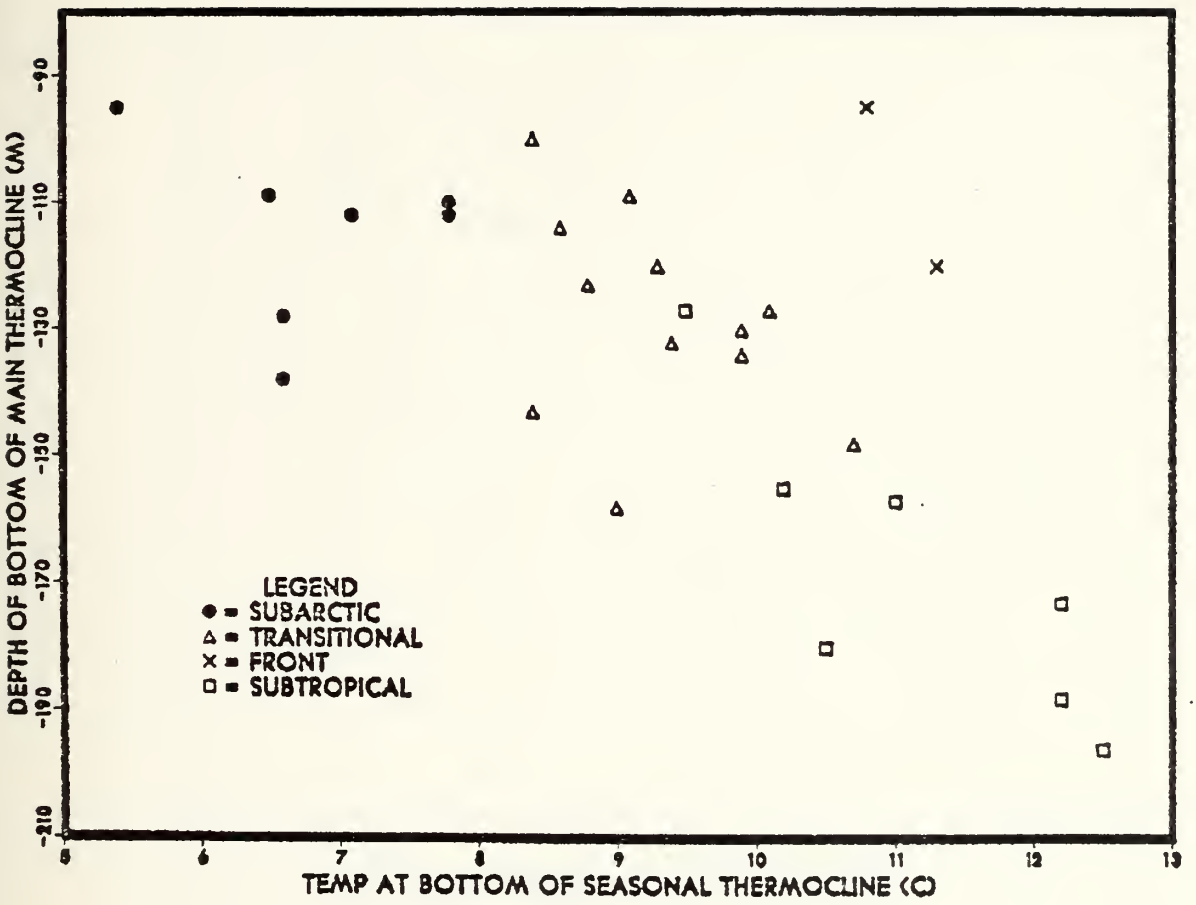

Figure E.5. Regional Scatter Diagram - BUZ Versus TBOT.

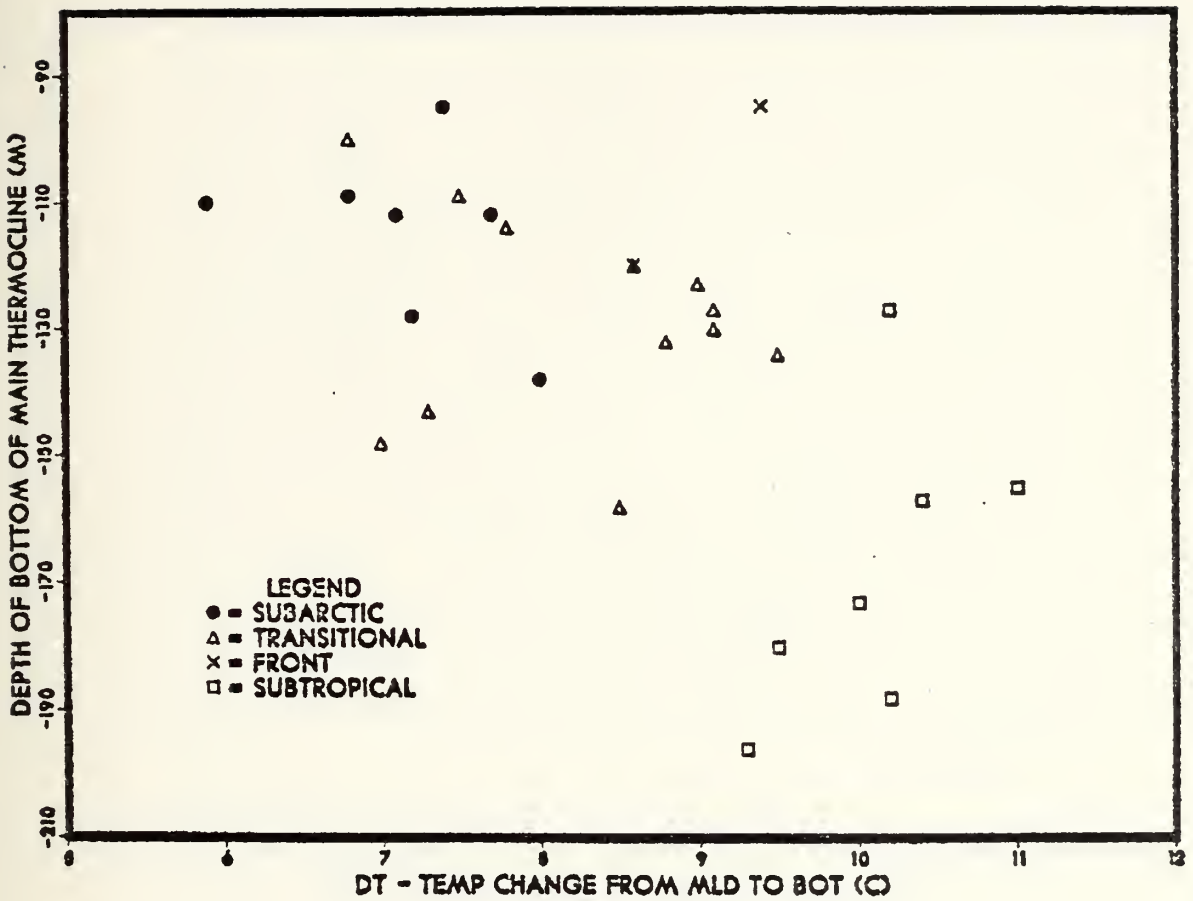

Figure E.6. Regional Scatter Diagram - BUZ Versus DT.

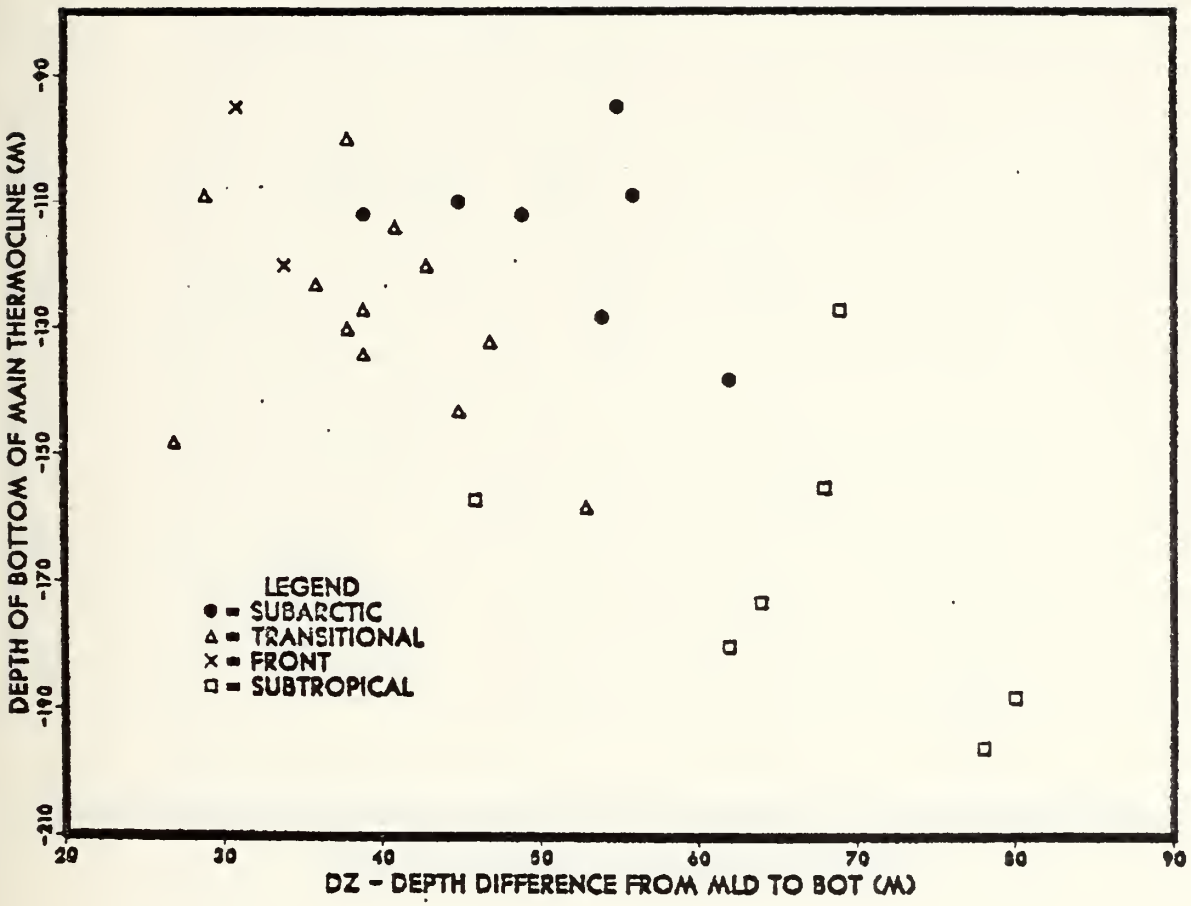

Figure E.7. Regional Scatter Diagram - BUZ Versus DZ.

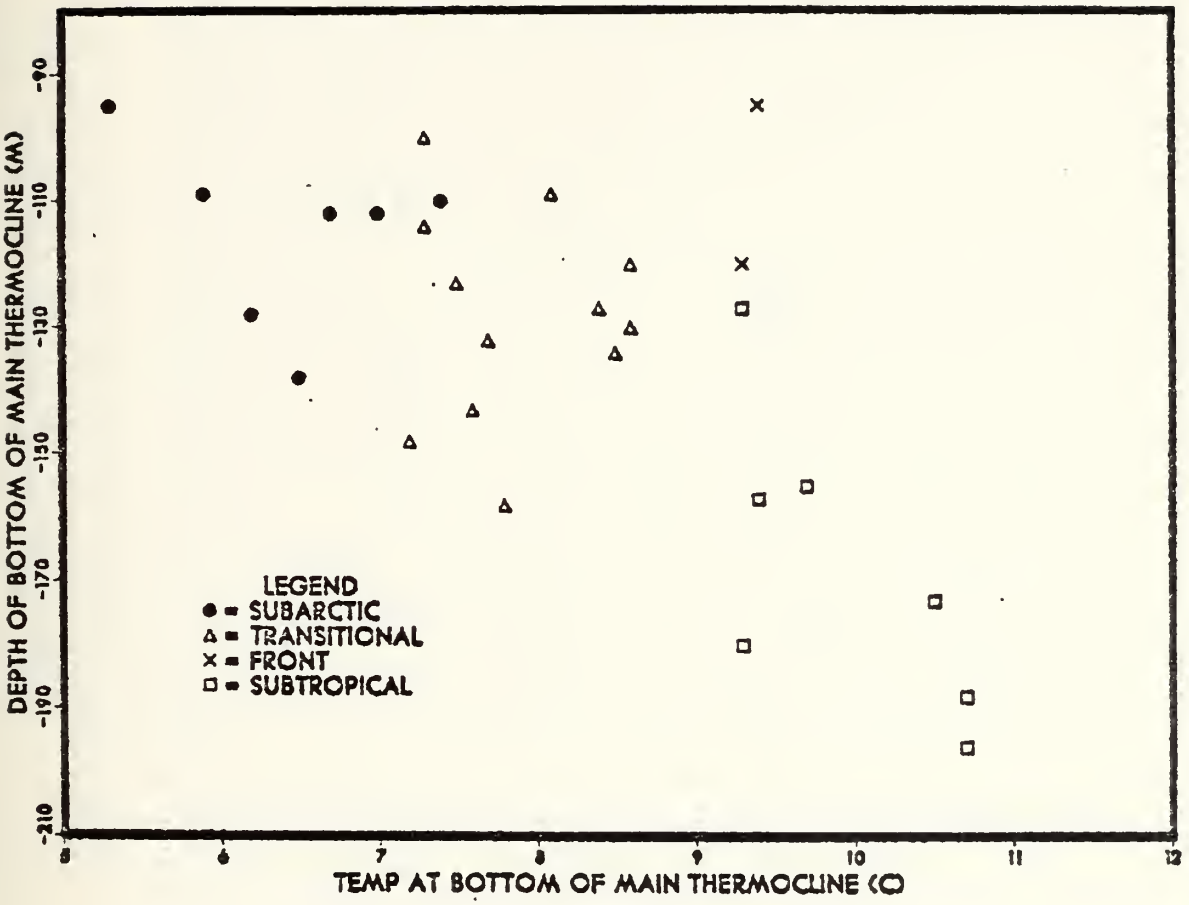

Figure E.8. Regional Scatter Diagram - BUZ Versus TBUZ.

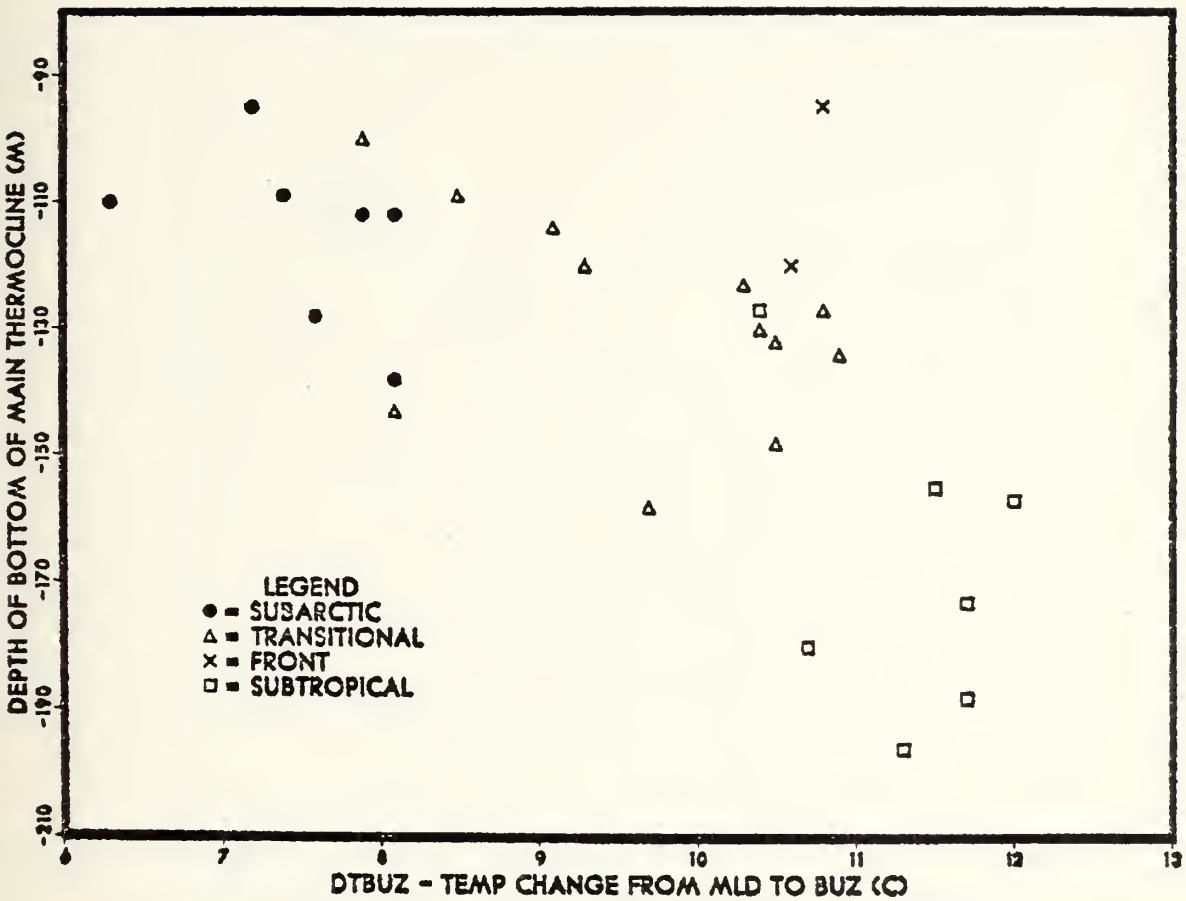

Figure E.9. Regional Scatter Diagram - BUZ Versus DTBUZ.

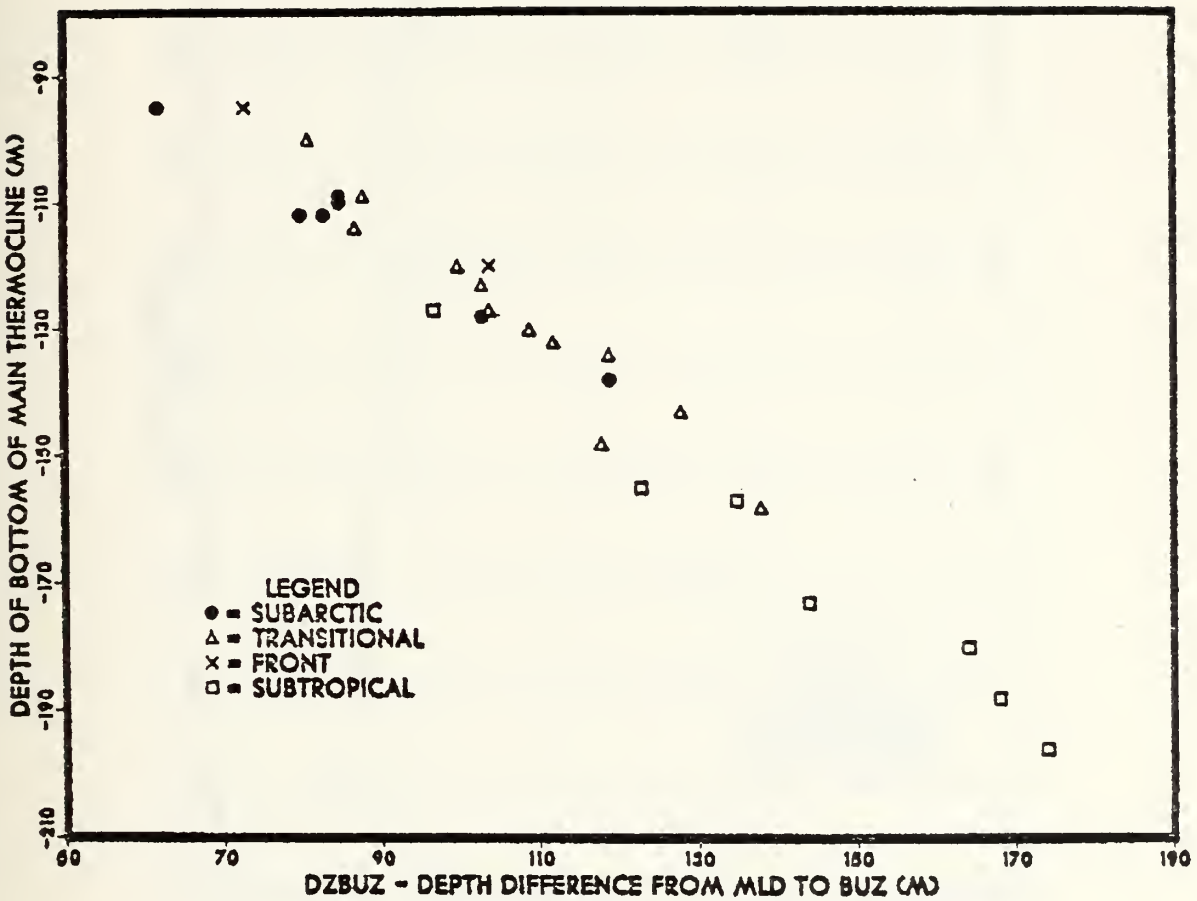

Figure E.10. Regional Scatter Diagram - BUZ Versus DZBUZ.

APPENDIX F

OBSERVED AND PREDICTED THERMAL PROFILES ALONG TRACK

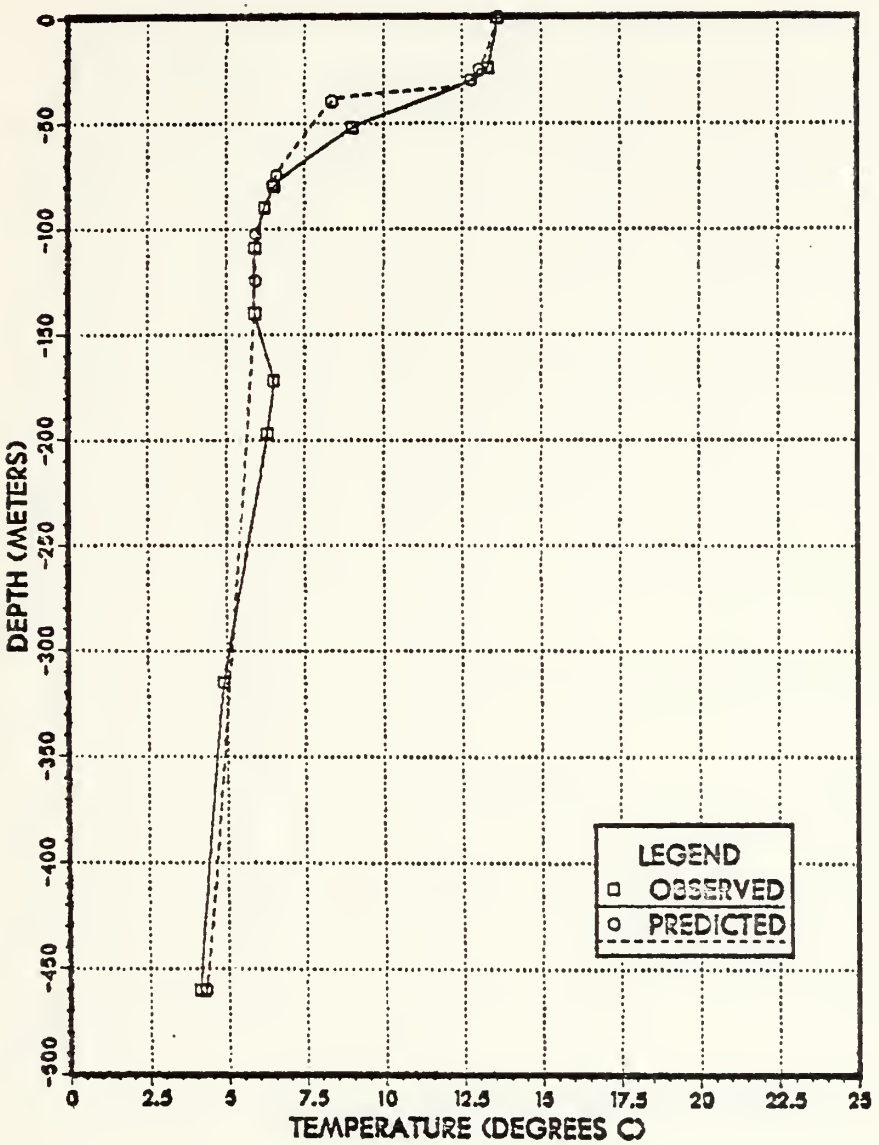

Figure F.1. Observed and Predicted Thermal Profiles at XBT Sta. 340.

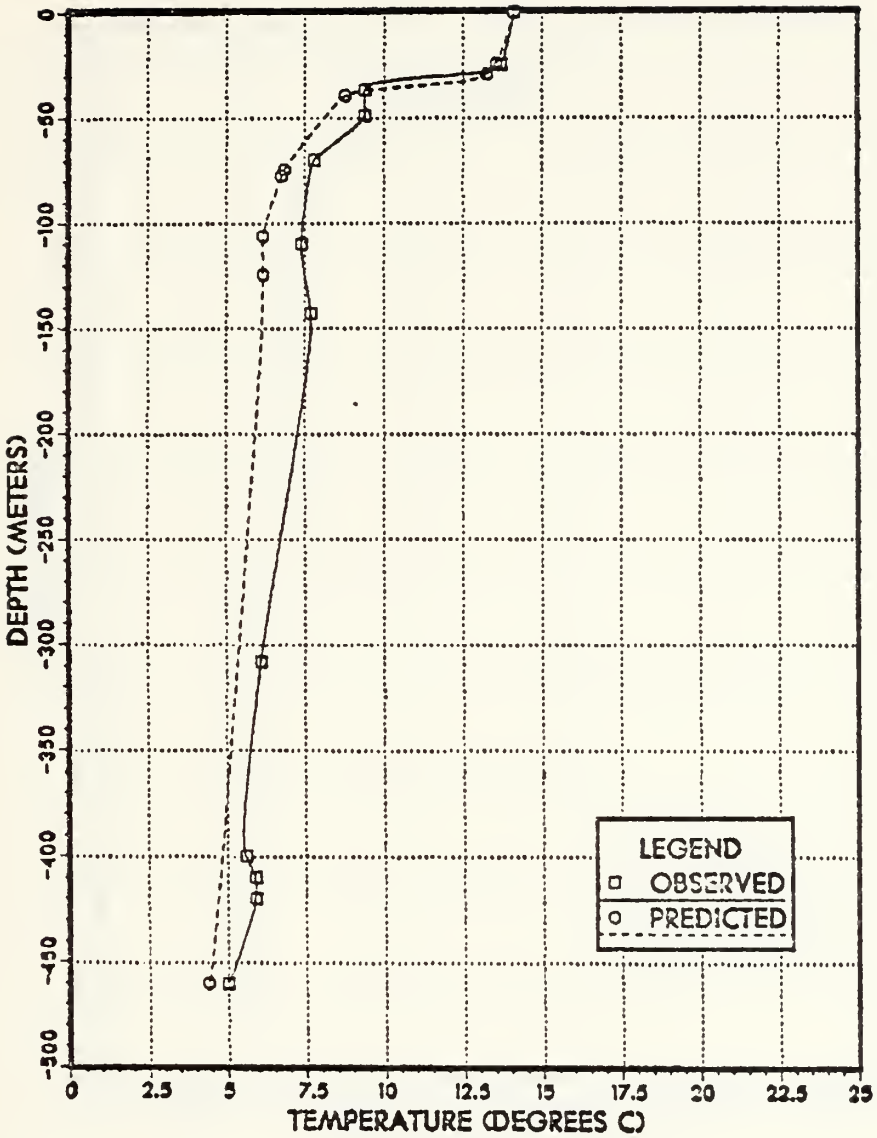

Figure F.2. Observed and Predicted Thermal Profiles at XBT Sta. 341.

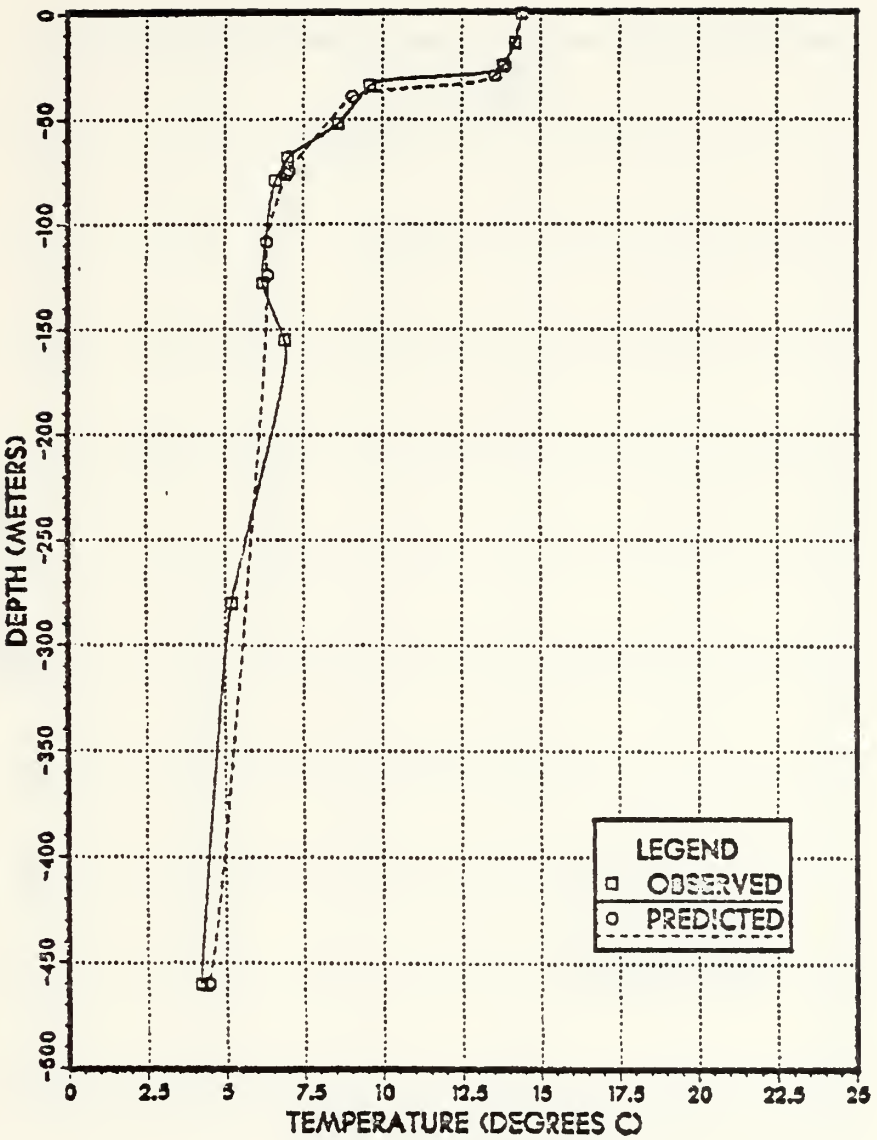

Figure F.3. Observed and Predicted Thermal Profiles at XBT Sta. 342.

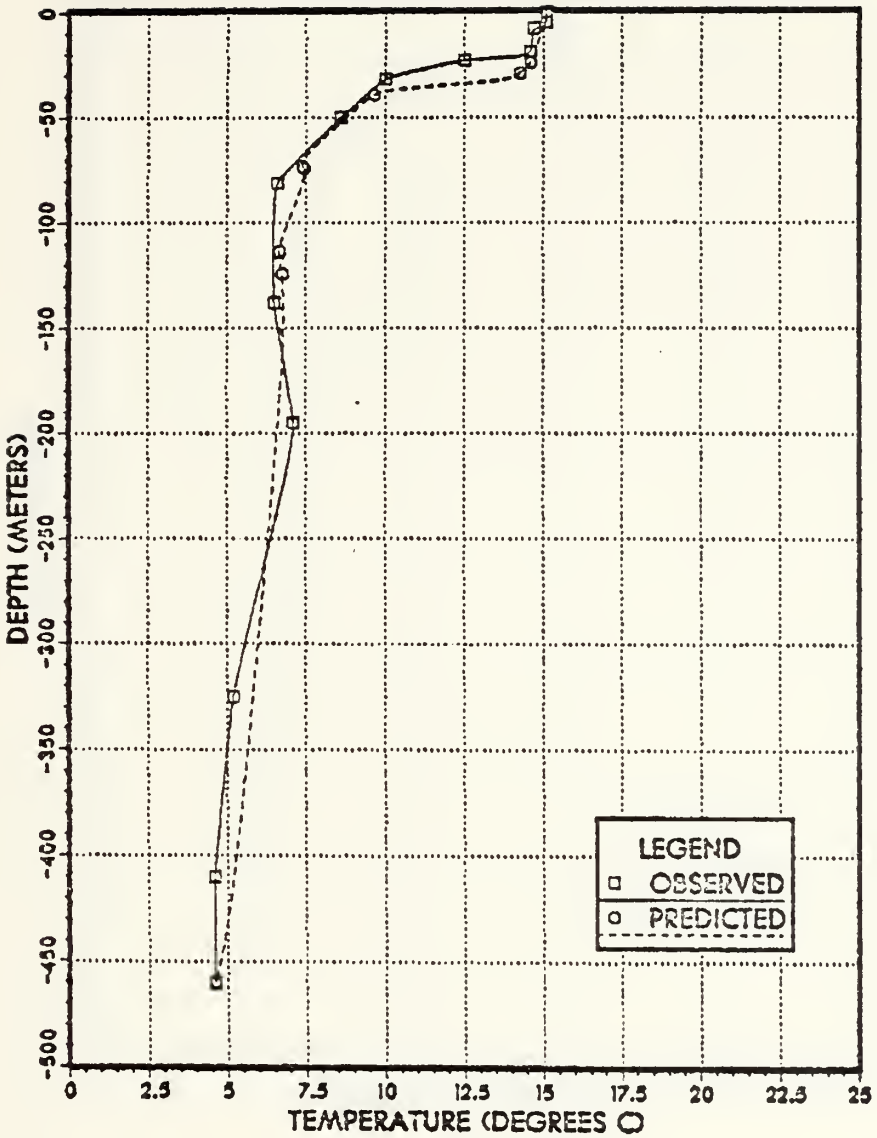

Figure F.4. Observed and Predicted Thermal Profiles at XBT Sta. 343.

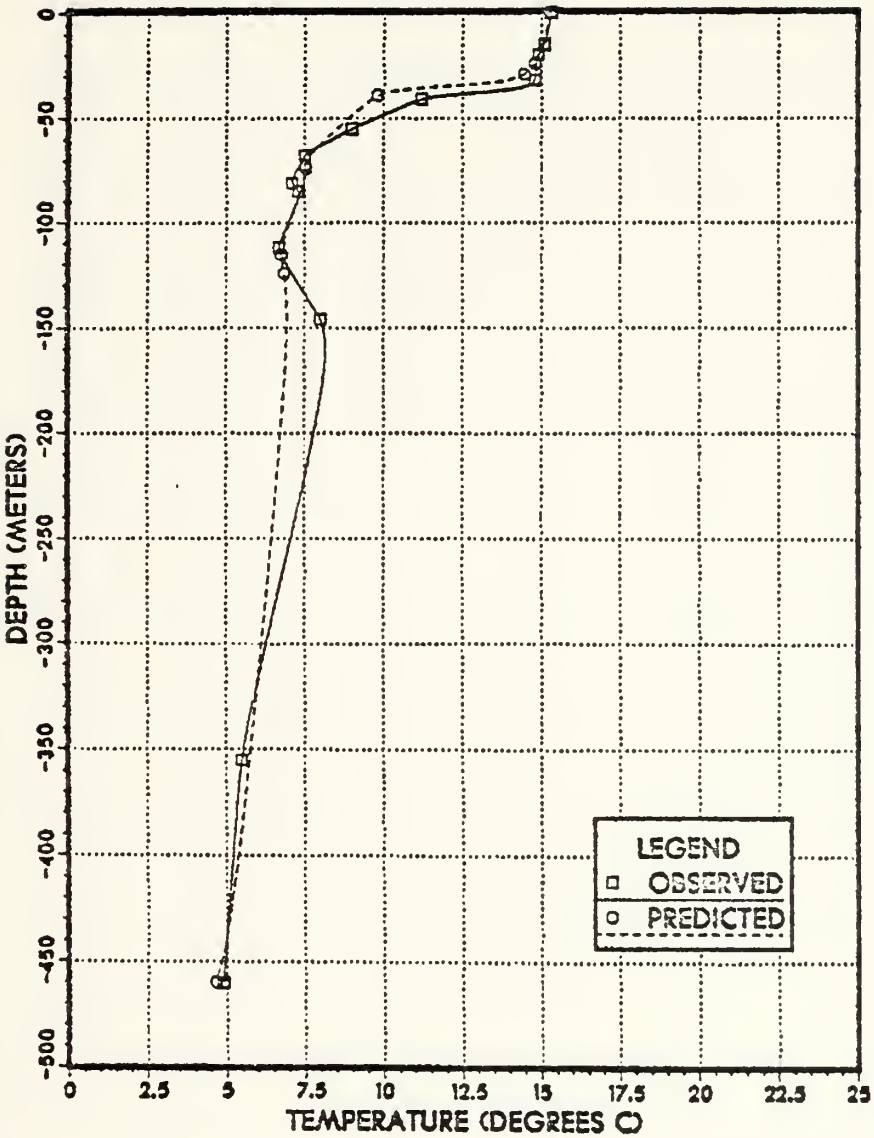

Figure F.5. Observed and Predicted Thermal Profiles at XBT Sta. 344.

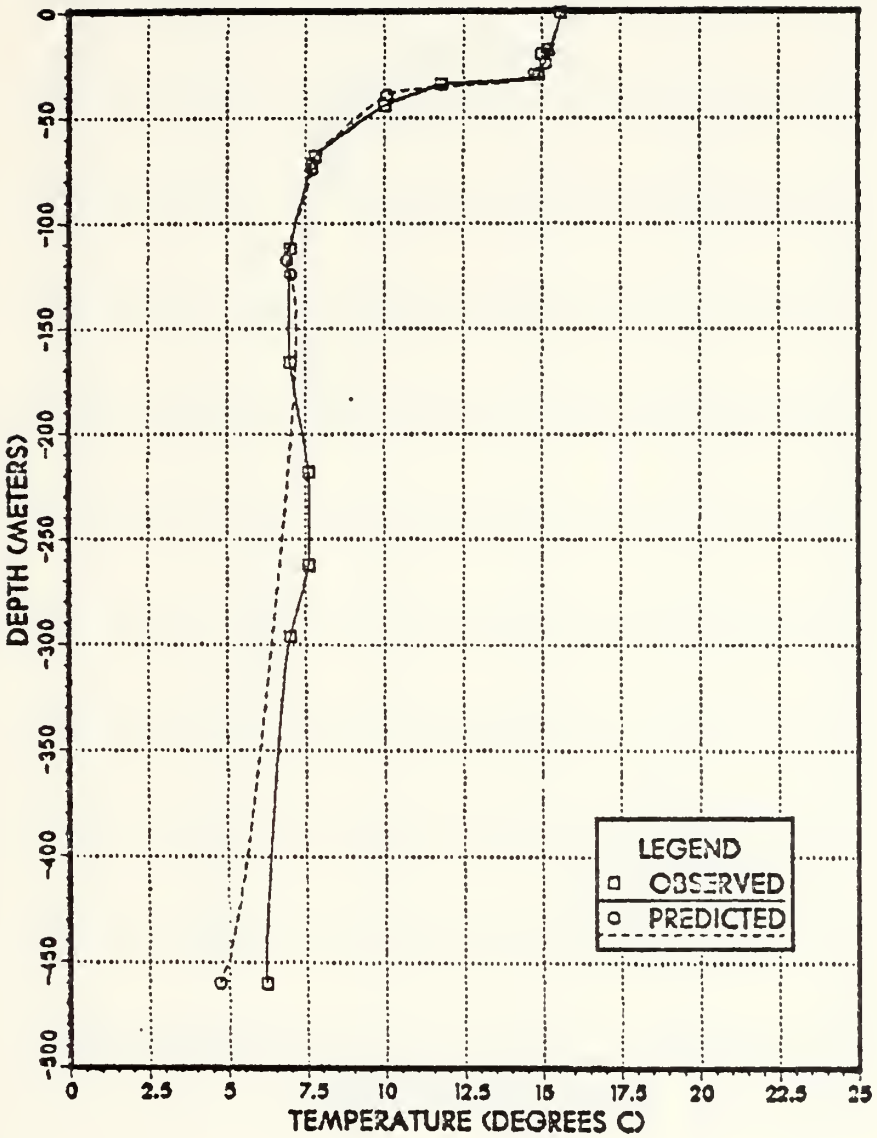

Figure F.6. Observed and Predicted Thermal Profiles at XBT Sta. 345.

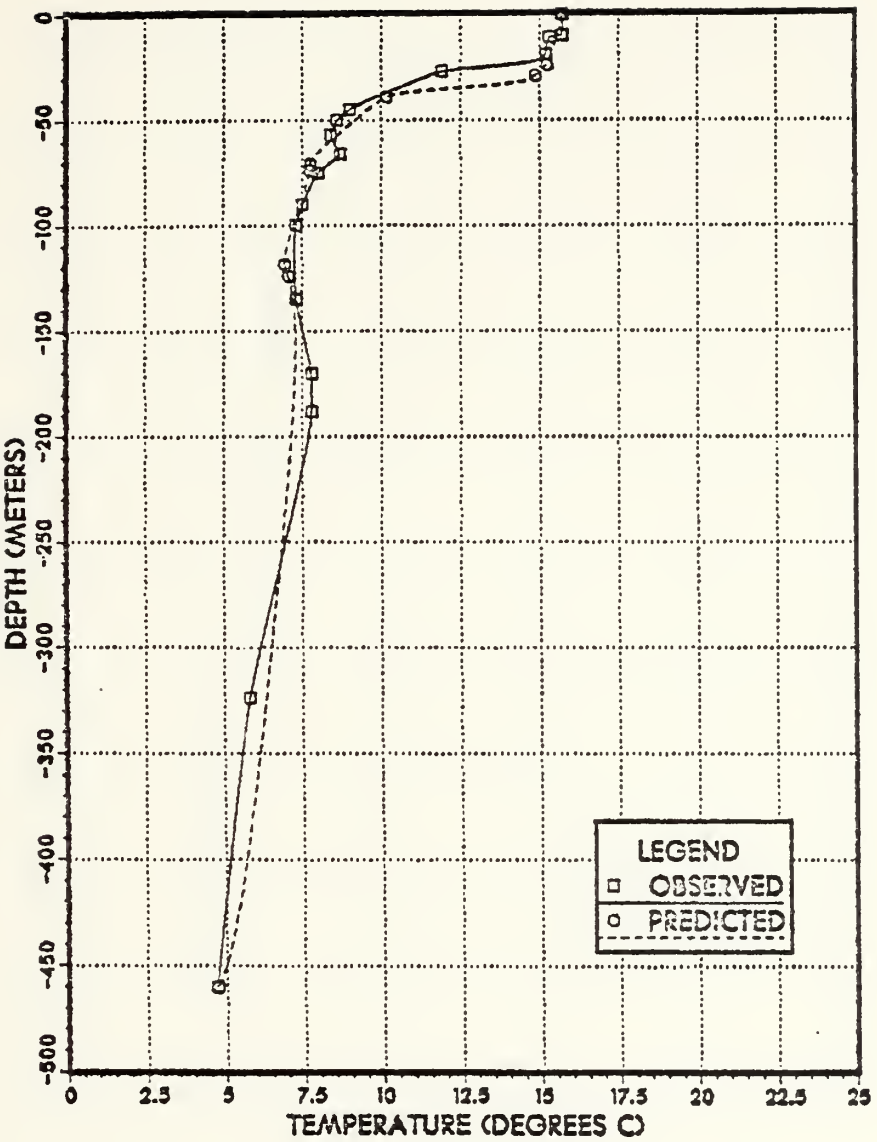

Figure F.7. Observed and Predicted Thermal Profiles at XBT Sta. 346.

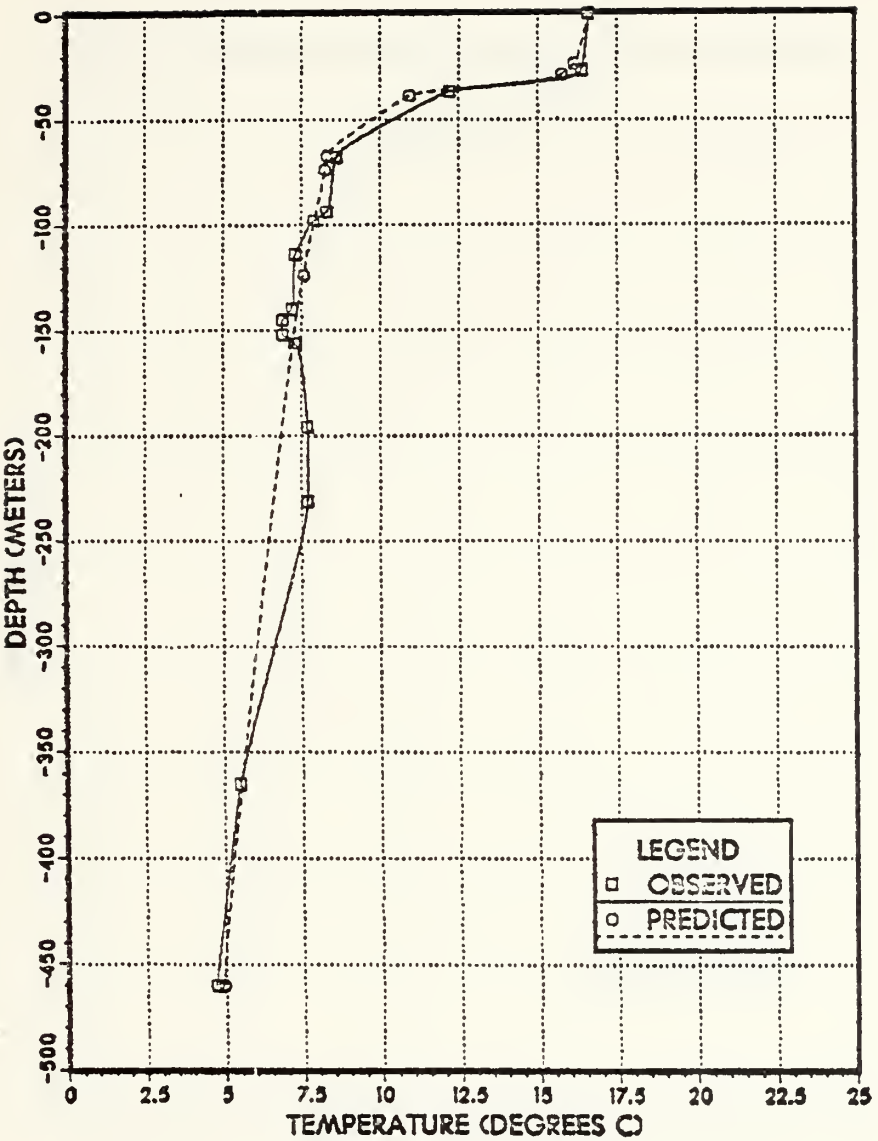

Figure F.8. Observed and Predicted Thermal Profiles at XBT Sta. 347.

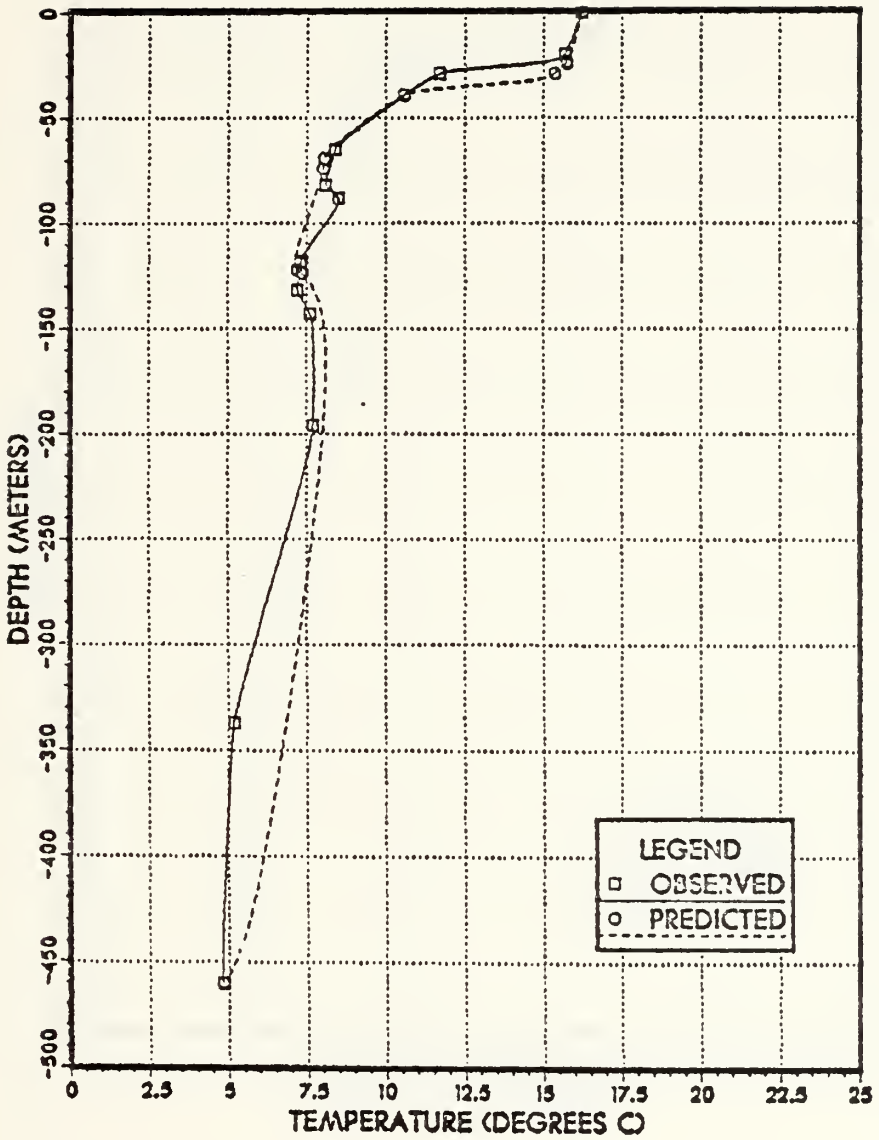

Figure F.9. Observed and Predicted Thermal Profiles at XBT Sta. 348.

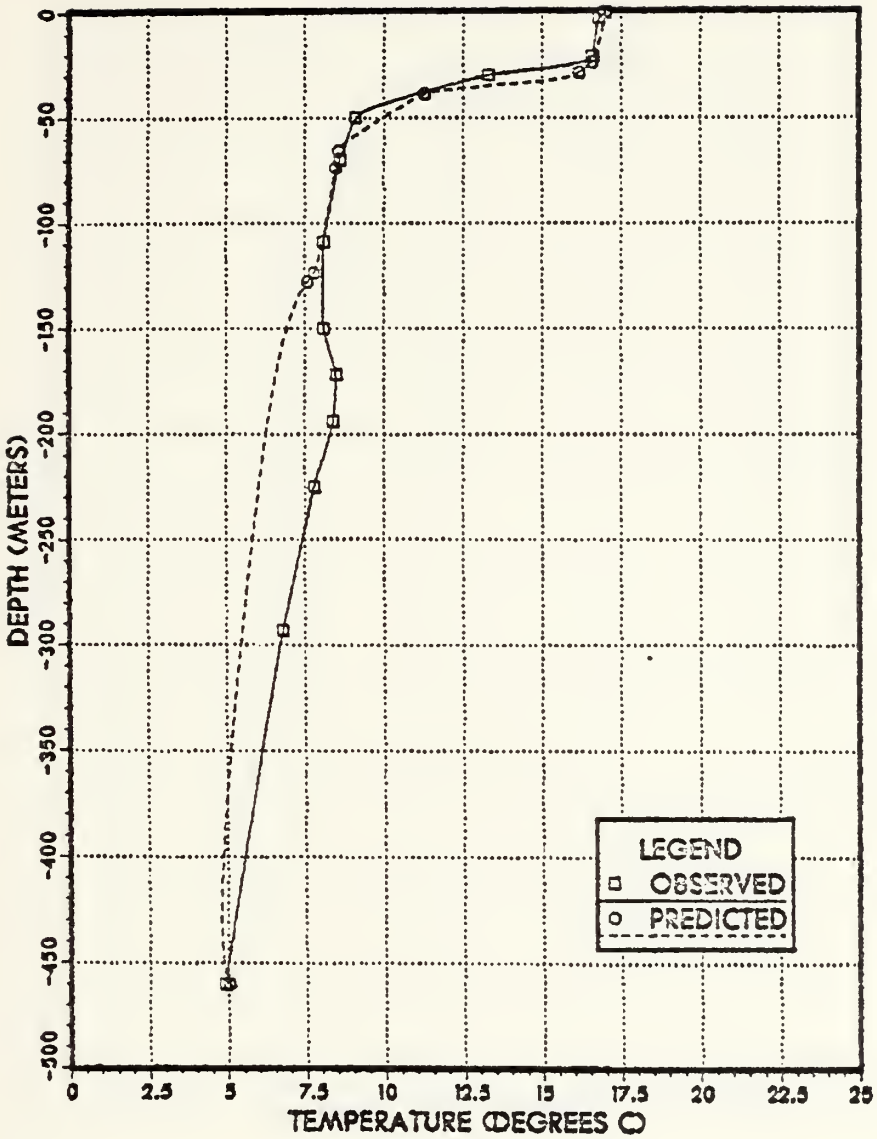

Figure F.10. Observed and Predicted Thermal Profiles at XET Sta. 349.

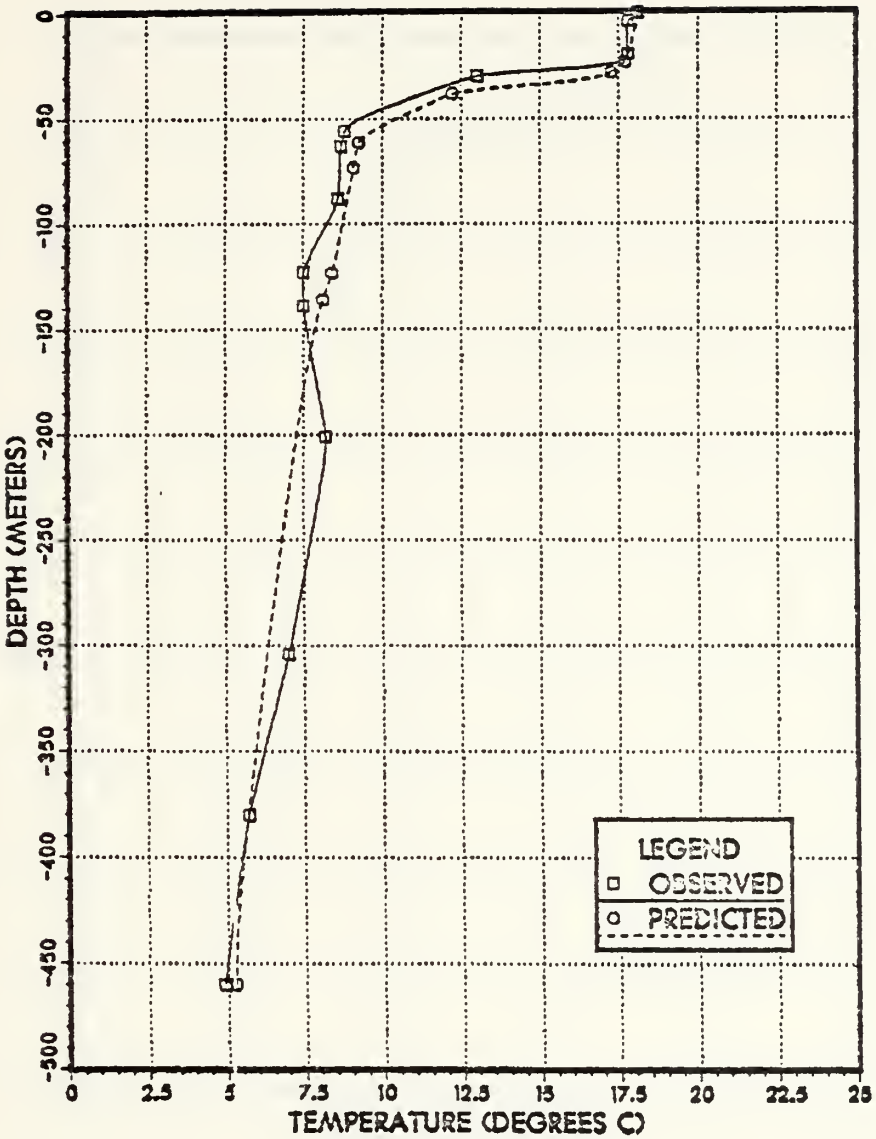

Figure F.11. Observed and Predicted Thermal Profiles at XBT Sta. 350.

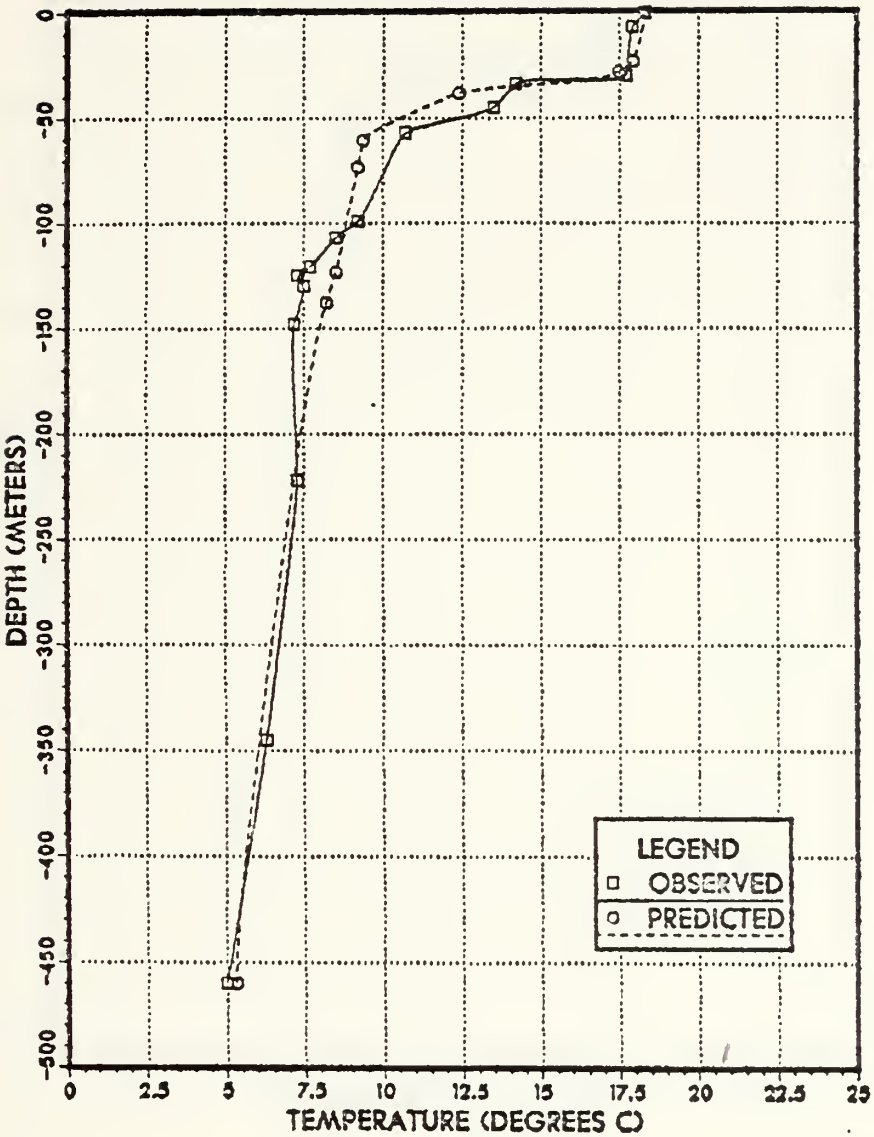

Figure F.12. Observed and Predicted Thermal Profiles at XBT Sta. 351.

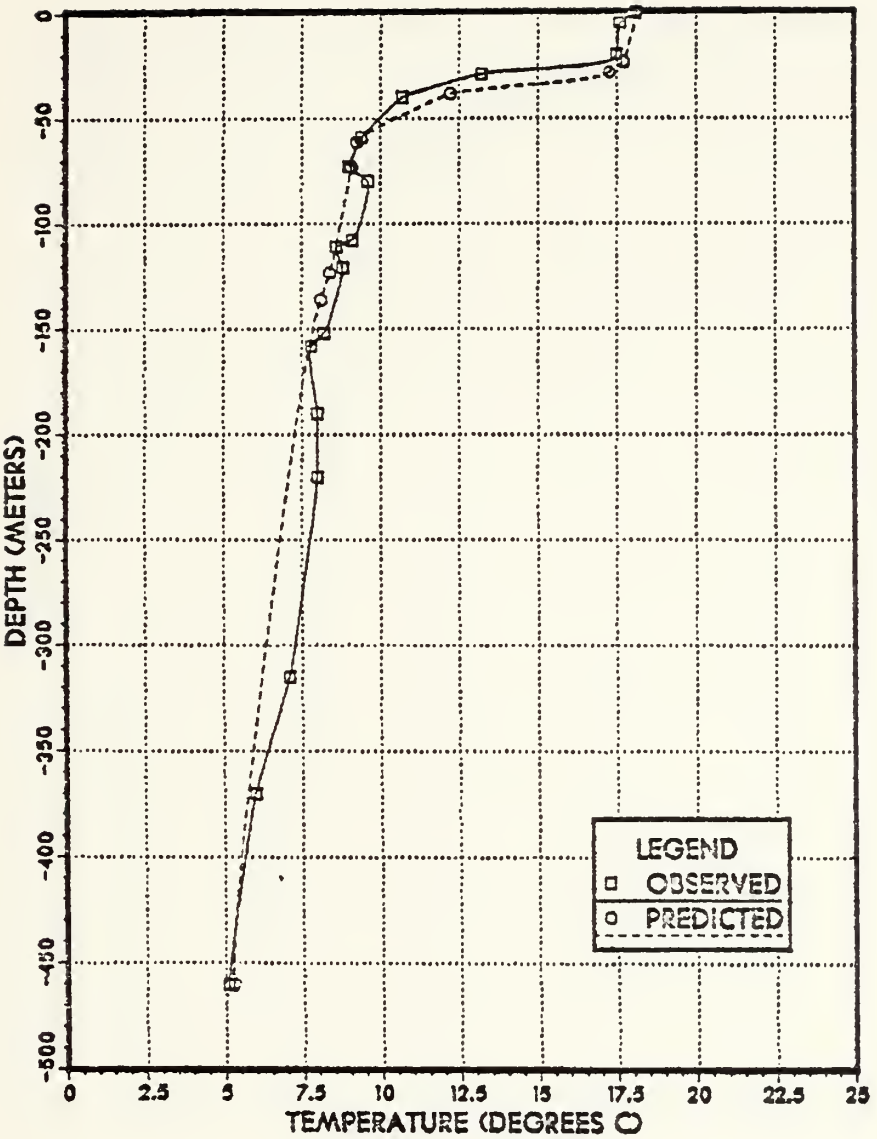

Figure F.13. Observed and Predicted Thermal Profiles at XET Sta. 352.

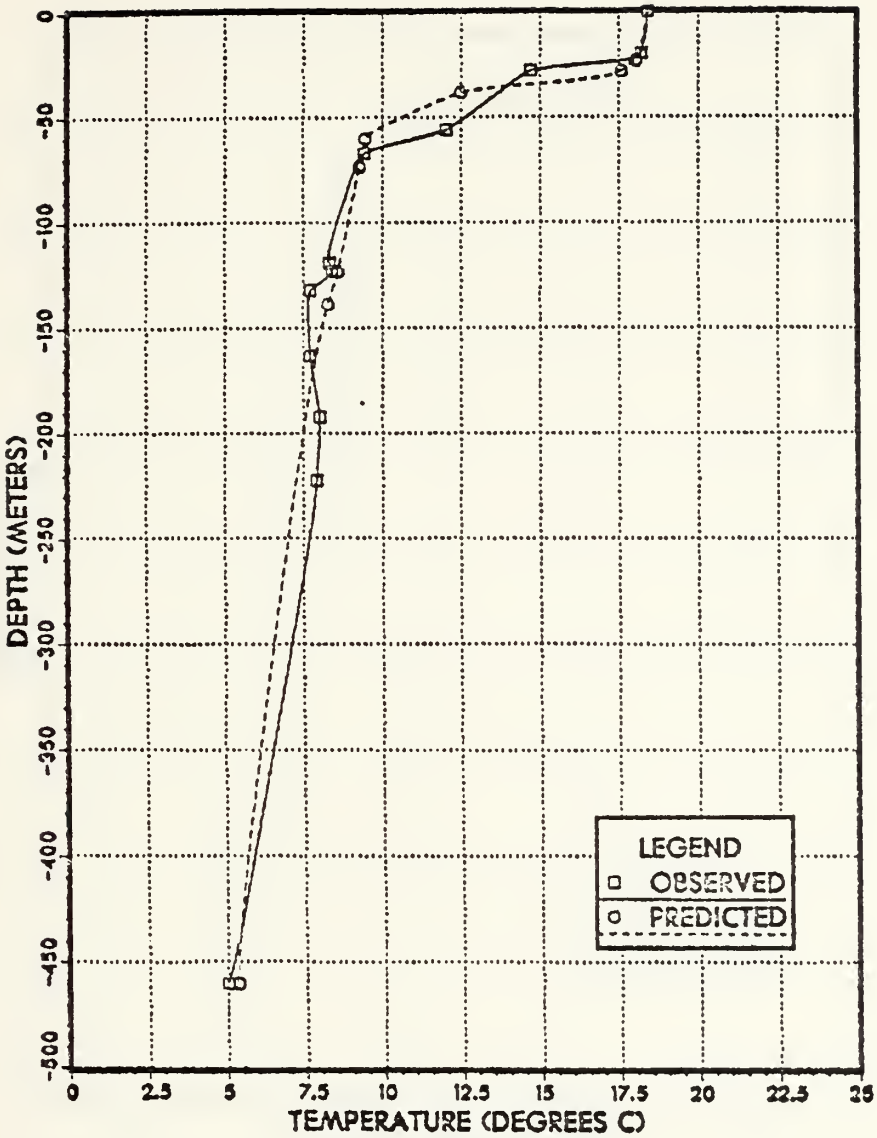

Figure F.14. Observed and Predicted Thermal Profiles at XBT Sta. 353.

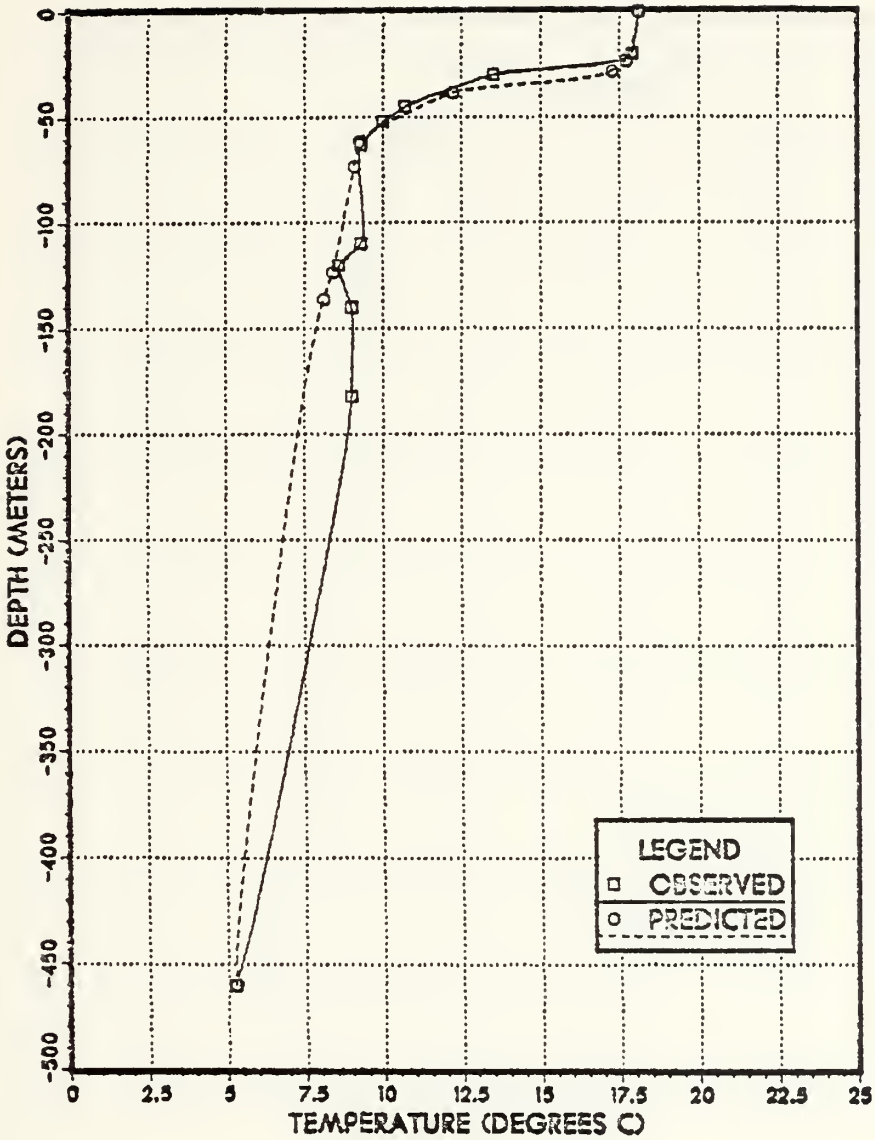

Figure F.15. Observed and Predicted Thermal Profiles at XBT Sta. 354.

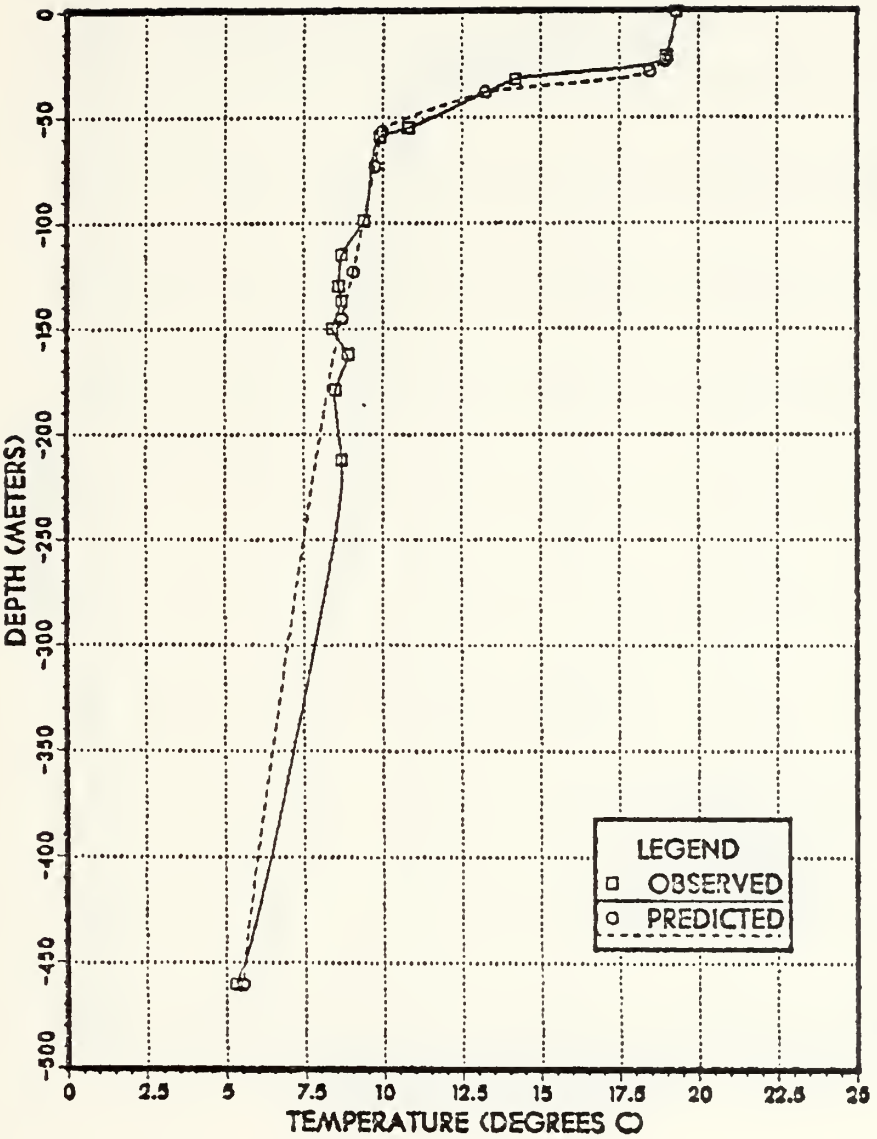

Figure F.16. Observed and Predicted Thermal Profiles at XBT Sta. 355.

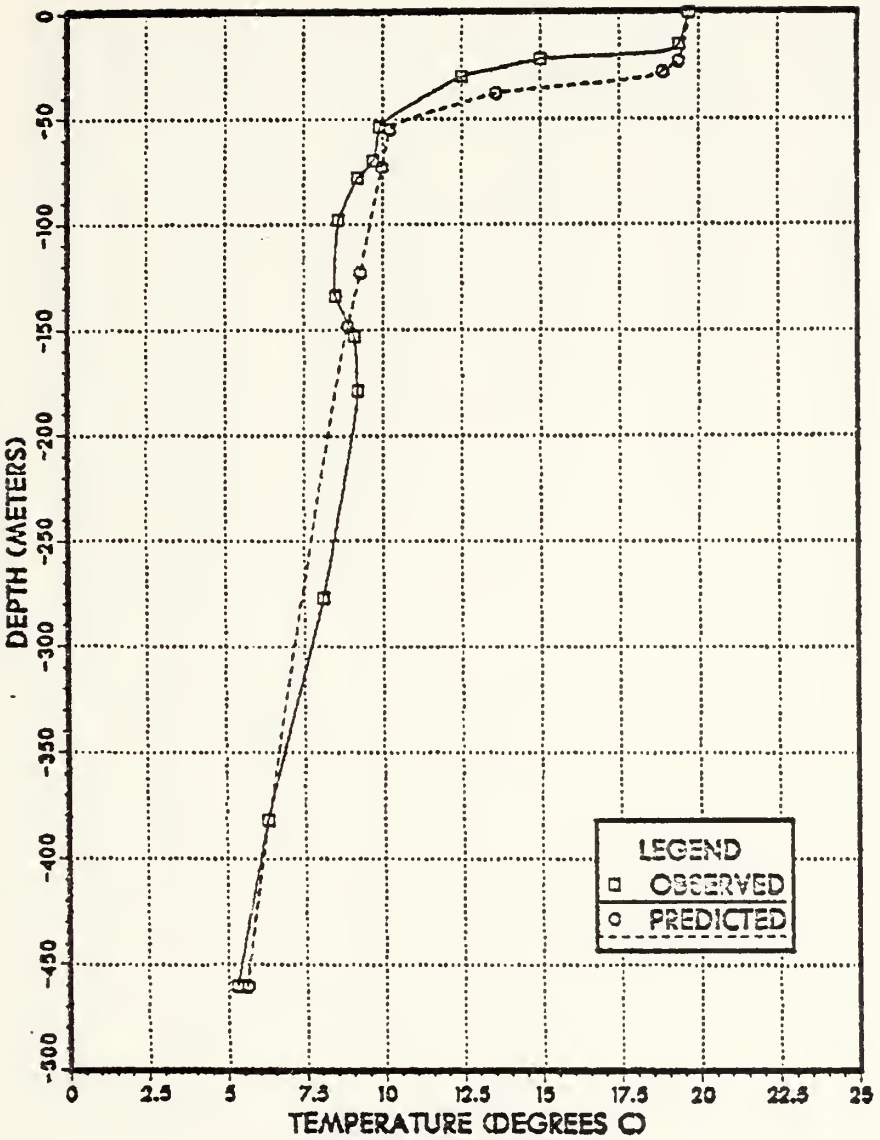

Figure F.17. Observed and Predicted Thermal Profiles at XBT Sta. 356.

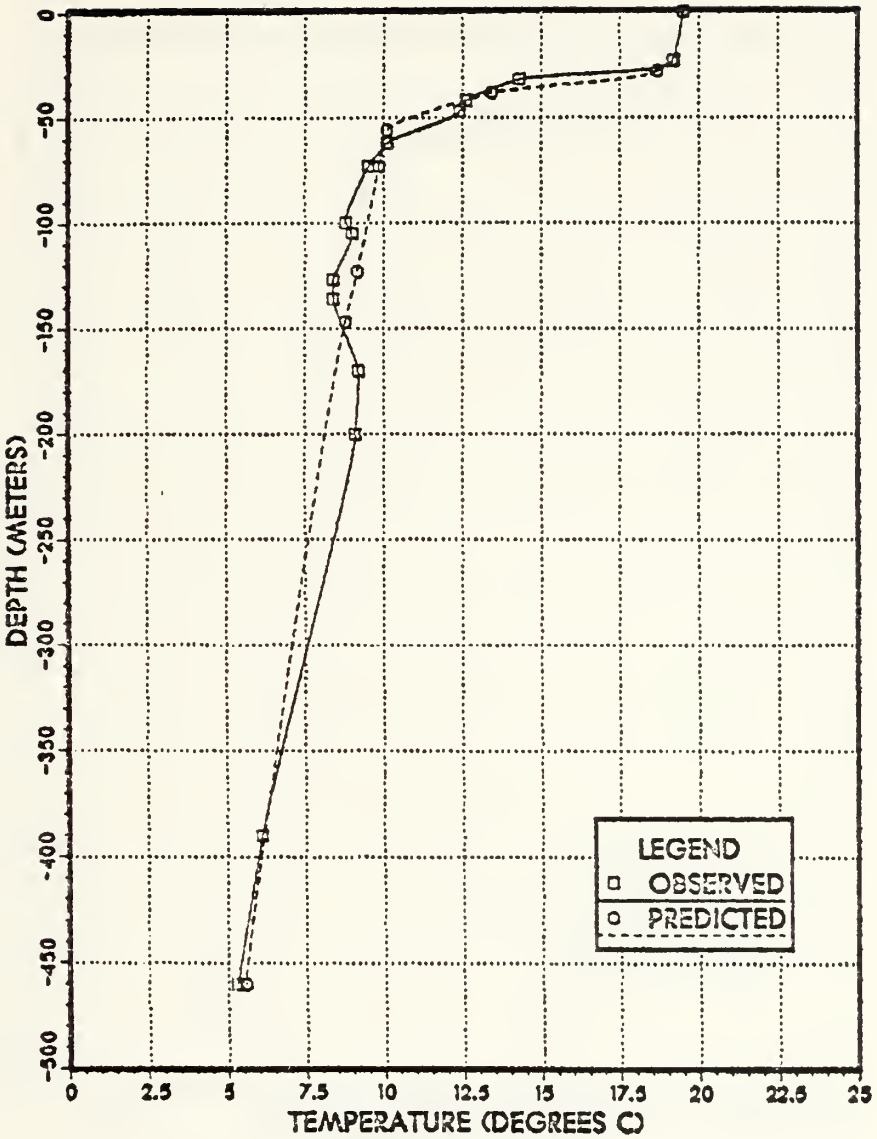

Figure F.18. Observed and Predicted Thermal Profiles at XBT Sta. 357.

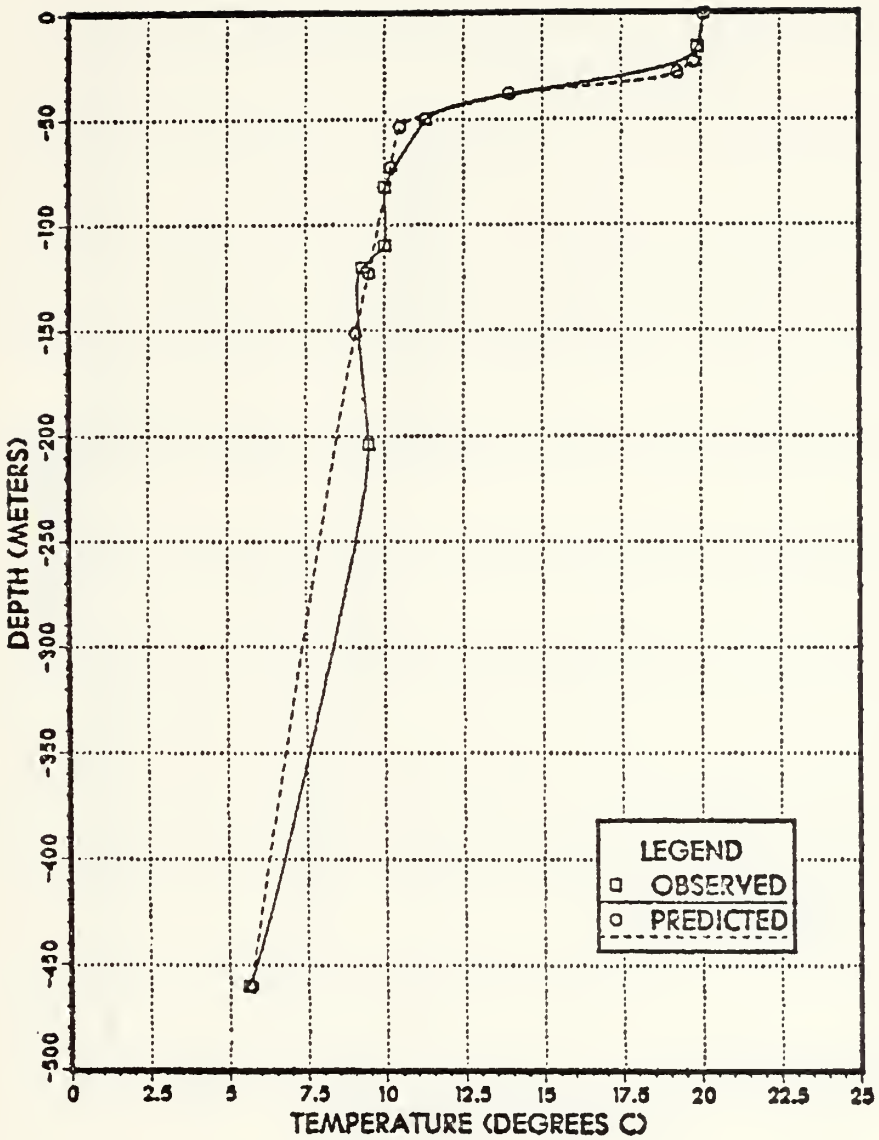

Figure F.19. Observed and Predicted Thermal Profiles at XET Sta. 358.

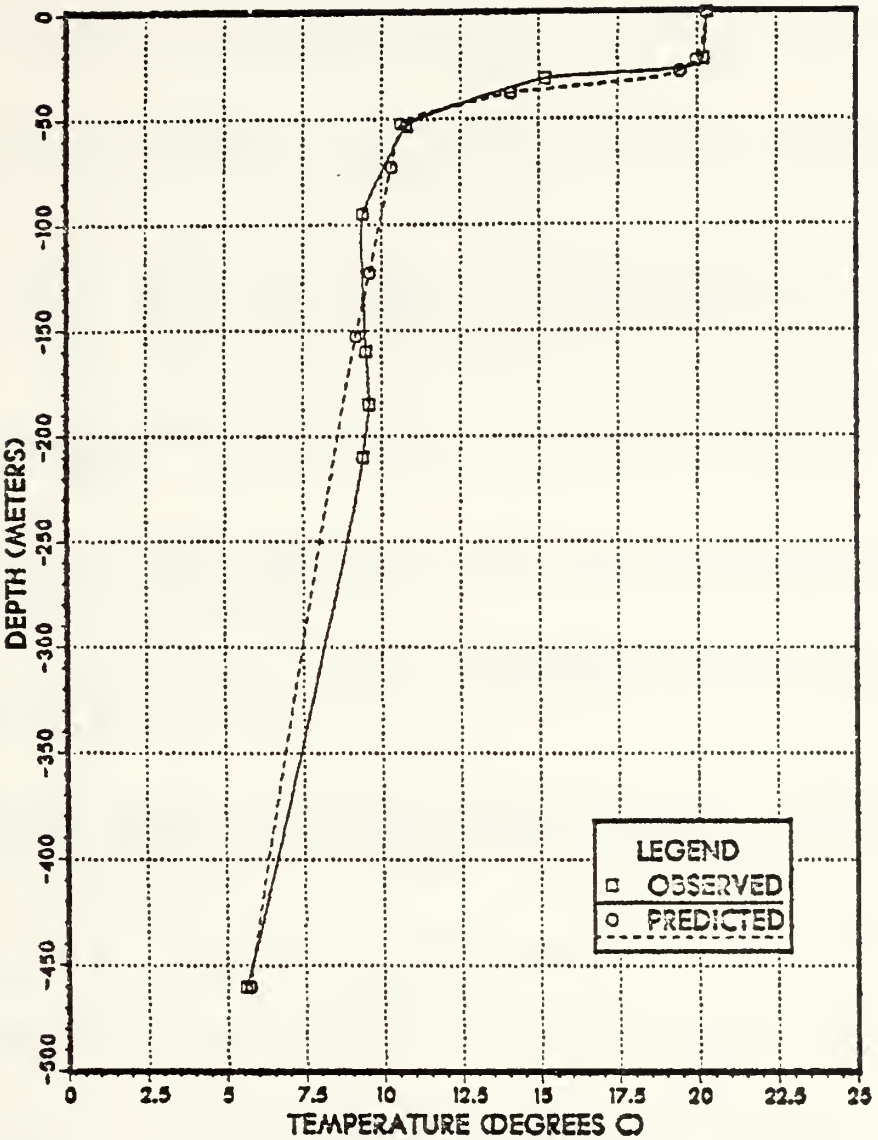

Figure F.20. Observed and Predicted Thermal Profiles at XBT Sta. 359.

LIST OF REFERENCES

Bathen, K.H., "On the Seasonal Changes in the Depth of the Mixed Layer in the North Pacific Ocean", Journal of Geophysical Research, v.77, n.36, 7138-7150, December, 1972.

Bathythermograph Log Sheets 113-122 for SILAS BENT cruise 343722, Phase III, September 1977.

Bernstein, R., Breaker, L., and Whritner, R., "California Current Eddy Formation: Ship, Air and Satellite Results", Science, v.195, 353-359, January 1977.

Clancy, R.M., and Martin, P.J., "Synoptic Forecasting of the Oceanic Mixed Layer Using the Navy's Operational Environmental Data Base: Present Capabilities and Future Applications", Bulletin of the American Meteorological Society, v.62, n.6, 770-784, June 1981.

Cox, S.A., Satellite Application to Acoustic Prediction Systems, Master's Thesis, Naval Postgraduate School, Monterey, 1982.

Denman, K.L., and Miyake, M., "Upper Layer Modification at Ocean Station Papa: Observations and Simulations", Journal of Physical Oceanography, v.3, n.2, 185-196, April 1973.

Dixon, W.J., and Brown, M.B., Biomedical Computer Programs P-Series, BMDP-79, University of California Press, Berkeley, California, 1-880, 1979.

Dodimead, A.J., Favorite, F., and Hirano, T., Review of Oceanography of the Subarctic Pacific Region, v.1, figure 216, Paper prepared for the International North Pacific Fisheries Commission, 1 October 1962.

Fleet Numerical Oceanography Center, Sea Surface Temperature Evaluation for 101200Z September 1977.

Fleet Numerical Oceanography Center, Surface Weather Analysis for September 1977

Frankignoul C., "Low Frequency Temperature Fluctuations Off Bermuda", Journal of Geophysical Research, v.86, n.7, 6522-6528, July 1981.

Kenyon, K.E., "A Shallow Northeastern Current in the North Pacific", Journal of Geophysical Research, v.86, n.7, 6529-6536, July 1981.

Kenyon, K.E., "The Surface Layer of the Eastern North Pacific in Winter", Journal of Geophysical Research, v.83, n.12, 6115-6122, December 1978.

Legeckis, R., "A Survey of Worldwide Sea Surface Temperature Fronts Detected by Environmental Satellites", Journal of Geophysical Research, v.83(C9), 4501-4522, September 1978.

Legeckis, R., and Gorden, A.L., "Satellite Observations of the Brazil and Falkland Currents - 1975 to 1976 and 1978", Deep-Sea Research, v.29, 392-405, March 1982.

Miller, I., and Freund, J.E., Probability and Statistics for Engineers, Prentice-Hall, Inc., Englewood Cliffs, New Jersey, 321-328, 1977.

Monin, A.S., and Fedorov, K.N., "The Fine Structure of the Upper Layers of the Ocean", Atmospheric and Oceanic Physics, v.9, n.4, 442-444, July 1972.

Renner, J.A., "Fishing Information", Southwest Fisheries Center - La Jolla, California, n.9, 1-13, September 1977.

Roden, G.I., "Aspects of the Mid-Pacific Transition Zone", Journal of Geophysical Research, v.75, n.6, 1097-1109, February 1970.

Roden, G.I., "On North Pacific Temperature, Salinity, Sound Velocity and Density Fronts and Their Relation to Wind and Energy Flux Fields", Journal of Physical Oceanography, v.5, n.4, 557-571, October 1975.

Roden, G.I., "Shallow Temperature Inversions in the Pacific Ocean", Journal of Geophysical Research, v.69, n.14, 2899-2913, July 1964.

Tabata, S., "Characteristics of Water and Variations of Salinity, Temperature, and Dissolved Oxygen Content of the Water at Ocean Weather Station 'P' in the Northeast Pacific Ocean", Journal of the Fisheries Research Board of Canada, v.17(3), 353-370, 1960.

Tabata, S., "Comparison of Observations of Sea Surface Temperatures at Ocean Station P and NOAA Bouy Stations and Those Made by Merchant Ships Traveling in Their Vicinities, in the Northeast Pacific Ocean", Journal of Applied Meteorology, v.17, 374-385, 1978.

Tabata, S., "Variability of Oceanographic Conditions at Ocean Station 'P' in the Northeast Pacific Ocean", Transactions of the Royal Society of Canada, v.3, Series 4, 367-418, June 1965.

Tabata, S., Boston, N.E.J., and Boyce, F.M., "The Relation Between Wind Speed and Summer Isothermal Surface Layer of Water at Ocean Station P in the Eastern Subarctic Pacific Ocean", Journal of Geophysical Research, v.70, n.16, 3867-3877, August 1965.

Tabata, S., and Kimber, P.M., "Satellite Observations of Sea Surface Temperature Patterns Off the Pacific Coast of Canada", Pacific Marine Science Report 79-19, Institute of Ocean Sciences, Patricia Bay, British Columbia, Canada, 1-77, 1979.

Tully, J.P., "Oceanographic Regions and Assessment of Temperature Structure in the Seasonal Zone of the North Pacific Ocean", Journal of the Fisheries Research Board of Canada, v.21(5), 941-970, September 1964.

Tully, J.P., and Giovando, L.F., "Seasonal Temperature Structure in the Eastern Subarctic Pacific Ocean", Marine Distributions, The Royal Society of Canada Special Publication No. 5, 10-35, 1963.

Uda, Michitake, "Oceanography of the Subarctic Pacific Ocean", Journal of the Fisheries Research Board of Canada, v.20(1), 119-179, 1963.

White, W., Bernstein, R., McNally, G., and Pazan, S., "The Thermocline Response to Transient Atmospheric Forcing in the Interior Mid-Latitude North Pacific 1976-1978", Journal of Physical Oceanography, v.10, 372-384, March 1980.

INITIAL DISTRIBUTION LIST

		No. Copies
1.	Defense Technical Information Center Cameron Station Alexandria, Virginia 22314	2
2.	Library, Code 0142 Naval Postgraduate School Monterey, California 93940	2
3.	Chairman (Code 68Mr) Department of Oceanography Naval Postgraduate School Monterey, CA 93940	1
4.	Chairman (Code 63Rd) Department of Meteorology Naval Postgraduate School Monterey, CA 93940	1
5.	Superintendent Attn: Code 68Jg Naval Postgraduate School Monterey, California 93940	2
6.	Superintendent Attn: Code 68Du Naval Postgraduate School Monterey, California 93940	2
7.	Director Naval Oceanography Division Naval Observatory 34th and Massachusetts Avenue NW Washington, D.C. 20390	1
8.	Commander Naval Electronics Systems Command Attn: PME-124-60 Naval Electronics Systems Command Headquarters Washington D.C. 20360	1
9.	Commander Oceanographic Systems, Pacific Box 1390 Pearl Harbor, HI 96860	1
10.	Commander Attn: Code 531 Naval Ocean Systems Center San Diego, CA 92152	1

11. Chief of Naval Operations 1
Attn: OP951F
Navy Department
Washington D.C. 20350

12. Commanding Officer 1
Fleet Numerical Oceanography Center
Monterey, CA 93940

13. Commanding Officer 1
Naval Ocean Research and Development Activity
NSTL Station
Bay St. Louis, MS 39522

14. Commanding Officer 1
Naval Environmental Prediction Research Facility
Monterey, CA 93940

15. Chairman, Oceanography Department 1
U.S. Naval Academy
Annapolis, MD 21402

16. Chief of Naval Research 1
800 N. Quincy Street
Arlington, VA 22217

17. Office of Naval Research (Code 480) 1
Naval Ocean Research and Development Activity
NSTL Station
Bay St. Louis, MS 39522

18. Scientific Liason Office 1
Office of Naval Research
Scripps Institute of Oceanography
La Jolla, CA 92037

19. Library 1
Scripps Institute of Oceanography
P.O. Box 2367
La Jolla, CA 92037

20. Library 1
Department of Oceanography
University of Washington
Seattle, WA 98105

21. Library 1
CICESE
P.O. Box 4803
San Ysidro, CA 92073

22. Library 1
School of Oceanography
Oregon State University
Corvallis, OR 97331

23. LT T.A. Howell 1
Naval Western Oceanography Center
Box 113
Pearl Harbor, HI 96860

24. Commander 1
Naval Oceanography Command
NSTL Station
Bay St. Louis, MS 39522

25. Commanding Officer 1
Attn: Dr. William Jobst, Code 7300
Naval Oceanographic Office
NSTL Station
Bay St. Louis, MS 39522

26. Commanding Officer 1
Attn: Code 5101
Naval Research Laboratory
Washington D.C. 20375

201550

Thesis
H8247 Howell
c.1 A statistical approach for determining subsurface thermal structure from sea surface temperature in the northeast Pacific Ocean.

201550

Thesis
H8247 Howell
c.1 A statistical approach for determining subsurface thermal structure from sea surface temperature in the northeast Pacific Ocean.

thesH8247
A statistical approach for determining s
3 2768 002 06755 5
DUDLEY KNOX LIBRARY